Fabrication Aspects of Porous Biomaterials in Orthopedic Applications: A Review

Article *in* ACS Biomaterials Science and Engineering · November 2017
DOI: 10.1021/acsbiomaterials.7b00615

2 authors:

Elham Babaie
Rice University
13 PUBLICATIONS **24** CITATIONS
SEE PROFILE

Sarit B Bhaduri
University of Toledo
181 PUBLICATIONS **3,160** CITATIONS
SEE PROFILE

ACS Biomaterials SCIENCE & ENGINEERING
Review
Cite This: ACS Biomater. Sci. Eng. XXXX, XXX, XXX−XXX

Fabrication Aspects of Porous Biomaterials in Orthopedic Applications: A Review

Elham Babaie*,† and Sarit B. Bhaduri‡

†Department of Bioengineering, Bioscience Research Collaborative, Rice University, Houston, Texas 77030, United States
‡Department of Mechanical and Industrial Engineering and Division of Dentistry, University of Toledo, Toledo, Ohio 43606, United States

ABSTRACT: Porous biomaterials have been widely used in a variety of orthopedic applications. Porous scaffolds stimulate the cellular responses and accelerate osteogenesis. The porous structure of scaffolds, as well as their compositions, dictate cellular responses such as their adhesion, penetration, differentiation, nutrition diffusion, and bone in-growth. During the last two decades, tremendous efforts have been devoted by researchers on innovative processing technologies of porous ceramics, metals, polymers, and glasses, resulting in a wide variety of porous architectures with substantial improvements in properties. Design and fabrication of porous scaffolds are complex issues that can jeopardize scaffolds' biological, mechanical, and physiochemical properties. This paper intends to comprehensively review the processing techniques used in fabricating porous biomaterials including ceramics, polymers, metals, and glasses along with correlating with their biological and mechanical performances. From a macroscopic perspective, pore size distribution, interconnectivity, pore morphology, and porosity play critical roles in bone formation in vivo. From a microscopic viewpoint, the adhesion−retention of proteins, which eventually affect some cellular fates, and absorption−delivery of therapeutic agents can be tailored by microtextured surfaces. Various processing techniques such as partial sintering, sacrificial fugitives, foaming, freeze casting, metal injection molding, rapid prototyping, etc., and their associated parameters in designing of porous biomaterials are reviewed, with specific examples of their applications. The remainder of the paper is organized as follows. First, the paper describes correlations of porosity characteristics with biological properties. Subsequently, mechanical properties of porous scaffolds are discussed. Finally, a summary of this review and future directions are presented.

KEYWORDS: *Porosity, fabrication, biomaterials, properties, orthopedics*

1. INTRODUCTION

Porous biomaterials are of significant interest in a wide range of biomedical applications. A case in point is orthopedic applications where there are uses as bone graft substitutes,[2,3] scaffolds,[4−6] coatings,[7,8] and drug delivery systems.[6,9] A key requirement in bone regeneration is a scaffold that allows for cells to migrate, proliferate, differentiate, and eventually synthesize new bone. To function as drug delivery media, sustained release of the therapeutic agents over a long period of time at targeted sites is an important requirement. The sustained release kinetics of agents is dependent upon the characteristics of drugs as well as microstructure of porous biomaterials such as pore content, size distribution, and tortuosity. From a different perspective, the presence of pores compromises the load-bearing ability of the materials, especially in brittle ceramics. The main concern with ceramics in general is their inherent brittleness and low fracture strength in load bearing applications.[10]

Lastly, there are myriads of choices in selecting processing technologies to fabricate porous biomaterials, for example, metals, ceramics, and polymers. These considerations necessitate a comprehensive understanding of correlations among the processing parameters, the resulting porous microstructures, and the physical, mechanical, and in vitro/in vivo behaviors of materials. These correlations are in fact ubiquitous in Materials Science textbooks that are organized based on triangular structure−processing−properties relationships. The only difference here is that there is a fourth vertex that represents biological (in vitro/in vivo) responses. This situation is represented by the tetrahedron as shown in Figure 1a.

There are several signatures of this effort. First, Figure 1a is drawn in a way to reflect that processing is the main theme here. However, a comprehensive review of this magnitude remains always incomplete if the related issues are not addressed. Second, as mentioned before, porous biomaterials are becoming important from the viewpoint of their applications. For example, synthetic bone graft substitutes (BGS) have been developed in different pore shapes and sizes using diverse manufacturing techniques. The growing marketplace of synthetic bone graft substitutes can effectively reduce the need for the applications of autologous or allogeneic bones that have been conventionally in use for the last several decades. More importantly, there is a lesser risk of disease transfer and rejection and morbidity at the harvest sites with the

Received: August 30, 2017
Accepted: November 22, 2017
Published: November 22, 2017

DOI: 10.1021/acsbiomaterials.7b00615
ACS Biomater. Sci. Eng. XXXX, XXX, XXX−XXX

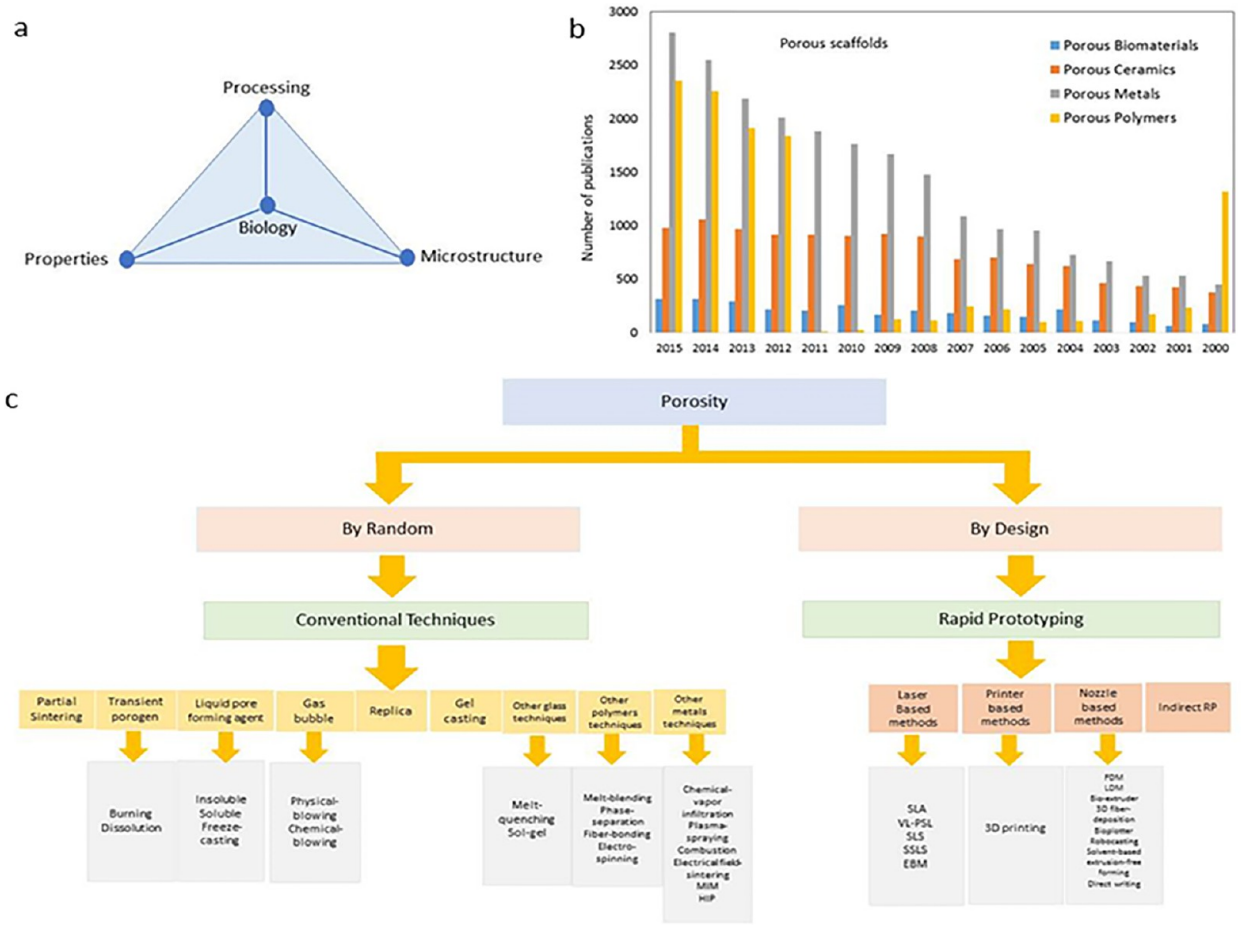

Figure 1. (a) Triangular structure−processing−properties relationships, (b) keywords and the number of porous-materials-related studies over the last 15 years (2000−2015), and (c) classification of porous scaffold fabrication techniques.

synthetic materials compared to autografts or allografts.[11] It is hoped that a comprehensive understanding of this interdisciplinary topic will expand and broaden successful uses of porous biomaterials with an emphasis on orthopedics. Third, in the literature, there are individual reviews about theoretical developments on porous materials and their use in structural or energy related applications.[12,13] There are also reviews on porous scaffolds made from biopolymers for use in regenerative medicine.[5,14] The results of recent keyword searches in the Scopus database spanning 2000 until 2015 are described in Figure 1b. Keywords such as "Porous metals", "Porous ceramics", "Porous polymers", and "Porous biomaterials" were used in conducting the search. Inherent in these searches is the fact the pore sizes could range from microscale to macroscale. To deal with all kinds of pore sizes is a daunting task. Thus, this review will mostly limit itself to presence of macroporosities, which is important in orthopedics.[11] Figure 1b reveals that porous biomaterials are a smaller subclass of the three main classes of porous materials. At the same time, research in porous biomaterials has been growing at a rapid pace, outpacing its larger parents. In spite of the explosive growth, to the best of our knowledge, there has been no comprehensive review in the literature on processing of these materials. Many times, a processing technique is chosen on an *ad hoc* basis without determining a clear strategy. All of these considerations motivate this compilation.

As mentioned before, there has been a three-decade old research effort on porous materials led by Sir Michael Ashby at Cambridge University.[1,5,15−17] Over this time, several review papers were published by the group in the literature. The paper by Gibson and Ashby is the very first attempt to review the properties of porous materials from their mechanical properties aspects.[1] Ashby refers to these materials as "Cellular" or "Lattice" materials while discussing their ductile and brittle mechanical properties in a comprehensive text on the topic including processing, properties, and uses. Conventionally, these materials are used as catalyst carriers, filters, and membranes in chemical, transportation, and energy related industries. Such uses take advantage of their interesting properties such as the strength-to-weight ratios. From the perspective of applications, their uses in biomedical fields are of recent origin. In most such applications their biomedical properties are emphasized without realizing that the mechanical properties can also be taken advantage of. Salimon et al. reviewed properties and applications of metallic foams.[17] However, none of the commercially available foams described in ref 17 have any biomedical applications.

The use of the keyword, "Porous Biomaterials" results in several important reviews, all related to porous scaffolds in regenerative medicine. The common trends of these papers are noted in the following. First, many of these review papers are related to biopolymers, which is an indication of the popularity of these materials in the fabrication of scaffolds, as opposed to metals and ceramics. Second, deliberate advantage is taken of osteoconductive, osteoinductive, and osteointegrable materials in the fabrication of scaffolds. Osteoconduction implies ease (or

DOI: 10.1021/acsbiomaterials.7b00615
ACS Biomater. Sci. Eng. XXXX, XXX, XXX−XXX

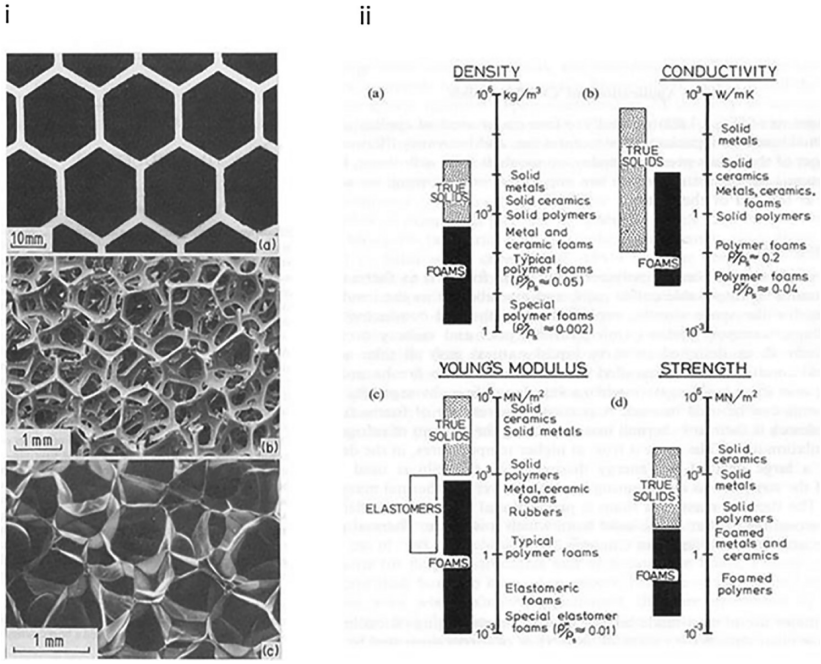

Figure 2. (i) Examples of cellular solids: (a) a two-dimensional honeycomb; (b) a three-dimensional foam with open cells; (c) a three-dimensional foam with closed cells.[1] (ii) The range of properties available to the engineer through foaming: (a) density, (b) thermal conductivity, (c) Young modulus, (d) compressive strength.[1]

difficulty) of formation of bone on a surface. Implant materials of low biocompatibility such as copper or silver show little or no osteoconduction.[18] Osteoinduction encompasses the process of mesenchymal cell recruitment, mesenchymal differentiation to bone-forming osteoblasts, and ectopic bone formation in vivo.[19] Finally, the process of osteointegration means direct bonding of bone to an implant surface.[20,21] In his highly cited review, Hutmacher emphasized these issues.[20,21]

Attention was drawn to enhanced capabilities of such materials via incorporation of biological molecules (e.g., proteins, nucleic acid sequences etc.) or cells. The appropriate delivery of these molecules increases the cell signaling, vascular networks, and growth. Hutmacher's paper primarily focuses on design and fabrication of porous polymers. The advantages of 3-D printing on carefully tailored porosities are discussed.

The review paper by Rezwan et al. is more related to the present paper.[5] The focus in ref 5 is biopolymer/ceramic composites and their microstructure−processing−property correlations. The authors collected a large amount of data for both polymers and ceramics. The absence of useful properties as mentioned in the previous paragraph lead to a reduced chance of success for these materials. When pores are sufficiently large, bone ingrowth occurs due to the larger availability of space preventing peripheral cellular growth and fibrosis. Larger surface area provides higher bone inducing protein adsorption, thus enhancing cell adhesion in overall scaffold. These considerations highlight the importance in understanding processing aspects of porous biomaterials in regenerating bone.[5,8]

Karageorgiou and Kaplan reviewed the biological aspects of presence of pores in scaffolds for osteogenesis.[22] The paper, published in 2005, focused on different types of porous biomaterials including metals, ceramics, glass, and polymers. The porosity content, their microstructural architecture, and the size distributions in various materials were correlated to the biological responses. It was found that the in vitro and in vivo responses differed. The paper did not go into detailed review of processing related issues and characterization methods. A review paper by Chevalier et al., on the other hand, focused the fabrication aspects of porous biomaterials, albeit in a less than comprehensive manner.[23] No correlating relationship was addressed. Ohji and Fukushima[24] also reviewed several techniques for fabrication of macroporous ceramics. Those techniques mostly focused on sintering and foaming methods aiming at a variety of industrial applications. However, processing of porous ceramics in biomedical applications has not been addressed.

A more recent review paper by Perez and Mestres focuses on the correlations between pore size and morphology of porous scaffolds on their in vitro and in vivo responses.[16] Within that framework, various materials and their processing as porous scaffolds are described but given lesser importance. The mechanical properties have been briefly mentioned. This being a very recent paper, many recent advances are incorporated.[16]

The present review attempts to present a comprehensive discussion of the fabrication and related materials aspects of macroporous biomaterials such as polymers, metals, ceramics, and glasses with potential orthopedic applications. It is noted that research on porous scaffolds has been extensive. However, excepting the paper by Perez and Mestres, many other reviews are already a decade old. In most papers, scaffolds for tissue (e.g., bone) regeneration is the focus without processing getting much attention. While biological responses have been discussed in previous literature, the mechanical properties aspects are mostly ignored. Thus, correlations between various aspects of porous biomaterials are not possible. In view of these observations, we have focused on the processing aspects more than the other signatures of porous biomaterials. However, we have not ignored the resulting structures, the architecture, and last but not least, their mechanical properties.

DOI: 10.1021/acsbiomaterials.7b00615
ACS Biomater. Sci. Eng. XXXX, XXX, XXX−XXX

Table 1. Geometric Properties of Isolated Cells[1]

cell shape	number of faces, f[a]	number of edges, n[b]	number of vertices, v[c]	cell volume[d,e]	surface area[a,d,e]	edge length[b,e]	comments[f]
tetrahedron	4	6	4	$0.118l^3$	$\sqrt{3}l^2$	$6l$	regular
triangular prism	5	9	6	$(\sqrt{3}/4)l^3A_r$	$(\sqrt{3}/2)l^2(1 + 2\sqrt{3}A_r)$	$6l(1 + A_r/2)$	packs to fill space
square prism	6	12	8	l^3A_r	$2l^2(1 + 2A_r)$	$8l(1 + A_r/2)$	packs to fill space (cube is regular)
hexagonal prism	8	18	12	$3(\sqrt{3}/2)l^3A_r$	$3\sqrt{3}l^2(1 + 2A_r/\sqrt{3})$	$12l(1 + A_r/2)$	packs to fill space
octahedron	8	12	6	$0.471l^3$	$3.46l^2$	$12l$	regular
rhombic dodecahedron	12	24	14	$2.79l^3$	$10.58l^2$	$24l$	packs to fill space
pentagonal dodecahedron	12	30	20	$7.663l^3$	$20.646l^2$	$30l$	regular
tetrakaidecahedron	14	36	24	$11.31l^3$	$26.80l^2$	$36l$	packs to fill space
icosahedron	20	30	12	$2.182l^3$	$8.660l^2$	$30l$	regular

[a]In an infinite, packed array, every face is shared between two cells; the number of faces per cell and surface area per cell in the array are one-half of these values. [b]In an infinite, packed array, every edge is shared between Z_f faces (usually three); the number of edges per cell and the edge length per cell in the array are $1/Z_f$ of these values. [c]In an infinite, packed array, every vertex is shared between Z_e edges (usually four); the number of vertices per cell in the array is $1/Z_e$ of these values. [d]See, for instance, De Hoff and Rhines[25] and the Handbook of Chemistry and Physics.[26] [e]A_r is the aspect ratio: $A_r = h/l$ where h and l are defined in Figure 2.11 in ref 1. [f]Regular polyhedra have faces and edges that are all identical. Most do not pack to fill the space.

The present review's topic is introduced here by describing and critiquing the important aspects of recent reviews. This is followed by a short introduction on "Porous Biomaterials" with bone as the prime example. The next section represents the core of the paper. As shown in Figure 1c, the fabrication techniques are categorized according to the pores created randomly or by design. To begin with, the fabrication methods common to all classes of materials are described. Subsequently, processing techniques related to one specific class of materials are presented. In addition, the correlating relationship of the porous characteristics with pertinent materials issues is discussed. The effects of pore size, porosity, interconnectivity, and permeability on cell responses, mechanical performance, and drug delivery manners are elaborated. Finally, the summary of this review and future directions in porous biomaterials are discussed.

1.1. Description of Bone as a Porous Material. Porous materials are also referred to as cellular materials. From a biological (or otherwise) viewpoint, the word "cell" represents a small space and has its origin in the Latin word "cella". A cellular solid comprises a number such cells. Specifically, the architecture of a cellular solid can consist of solid struts or plates, resulting in edges and faces of walls.[1]

Figure 2i shows three such examples. To begin with, a lattice of polygons can fill a two-dimensional plane. A case in point is a cluster of hexagons leading to two-dimensional structures, which are referred to as "honeycombs" (Figure 2i-a). Translating from two-dimensions to three-dimensions in order to fill the three-dimensional space, polygons become polyhedra, which can serve the purpose of space-filling. The two-dimensional "honeycomb" cellular materials become three-dimensional "foams", which can be classified into "open cell" and "closed cell" categories. The "open cell" foams have the solid material only on the cell edges with the rest of the cell empty (Figure 2i-b). The "closed-cell" foams have solid materials on faces as well, leading to isolation of each cell from one another (Figure 2i-c). Often times, foams possess both open and closed cell characteristics. This review will concentrate on the open cell foams, which are of more biomaterial significance than the closed cell foams.

The three-dimensional geometrical aspects of foams (or cellular solids) can be easily described by the organization of two-dimensional components (faces), one-dimensional components (edges), and zero-dimensional components (vertices).[15] The following definitions are arrived at, based on this scheme:

(1) Edge connectivity, Z_e. This is the number of edges that meet at a vertex. For example, in a honeycomb, Z_e is 3 and in a foam Z_e may be 4.

(2) Face connectivity, Z_f. The number of faces that meet at an edge. In foams, this may be 3 but can take other values. Furthermore, the number of vertices, V, of edges, E, of faces, F, and of cells, C, is related by Euler's law,

$$F - E + V = 1 \quad \text{(for two-dimensional geometry)} \tag{1}$$

$$-C + F - E + V = 1 \quad \text{(for three-dimensional geometry)} \tag{2}$$

Figure 2i shows various arrangements of the space-filling characteristics of polyhedral cells. Table 1 describes the topological properties of various individual geometries.

The ability to process cellular solids can result in significant extension of values of important properties. Figure 2ii-a–d shows the range of four different properties: the density, conductivity, the Young's modulus, and the compressive strength. The dotted bar shows typical property values in conventional solids. The solid bar, on the other hand, shows values achieved in foamed structures of the same solids.[1] This extension of property values results in diverse applications.

Bone can be described from the viewpoint of above perspectives as a complex composite, mainly composed of hydroxyapatite crystals deposited within an organic matrix of collagen. It consists of cortical bone with 5–13% porosity and cancellous bone with 30–90% porosity. Haversian canals as a part of cortical bone have cross-sectional area of 2500–12000 μm, and 3–12% porosity. Mechanical properties such as a range of compressive strengths of cortical bone of 130–180 MPa, flexural strengths of 135–190 MPa, tensile strengths of 50–151 MPa, and an elastic modulus of 12–18 GPa were reported for compacted bone. Cancellous bone, on the other hand, exhibits a compressive strength of 4–12 MPa, a tensile

DOI: 10.1021/acsbiomaterials.7b00615
ACS Biomater. Sci. Eng. XXXX, XXX, XXX–XXX

Table 2. Pore Sizes and Porosities of Ceramic Scaffolds for Bone Tissue Engineering[a]

material	fabrication method	pore size (μm)	porosity (%)	ref
β-TCP	emulsion/sintering	170, 217,416, and 972	~52	288
β-TCP	PMMA porogen leaching/sintering	337, 415, 557 and 632	60, 52, 41, and 37	248
HA	pressing/firing		~17	29
HA-45S55	freeze casting/polymeric sponge	1−10, 50−1100	80−92	103
HA cement	liquid foaming agent/hydrolysis	0.06−1000	45−66	88
HA	polymeric sponges/sintering	750−1100	76 (single coat), 82 (double coat)	107
Injectable CPC	solid foaming agent	0.005−10, 10−1000	47−75	289
HAp-(a-TCP)	gel casting	0.2−0.9, 25−250, 250−900	~90	290
HA	gel casting/polymer sponge	200−400	~76	291
calcium silicate phosphate cement	salt leaching	2−5, 200−500		56
HA-βTCP	indirect RP/sintering	340	26−72	235
CPC	PLGA porogen	40−1	up to 100	54
brushite block	low-temperature direct 3D printing	open channel of 1.3 mm	~38 ($p_{microporosity}$)	209
monetite block	low-temperature direct 3D printing	10−20, closed pore channels of 2.5 mm	~44 ($p_{microporosity}$)	209
calcium sulfate ($CaSO_4$)	selective laser sintering	1.2 mm	~34	292

[a]Pore sizes are shown either by the range or by the average size.

Table 3. Pore Sizes and Porosities of Polymer (Natural and Synthetic) Scaffolds for Bone Tissue Engineering[a]

material	fabrication method	pore size (μm)	porosity (%)	ref
polycaprolactone (PCL)	selective laser sintering	2 mm × 2 mm square pore channels	57−83	196
collagen−glycosaminoglycan	freeze-drying	85−325		80
corn starch/poly(ε caprolactone)	three-dimensional plotting	gradient pore size 100−750−100	up to 90	244
silk fibroin	freeze-drying	50−300	71−94	293
PLGA	CO_2 blowing agent	-	~95	100
poly(D,L-lactide)	partial sintering of microsphere		39−58	61
PEO/PBT	compression molding/salt leaching		73−85	61
PCL	coagulation/molding/leaching		65−95	61
poly(L-lactide)	co-continuous blend	1.5−88	~60	131
PCL	solvent casting/particulate/polymer leaching	378−435	91−93	60
chitosan/PLGA	microsphere sintering	170−200	28 and 37	36
PLGA/PVA	melt-molding/particulate-leaching	200−300	~90	64
gelatin−cornstrach−dextran	3-D printing	2.5 mm (cylindrical), 2.5 mm × 2.5 mm (square)	up to 0.590 (m^3)	294
PCL	bioextruder	670	~67	214
PEOT/PBT	3-D fiber deposition	1850	~78	219
PCL	stereolithography	465	~70	194
PVA	selective laser sintering		~68	295
spongiform PGA	wet electrospinning		~97	161
PCL	electrospinning (spherical dish and metal array collector)	2−5		134

[a]Pores are shown either by the range or by the average size.

strength of 1−6 MPa, and an elastic modulus of 0.1−0.5 GPa.[27,28] Substitutions used for such bone-mimicking biomaterials should optimize bone morphology, structure, and functions of bone. The next few sections of the paper focus on processing aspects as well as various correlations, as described earlier.

2. CREATION OF RANDOM POROSITY

Summaries of pore sizes and porosities achieved by different methods are collected for ceramic, polymer, and metal materials in Tables 2, 3, and 4, respectively. Table 5 summarizes the advantages and challenges of different fabrication techniques.

2.1. Partial Sintering. In this technique, the mechanisms of surface diffusion or evaporation−condensation at high temperature exposures can be preferentially triggered in an assembly of particles. This results in grain/pore coarsening without densification. Alternatively, a homogeneous porous structure can be formed when sintering is stopped before full densification is achieved as shown in Figure 3a. The porous structure or the size and morphology of pores can be modified by the size of starting powders, level of initial compaction, and subsequent sintering parameters including pressure, sintering temperature, and time. For instance, the porosity content decreases by the decrease in powder size because of faster sintering.

2.1.1. Ceramic. The ball milled and sieved hydroxyapatite (HA) powder, the most important bioceramic, can be uniaxially compressed to form green bodies prior to the sintering step. After sintering, the shapes of the pores change with increasing temperature soaks. Additionally, with increasing temperature, the number of pores decreases as their individual volumes increase.[29−31] Activated processes such as microwave sintering and microwave heating can be applied for processing of bioceramic powders. Sintering using the microwave radiation

DOI: 10.1021/acsbiomaterials.7b00615
ACS Biomater. Sci. Eng. XXXX, XXX, XXX−XXX

Table 4. Pore Sizes and Porosities of Metal Scaffolds for Bone Tissue Engineering[a]

material	fabrication method	pore size (μm)	porosity (%)	ref
open porous Ti_6Al_4V	selective laser melting	700 × 700 orientated perpendicular		296
Ti	indirect rapid prototyping/sintering	300−1000	∼67	239
Ti_6Al_4V	selective laser melting	500, 1000		202
Ti filled with chitosan/HA sponge	EBM/freeze-casting	50−250	60−75	206
Ti	liquid foaming agent	10100−400	∼76	297
Ti	fugitive filler	50−500	10−60	298
Ti	Mg as filler	0−500	50, 60, and 70	48
Ti	microwave assisted	10−100		299
Ti	plasma spray	300−500	40−60	167
Ti	freezing TiH_2-camphene slurries	up to 100	49−63	77
NiTi	pore-forming agent/capsule-free HIP	300	∼50	183
NiTi	polymeric sponge	250−500	65−72	106
NiTi	MIM/salt leaching	100−500	50−70	178
Ti	inkjet 3D printing	1200−1400, 20−30	13−16 ($p_{microporosity}$), $p_{macroporosity}$ < 70	211
Ti_6Al_4V	3D-fiber depositing	400	74	300
Ti_6Al_4V	direct laser forming (DLF)	500, 700, and 1000		204

[a]Pores are shown either by the range or by the average size.

saves time, energy, and the concomitant processing cost. This technique usually results in nanoscale or fine grain structures. Magnesium phosphate and calcium phosphate are examples of bioceramics processed with microwave radiation.[32,33] Nanocrystalline structure of HA/β-TCP with porosity of 65% was fabricated via sintering for about 5 min through adjusting the parameter such as temperature, heating rate, and holding time.[33]

2.1.2. Microsphere Sintering for Polymer. Polymer microspheres prepared via the emulsion/solvent evaporation technique can be sintered to yield 3D porous scaffolds. Poly(lactic-*co*-glycolic acid) (PLGA) scaffolds were formed via sintering of microspheres.[34] There is a positive correlation between sphere diameter and pore diameter[35] (Figure 4i). By modifying processing parameters including sphere diameter and temperature, a biomimetic pore system equivalent to the structure of trabecular bone was fabricated (Figure 4i-a−d). The soaking times at high temperature did not correlate with the pore structure.[35] Sintering of composite chitosan/poly(lactic acid-*co*-glycolic acid) (PLGA) microspheres can successfully fabricate 3-D chitosan/PLGA porous scaffolds for bone tissue engineering applications.[36] The study showed that fabrication parameters, such as sintering temperatures and times, dictate pore sizes, pore volume, and mechanical properties of as-fabricated scaffolds. The resulting sintered microsphere scaffolds showed total pore volume between 28% and 37% with median pore size in the range 170−200 μm.[36] Supercritical CO_2 can be also useful in creating 3-D macroporous scaffolds for bone and cartilage tissue engineering.[37] In processing porous PLGA, parameters such as pressures of supercritical gaseous CO_2 and the ratios of lactic acid to glycolic acid were proven to be important parameters in yielding different pore geometry.[38]

2.1.3. Powder Metallurgy. In orthopedics, porous metallic implants have many applications including spinal fixation to acetabular hip prostheses, dental implants, permanent osteosynthesis plates, intervertebral discs etc.[39] Porous metallic implants range from titanium and its alloy (Ti_6Al_4V), Co−Cr, 316L stainless steel, Co−29Cr−6Mo, NiTi, etc. They are useful in preventing the phenomenon of stress shielding in vivo. Partial sintering of powders[40] or wires has been reported.[41] The final scaffold structure can be weak because of the presence of thin contacts between individual powder particles. Important parameters for subsequent processing include powder size, shape, and surface conditions. Sintering of powders and wires can also be used to create porous coatings on the surfaces of dense substrates.[42] In sintering of metallic scaffolds, both total and open porosity decrease gradually with increasing sintering temperatures. In one study, Ti powders with three different particle sizes were stacked and compacted sequentially, starting with a size of 65 μm then 189 μm followed by 374 μm in the mold. To attain uniform densification of the powders, the stacked powders needed precompaction. Pore content and size of vacuum sintered Ti scaffolds decrease with reduction of the initial powder size and by applying pressure.[40] In the wire densification approach, a uniform open structure can be attained by coiling the wire into an elongated helix and compacting it in a die set of relevant shape. The resulting sintered solid sample can be subsequently drilled, ground, and resintered to obtain the final shape.[41] Microwave sintering has been used in densifying metals, even though it is contrary to common life experiences unlike ceramics. As long as metals are in powder form, they absorb microwaves. Microwave absorbers can also be employed. Ti_6Al_4V powders can be mixed with multiwalled carbon nanotubes (MWCNTs) and the particle size of Ti_6Al_4V is ∼5 μm. In this case, the MWCNTs acted in a bifunctional way: as microwave susceptors as well as to provide paths for rapid sintering of Ti alloys. The green compacts can be sintered in the microwave within 2 min without using any protective gas environment. The composite showed a porosity of approximately 25% and pore size in the range of 5−80 μm.[43]

2.2. Porosity Using Transient Porogen. Sintering of powders around a transient porogen can be beneficial in creating porous structures.[44,45] The porogens can be incorporated in three different ways by (1) mixing into the melt, (2) introducing into a casting mold, or (3) adding into a die set. As shown in Figure 3b, mixing appropriate amounts of transient porogen with powders followed by evaporation, burn out, or dissolution of the porogen also helps. Varying the shape, size, and volume fraction of the porogens affects the porosity, pore shape, and macropore-size. Micropores may form due to the incomplete sintering of powders.

2.2.1. Use of Porogens for Metals. Open cellular titanium pores ranging from 200 to 500 μm can be manufactured by

DOI: 10.1021/acsbiomaterials.7b00615
ACS Biomater. Sci. Eng. XXXX, XXX, XXX−XXX

Table 5. Advantages and Challenges of Different Fabrication Techniques

fabrication route	advantage	challenge	reference
partial sintering	graded porosity	low interconnectivity, isotropic structure	32−43
porosity using transient porogen	controlled porosity, graded porosity, can create complex shapes	some techniques use of organic solvent, low interconnectivity, isotropic structure	29,44−55,61,62,65−67
porosity using a liquid pore forming agent	can create directional pores, anisotropic porous structure, high porosity, good interconnectivity	use of organic solvent, associated with small pore sizes, sometimes shows poor homogeneity of the pore structure	70−76,79,80,82,83
gas foaming	high porosity when combined with salt leaching improve interconnectivity	low mechanical strength, normally leads to smaller pore size	42,86−88,96,99,101
replication technique	can create open and interconnected cell, can create anisotropic pore structure with elongated pores	slurry rheology and homogeneity	24,87,102,103,107
gel-casting	near-net shape, high homogeneity, good interconnectivity when combined with foaming	slurry rheology and homogeneity	91,92,108−110,113,114
sol−gel	highly mesoporous structure	large content of nanoporosity	118,119,121,122
phase separation	highly porous structure, tubular pore morphology, extensive pore interconnectivity	no control over the scaffold morphology	124−128
melt blending of two immiscible polymers	fully interconnected porous structure, interconnectivity through cylindrical pores rather than smaller pores, narrow pore size distribution	needs highly controlled annealing step	65,131,132
electrospining	when combined with RP can create complex structure, larger pores size, oriented fibers	smaller pore size in conventional techniques, low cell infiltration, nonuniform distribution of fibers	134,135,156−158,164
electrical field activated sintering	shorter sintering time compared to conventional sintering	some techniques contain large holes at the cross-section of solids	172−176
MIM	near-net-shape parts	when combined with particle leaching	177−179
HIP	nearly spherical pore shapes when combined with space holders plus gas expansion can create different porosities, pore morphologies and increased pore size	little porosity compared to capsule free HIP, small pore size, can create higher porosity and larger pore size	180−185
laser based RP	can be fabricated into complex shape, porous structure can be tuned to match the host tissue, some techniques do not need the use of toxic organic solvents for binding	some methods require minimal surface finishing after manufacturing	191−193,196,197,204
printer based RP	porous structure can be tuned to match the host tissue, can be fabricated into complex shape, fine details in microscale features using finer particles	some methods use organic solvent, controlled porosity content due to unbounded powders, potential creation of random microporosity	207−209,211
nozzle based RP	porous structure can be tuned to match the host tissue, can be fabricated into complex shape, fine nozzles can be used in complex designs, functional graded scaffolds can be fabricated using a wide range of materials and pore morphologies, high reproducibility at a low-cost, protein and cell encapsulation possible in some cases	some methods use organic solvent	133,213,216,218,220,234
indirect RP	fully interconnected porous reproducible porosity and pore size	slurry rheology and homogeneity	66,235,237,238

DOI: 10.1021/acsbiomaterials.7b00615
ACS Biomater. Sci. Eng. XXXX, XXX, XXX−XXX

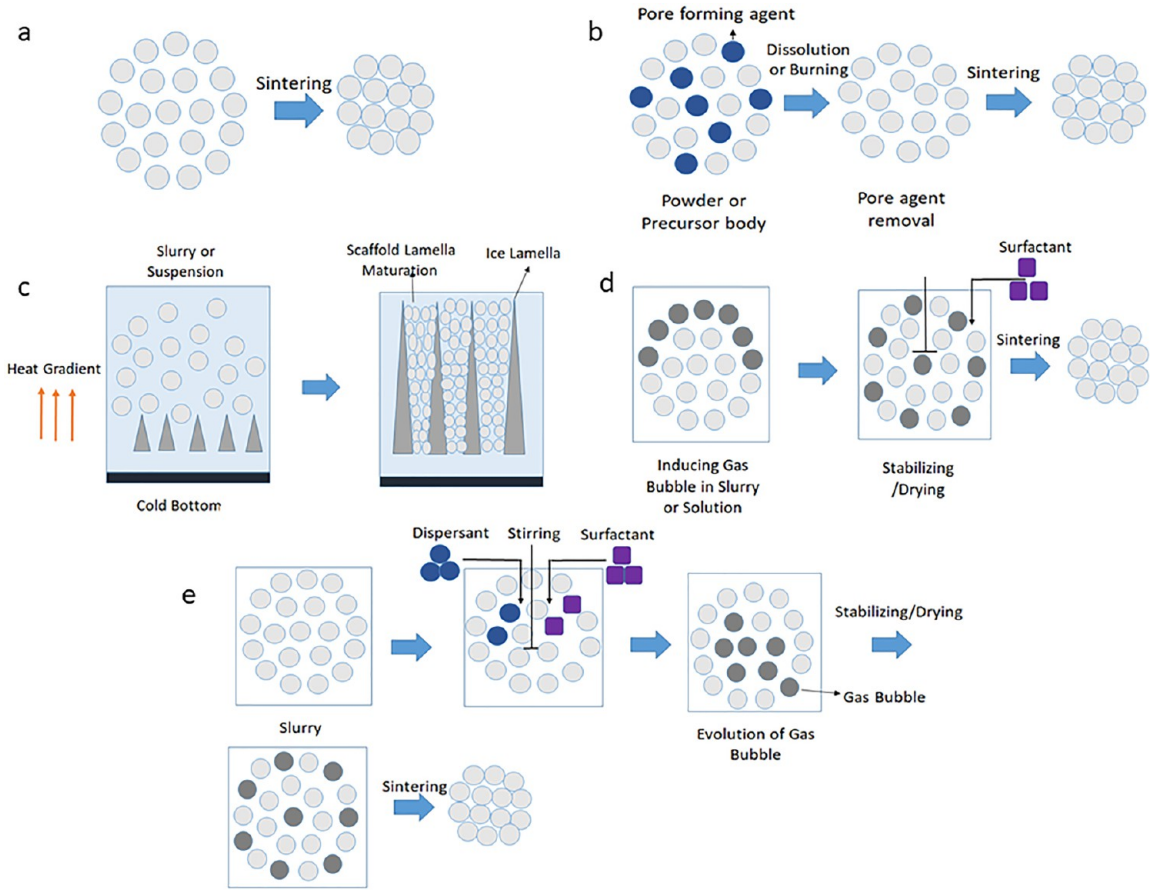

Figure 3. Random porosity generation by (a) partial sintering of polymers, metals, and ceramics, (b) fugitive porogen for use with polymers, metals, and ceramics, (c) liquid pore forming agent freeze-casting for polymers, metals, and ceramics, (d) direct gas-foaming/physical blowing for polymers, metals, and ceramics, and (e) gas-foaming/chemical blowing for polymers, metals, and ceramics.

adding a porogen (e.g., ammonium hydrogen carbonate) into the starting powder. The ingredients are mixed homogeneously and pressed into green compacts. Afterward, the green compacts are first heated at 200 °C to burn out the porogen, and then sintered at 1200 °C.[46] The pore sizes in porous NiTi alloys positively correlate with the size distribution of ammonium hydrogen carbonate particles. Use of porogen from polymer spheres made of paraformaldehyde (also known as polyoxymethylene) with mean diameter of 500 μm was also used.[47] Ti/Mg compacts were fabricated by warm compaction using magnesium granules as a spacer. Porous Ti scaffolds of complex geometries were fabricated by the removal of Mg granules by self-corrosion. The pores with a range of sizes of 132−262 μm were homogeneously distributed and interconnected. The results showed that due to the anisotropy and alignment of pores, the compressive strength varied with the direction of compression. A conventional machining process was also applied to control net-shape of the Ti/Mg scaffold.[48]

2.2.2. Ceramic. Powders synthesized by hydrothermal[29] or precipitation[49] methods are isostatically pressed and compacted before sintering. Subsequently, sintering is performed at high temperatures in the range between 900 and 1500 °C. The shape of pores changed with thermal treatments of specimens. Mechanical properties are a function of the amount and morphology of pores.[29] Ceramic scaffolds fabricated via pressing and firing usually have a disordered pore structure.[29] A transient porogen such as naphthalene was added into ceramic powder with varying volume fraction and pressed at 300 MPa to form a homogeneous mixture. Afterward, naphthalene was removed by heating at 300 °C, and the resultant porous structure was sintered at 1300 °C.[50]

2.2.3. Cements and Slurries. Casting is also employed in fabrication of porous structure using transient porogens. As-cast cements and slurries can be sintered to remove the porogen. Cement compositions are obtained by mixing calcium phosphate or magnesium phosphate powder with a liquid phase, which leads to a self-setting paste.[51,52] Afterward, the cast paste can be molded, dried, and sintered to improve mechanical properties. Slurries can also be prepared by dispersing ceramic powders in a liquid phase prior to sintering.[53] Poly(methyl methacrylate) (PMMA) microspheres are used as fugitive porogens to create micropores in HA scaffolds by burning at 900 °C and sintering at 1300 °C.[53] PLGA as a porogen was also used to fabricate porous bone cement compositions.[54] Various amounts of polymeric porogens of various molecular weights and sizes were incorporated into calcium phosphate-based self-setting cement formulations. The content and the size-range of porogens had significant effect on the characteristics of cements, while the molecular weight did not show any significant effect.[54,55]

2.3. Dissolution. In the dissolution approach or porogen leaching technique for ceramic, metal, and polymer, the porogens are removed simply by immersing the structure in an appropriate solvent at room temperature. The common porogens should be more soluble than the matrix. Examples of such porogens include granules of sugars, such as sucrose or

DOI: 10.1021/acsbiomaterials.7b00615
ACS Biomater. Sci. Eng. XXXX, XXX, XXX−XXX

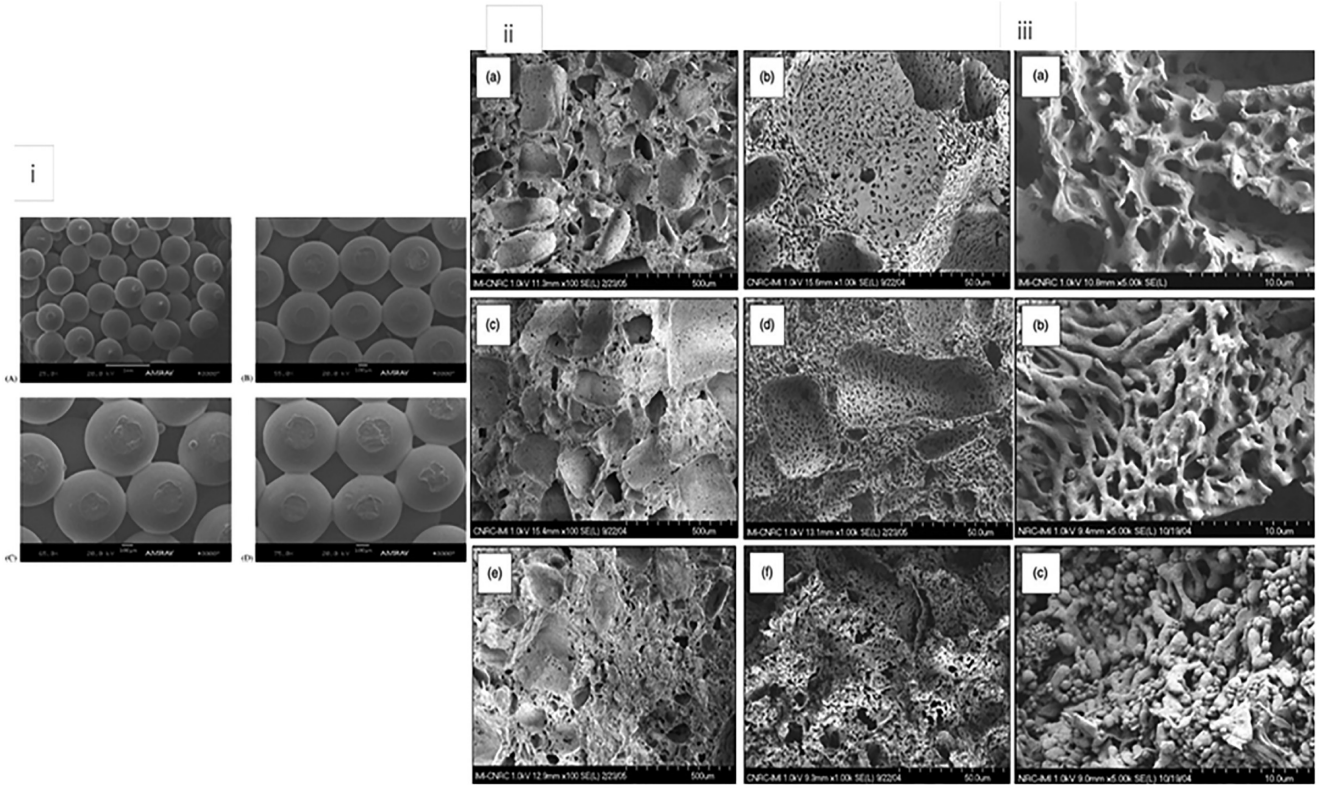

Figure 4. (i) Sintered PLGA microsphere based scaffolds: (A) a low magnification image showing the 600−710 μm sintered matrix with an interconnected structural framework (magnification = 25×); (B−D) different packing patterns commonly seen in the structure of the sintered matrix at higher magnification. Note the extensive connectivity and microsphere bonding (magnification = 55−75×).[35] Reproduced with permission from ref 35. Copyright 2003 Elsevier. (ii) Interconnected poly(ε-caprolactone) porous scaffold fabricated via combination of polymer and salt particulate leaching: SEM of PCL porous scaffolds generated after selective extraction of (a, b) 50% NaCl, (c, d) 60% NaCl, or (e, f) 70% NaCl and dissolution of PEO. In all blends, the PCL/PEO composition ratio is kept constant at 50/50.[65] Reproduced with permission from ref 65. Copyright 2006 Elsevier. (iii) SEM of PCL porous scaffolds after selective extraction of PEO and NaCl. The PCL/PEO composition ratio is changed while keeping the NaCl concentration at 50 vol %: (a) PCL/PEO = 50/50; (b) PCL/PEO = 40/60; (c) PCL/PEO = 30/70.[65] Reproduced with permission from 65. Copyright 2006 Elsevier.

mannitol, and NaCl. The porous structure of scaffolds with respect to the pore size, porosity, and pore shape depends on the size, shape, and amount of porogen used.[56] However, pores are not always interconnected, and precisely controlling the interconnectivity is difficult. Sometimes this technique combined with other techniques such as gas foaming can result in micro- and macroporosity.

2.3.1. Ceramic/Composite. Sugar granules have been used in a slurry of calcium phosphate particles and PLGA. Porous composite scaffolds were fabricated by dissolving sugar granules in deionized H_2O. The final scaffold had nominal macropore size in the range of 800−1800 μm with a porosity of 81−91%.[57]

2.3.2. Dissolution in Cement. A porous calcium phosphate cement composition (CPC) was developed through porogen leaching and gas foaming. Sucrose granules were sieved to obtain particle sizes in the range of 125 to 250 μm. Mixtures of CPC powders can set and harden with porogen containing setting liquid. The porosity content reached 50%. Sucrose was able to produce some macropores because it did not dissolve completely before the cement had hardened.[58]

2.3.3. Metal. Porous titanium scaffolds were fabricated by sintering Ti particles with added sodium chloride (NaCl) granules as the porogen. Fast dissolution of NaCl in water reduces etching of metals. Optimum sodium chloride content, finding optimal conditions to remove salt such as water temperature, maximum immersion time per cycle, and agitation are the factors that need to be adjusted to produce desirable porous structure.[59]

2.3.4. Polymer. The dissolution approach for polymers include solvent casting and particulate leaching, compression molding and salt leaching, polymer coagulation, compression molding, and particulate leaching, and melt-processing and particulate leaching.

2.3.4.1. Solvent Casting and Particulate Leaching. This is carried out by the casting of a polymer solution with dispersed porogens. Then, an appropriate solvent removes the porogen. Procedure of fabricating a porous polycaprolactone (PCL) scaffold by solvent casting and particulate leaching is described in ref 60.

2.3.4.2. Polymer Coagulation, Compression Molding, and Particulate Leaching. Leachable particles are homogeneously incorporated in a polymer matrix during the precipitation of a high molecular weight polymer solution into a nonsolvent. After filtration and drying, the polymer-salt composites can be compacted by hot pressing. The compression molded polymer−salt composite discs are gradually exposed to stirred demineralized water to leach out the salt. This technique can provide excellent control over pore size and porosity and yields scaffolds with a much more homogeneous pore morphology as compared to common methods such as sintering, compression molding and salt leaching, and freeze-drying. Poly(D,L-lactic acid) (PDLA) and a segmented poly(ether ester) based on

DOI: 10.1021/acsbiomaterials.7b00615
ACS Biomater. Sci. Eng. XXXX, XXX, XXX−XXX

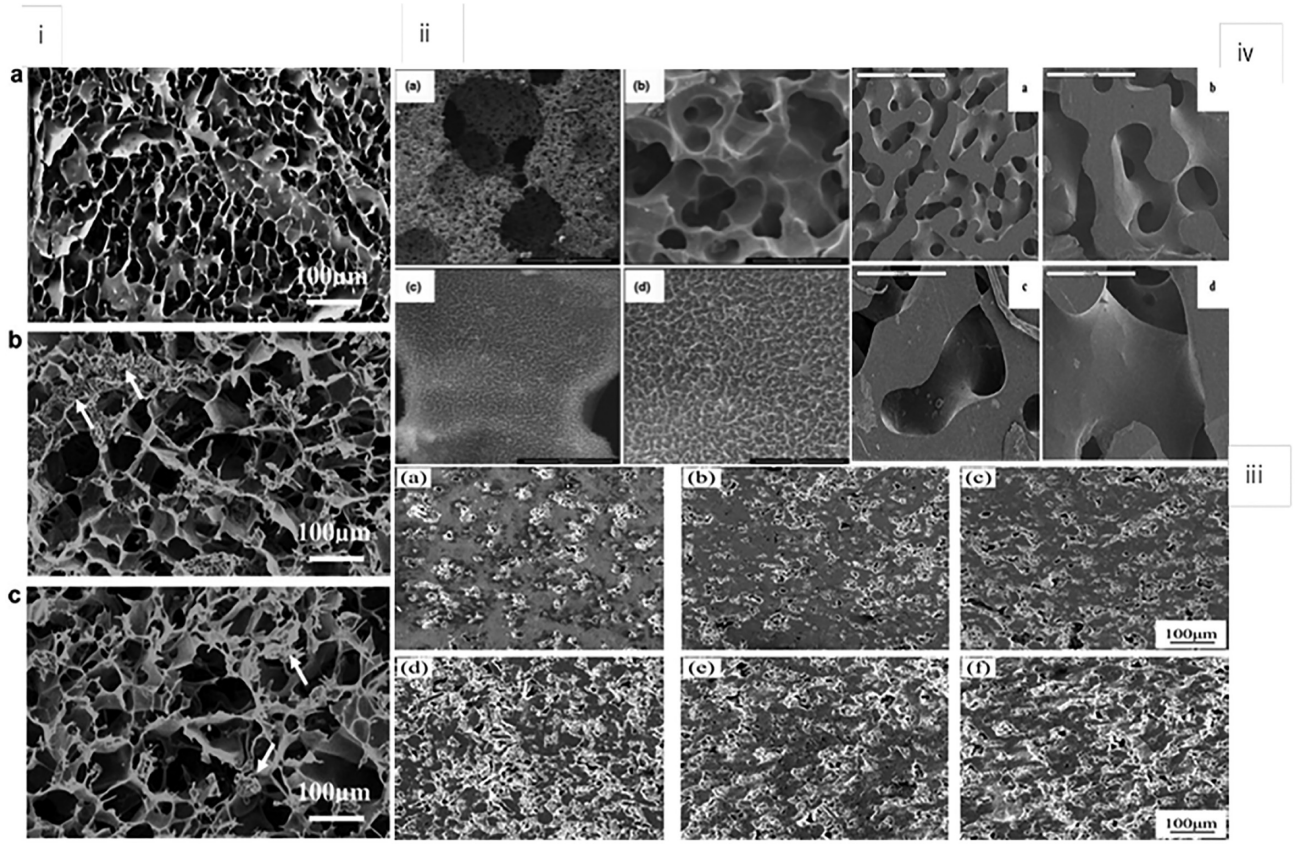

Figure 5. (i) Surface morphology of (a) porous silk, (b) MBG/silk, and (c) BG/silk scaffolds. The arrows indicate MBG or BG particles in silk scaffolds fabricated via freeze-drying method. MBG was incorporated into silk scaffolds in order to improve the osteoconductivity.[71] Reproduced with permission from ref 71. Copyright 2011 Elsevier. (ii) Three kinds of hierarchical pores in the Ti scaffold fabricated via liquid pore forming agent after sintering plus chemical treatment: (a) macropores, (b) micropores, (c) nanopores, and (d) higher amplification pictures of image c.[96] Reproduced with permission from ref 96. Copyright 2011 Springer. (iii) Gel casting for prepared near-shaped porous Ti−Mo and Ti−Nb alloy implants showing pore morphology and distribution in porous titanium alloys processed at 32% solid loading: (a) Ti-7.5Mo, (b) Ti-12.5Mo, (c) Ti-17.5Mo, (d) Ti-10Nb, (e) Ti-25Nb, and (f) Ti-35Nb alloys. Three-dimensional pore morphologies and total porosity range from 39% to 50% were achieved with gel casting.[114] Reproduced with permission from ref 114. Copyright 2012 Elsevier. (iv) SEM of 45PCL/55PEO vol % scaffolds of highly controlled porosity and interconnectivity derived from cocontinuous polymer blends annealed at 160 °C for (a) represent 30 min, (b) 1 h, (c) 2 h, and (d) 3 h. Scale bar = 200 μm.[132] Reproduced with permission from ref 132. Copyright 2014 Springer.

poly(ethylene oxide) (PEO) and poly(butylene terephthalate) (PBET) are the examples processed using this technique. Porosity could be adjusted by polymer-to-salt ratio to yield 70%−95% porosity content.[61] Interconnected and homogeneous porous PCL structure can also be fabricated with this technique where pore size and porosity could be precisely adjusted by salt particle size range and content.[62]

2.3.4.3. Melt Processing and Particulate Leaching. The presence of residual organic solvent in solvent casting and particulate leaching can be problematic. The melt molding and particulate leaching technique was proposed to address this shortcoming. This technique involves hot-pressing and compression molding of a homogeneously mixed polymer powder and porogen at temperatures slightly above the polymer melting point. Subsequently, samples are exposed to the same solid porogen leaching step as for the solvent-cast samples.[63] Porous PLGA/PVA scaffolds are fabricated by melt molding and particulate leaching. The scaffolds exhibit highly porous (about 90% porosity) and open-cellular pore structures with almost the same content of surface and interior porosities.[64]

In order to improve interconnectivity of pores in polymeric scaffolds, it may be possible to partially bond the porogen particles by locally melting the contact points. This may be achieved by working in humid conditions for NaCl porogen. Alternatively, a heat treatment in the case of paraffin spheres or sugar particles is useful. The standard leaching techniques as practiced in other fabrication techniques, such as phase separation, emulsion freeze-drying, gas foaming, or rapid prototyping, were also developed. The above techniques can be combined as well to enhance the connectivity of pores. This further enhances the ability to produce porous structures with different pore sizes or pore morphologies.[65−67] For example, a two-step process was developed for the fabrication of porous PCL scaffolds by combining selective polymer leaching and salt particulate leaching. In the first step, a twin screw extruder was used to produce a homogeneous blend of two biodegradable polymers, poly(3-caprolactone) (PCL) and poly(ethylene oxide) (PEO), with sodium chloride acting as the porogen. In the second step, a highly porous PCL scaffold with fully interconnected pores was fabricated by dissolving the PEO and mineral salts in water. The scaffold is shown in Figure 4ii,iii, which shows that the pore characteristics do not change significantly with the NaCl content varying from 50% to 70%. The as-fabricated samples showed multimodal distribution of pore sizes with their distinct locations (Figure 4ii). Figures 4iii-

DOI: 10.1021/acsbiomaterials.7b00615
ACS Biomater. Sci. Eng. XXXX, XXX, XXX−XXX

a−c depicts the effect of PEO content on the pore structure. For example, as shown in Figure 4iii-a, a structure with a PEO content of 50% PEO reveals a cocontinuous structure of PCL. A further increase in the PEO content to higher levels drastically alters the morphology of porous scaffolds (Figures 4iii-b,c). The nominal porosities of these scaffolds are 75%, 80%, and 85%, respectively.[61]

2.4. Porosity Using a Liquid Pore Forming Agent. In this section, the porogen can be soluble or insoluble liquid. In addition, emulsion, freeze-drying/freeze casting, and reverse freeze-drying are discussed using soluble/insoluble liquids as the porogen.

2.4.1. Insoluble Liquid Pore Forming Agent in Cement. An important example is commercially available bone cement (chronOS, Synthes Biomaterials) compounds,[68] mixed with oil and an emulsifier. An emulsion can either be cement droplets dispersed in oil (w/o) or oil dropped in the cement paste (o/w). After the cement sets, the oil is washed off to create a porous block. Varying emulsifier concentration results in different pore sizes while maintaining the volume fraction. A higher emulsifier concentration or lower oil content yields smaller pore size. A porous β-tricalcium phosphate (β-TCP) block can be manufactured by this emulsion technique that possesses a porosity content of 75%, with a different mean macropore sizes such as 150, 260, 510, and 1220 μm.[69]

2.4.2. Ice as a Porogen in Cement. A frozen sodium phosphate is allowed to melt during setting of the cement.[70] Different cement/ice (C/I) weight ratios of 0, 5, 4, and 3 were mixed with Na_2HPO_4 solution ice flakes. Exposure to a small quantity of liquid nitrogen prevents thawing. The resulting slurry can be poured into a mold and uniaxially compressed. Then, the mixture is allowed to set for 20 min through the melting of sodium phosphate ice prior to removing from the mold. The porogen can be made in a wide variety of shapes and sizes, without a need for a porogen removal stage. The macroporous cement manufactured with the ice is denser than that which can be obtained from slurry systems. This technique was able to produce up to 60% porosity containing macropore size >50 μm, and microporosity below 100 nm or between 100 nm and 50 μm.[70]

2.4.3. Freeze-Casting or Freeze-Drying. This technique is applied to polymers, metals, and ceramics. Freeze casting entails the freezing of a liquid slurry composed of the residual powder, solvent, and organic additives. In this technique, liquid solvent slowly solidifies in a dendritic manner at a specific temperature below its solidification point to induce solid−liquid phase separation (Figure 3c). Ice temporarily acts as a binder and the geometry of the frozen solvent crystals is replicated in the structures of pores. Thus, controlling the growth of ice crystals during freezing has to be carefully performed. This is followed by freeze-drying. The pore structures are significantly affected by a number of factors such as filler powder, organic additives, solvent, and freezing rate. Faster freezing results in smaller pores. Organic additives have important effects on the freezing behavior and crystal morphology. The solvent has a significant role to play in forming pores due to the freezing behavior of the solvent. Solvents like water and substances such as camphene, *tert*-butyl alcohol, and mixed solvents were used. An interesting signature of this method is to induce directional formation of pores, which can improve mechanical properties. To create aligned pores, an anisotropic thermal gradient is usually applied through the container to produce materials with unidirectional interconnected pores[71,72] (Figure 3c; Figure 5i-a−c). Additionally, lower solid loading provides some degree of increase of the macropore dimension albeit with some concomitant loss in mechanical strength.[73−75] As indicated in Figure 5i-a−c, the silk and composite scaffolds are highly porous. The pure silk scaffolds had a flat pore morphology (Figure 2a), whereas the mesoporous bioactive glass (MBG) or nonmesoporous bioactive glass (BG) composite scaffolds had a more open pore morphology (Figure 2b,c) compared to the silk scaffolds. MBG or BG particles were clearly visible in the pore walls of composite scaffolds.

2.4.3.1. Metal. Highly porous titanium (Ti) scaffolds were fabricated by freezing a titanium hydride (TiH_2)/camphene slurry. As the freezing time was prolonged from 1 to 7 days, the pore size increased significantly due to the continual overgrowth or fast diffusion of camphene dendrites.[76,77] The final scaffold showed large pores up to 100 μm surrounded by Ti metal strut. An increase in the initial TiH_2 content reduced the porosity from 63% to 49%.[77] Directional freeze-casting is yet another variation. In this process, an aqueous slurry containing titanium powders of size less than 45 μm was directionally solidified where pure ice was separated by interdendritic regions of high powder content. After drying, powders can be densified by sintering. Final porosity was 57−67%, and the structure showed aligned pores (~0.1 mm wide and several millimeters long). The use of coarser <125 μm powders exhibited lower porosities (39%), and the pores were not elongated.[78]

2.4.3.2. Polymer. Polymers are dissolved in the specific solvents and poured into a mold prior to freezing. After the freezing step is completed and phase separation has occurred, the solvent crystals are removed by freeze-drying. While highly porous structures can be obtained via this technique, small pore sizes and poor homogeneity of the pore structure can occur.[61] Chitosan and hyaluronic acid were mixed to form a polyelectrolytic solution, and then lyophilizing the solution yielded the 87% porosity with 77 μm pore size.[79] Collagen−glycosaminoglycan (CG) scaffolds were initially cooled to a temperature of −20 °C.[80] The temperature was then raised to −10 °C and held there for two specific annealing times to produce scaffolds with different mean pore sizes.[80] Emulsification with freeze-drying is also used for fabricating polymer scaffolds. This technique is based on the phase separation concept. To synthesize an emulsion, PLGA was dissolved in methylene chloride, followed by the addition of distilled water. The mixture was frozen in a mold by exposure to liquid nitrogen. The products were freeze-dried at −55 °C, leading to the removal of the dispersed water and polymer solvents. Scaffolds with large porosity content (up to 95%) but small pore sizes (13−35 μm) have been fabricated using this technique. Varying processing parameters such as water volume fraction, polymer weight percentage, and polymer molecular weight can yield different porosity as these values influence the emulsion's stability prior to quenching.[81]

2.4.3.3. Ceramic. This technique is also successfully applied to fabricate porous hydroxyapatite (HA) scaffold. The resultant structure showed well-defined pore connectivity along with directional and completely open porosity such as a lamellar morphology after sintering. Various parameters affected the porosity and compressive strength, including initial slurry concentration, freezing rates, and sintering conditions. The size of the porosity can be controlled by modifying the freezing rates of the slurries and the slurry concentration. Due to the

DOI: 10.1021/acsbiomaterials.7b00615
ACS Biomater. Sci. Eng. XXXX, XXX, XXX−XXX

lamellar pore structure, the scaffolds showed a compressive strength of 45 MPa with 47% porosity content and 65 MPa for 56% porosity content after sintering.[82] The change in porosity content of freeze-dried HA scaffolds was also studied by changing process parameters such as particle concentration, nature of the solvent, and temperature gradient.[83] The study showed that the thickness of the HA lamella decreased and the width of the pores increased with decreasing particle concentration. Also, lowering the substrate temperature from −20 °C to −196 °C created a finer lamellar microstructure. Finally, the use of water−glycerol mixtures as the solvent compared with water−dioxane mixtures resulted in the production of finer pores (1−10 μm) and a larger number of dendritic growths connecting the HA lamellae. However, the use of water−dioxane produced a cellular-type microstructure with larger pores (90−110 μm). In another study, the final porosity sizing and interconnectivity or lamellar structure of freeze-dried HA scaffold could be used to infiltrate with gelatin solution. Biohybrid HA/gel composite scaffolds (45−55 vol % of porosity) cross-linked with genipin, showed 5−6 times improved compressive mechanical strength.[84]

2.4.3.4. Reverse Freeze Casting. This technique was applied to fabricate porous Ti scaffolds with strongly aligned large pores as compared to freeze-casting. The idea of this method is based on the migration of raw powder, rather than the growth of camphene (solvent) dendrites. Highly porous titanium scaffolds with the average pore size of 400 μm (pores up to 500 μm in size possible), aligned structure, and high open porosity were fabricated with this technique. Camphene−Ti slurries were poured onto the prefrozen camphene. Ti powders migrated spontaneously along the prealigned camphene boundaries or channel and formed a titanium−camphene mixture with an aligned structure. Thereafter, the green bodies were freeze-dried to remove the frozen camphene and sintered at 1300 °C in a vacuum furnace. As the casting time increased from 24 to 48 h, the initial columnar structures turned into lamellar structures, with the porosity content decreasing from 69% to 51%.[85]

2.5. Porosity Formation Using Gas Bubbles.

2.5.1. Foaming. The foaming process takes advantage of a dissolved gas at elevated pressure (physical blowing agent or direct foaming) (Figure 3d)[86] or incorporation of a chemical that yields gaseous decomposition products (chemical blowing agent) (Figure 3e).[87] Foaming leads to the production of scaffolds with a compact skin and a porous core with high porosity content. However, the mechanical strength may be quite low.[87] Variation of the porosity content, the pore size (bubble size), and the shape is possible by changing different processing parameters such as the liquid-to-powder ratio, the concentration, the composition of the foaming agent in solution, the particle sizes of the starting powders, and finally the stirring conditions.[88]

2.5.1.1. Ceramics and Cement. The bubble generation technique is based on mixing the desired constituents and allowing the evolution of gas bubbles as shown in Figure 3e.[89] Porous ceramics with unidirectional channels have also been developed by using continuous bubble formation of ethanol in ceramic slurries.[90] Surfactant agents in mixtures stabilize the bubbles by reducing the interfacial energy of the gas−liquid boundaries.[91] Gel casting and foaming techniques were applied to create highly porous HA up to 90% porosity. Initially, a homogeneous suspension of ceramic powder, water, and monomer solution (i.e., acrylate monomers and methylene bis(acrylamide) monomers) is foamed by the addition of surfactants. The foaming of suspensions occurs prior to the *in situ* polymerization of organic monomers. Promoters of polymerization may be added before molding. Finally, the organic additives are eliminated at temperatures above 300 °C, and sintering is carried out for consolidation of the ceramic scaffolds. Porous HA showed spherical interconnected cells with sizes ranging from 20 to 1000 μm.[92] Another approach to generating bubbles is to take advantage of a gas evolving chemical reaction. Calcium phosphate powders were mixed with a diluted H_2O_2 solution that can foam. After foaming and drying at 60 °C, the cylinders were sintered at 1150 °C. This resulted in the distribution of pore sizes in the range of 1−10 μm.[93] Porous cement scaffolds can be obtained by adding $NaHCO_3$ to the starting cement powder of calcium phosphate using two different liquids: first, a basic liquid to form the paste and later an acid liquid to obtain CO_2 bubbles. The macropores with an average size of 100 μm were produced.[94] Recently, magnesium granules have been applied to fabricate porous bone cement scaffolds that yield a high porosity content of 90% and macropore size of 800 μm.[95]

2.5.1.2. Metal. Fabrication of porous metallic scaffolds can use argon or hydrogen gas as foaming agents. Micrometer-sized bubbles of pressurized inert argon gas can be entrapped within a matrix of Ti during the consolidation of titanium powders by hot isostatic pressing (HIP). By exposure of the compacts to elevated temperatures and ambient pressures, bubbles expand within titanium matrices. This results in porous foams with approximately 50% porosity with high strength. This high strength is attributed to the density of struts.[42] Alternatively, both liquid and solid foaming agents can be used. In the liquid approach, a slurry can be formed by mixing Ti powders, binders, dispersants, and hydrogen peroxide (H_2O_2) as the foaming agent (Figure 3e). The as-prepared slurry is poured into molds and dried. Subsequently, the dried material is sintered in a vacuum sintering furnace. Finally, Ti scaffolds are chemically treated with acid−alkali solution. The final scaffold showed pore sizes ranging from nanometer to micrometer scale and macropores with pore size larger than 100 μm and a total porosity content of 76% (Figure 5ii-a−d).[96]

2.5.1.3. Solid Foaming Agent Approach. This approach uses a polymeric binder and a foaming agent mixed with Ti powders to fabricate open celled structures. The process also uses a three-step thermal treatment. In the first step, two processes take place simultaneously: (1) creation of a suspension of Ti particles in a molten pool of the binder and (2) decomposition of the foaming agent by releasing gas. The second step is a careful binder removal process. These are followed by a final sintering step to impart strength to the porous structure. The process allows for the control of microstructural properties such as the size of pore openings, surface properties, and properties of the metal.[97,98] Irregularly shaped titanium powder was dry-mixed with low-density polyethylene as a polymeric binder, a foaming agent (*p*,*p*′-oxybis[benzenesulfonyl hydrazide]), and a cross-linking agent (dicumyl peroxide). The homogeneous mixtures can then be molded and heated through thermal treatments as described above. The final pore size of titanium foams can be controlled by optimizing the composition of the blend. The final scaffold had pore sizes ranging from 336 to 557 μm.[98]

2.5.1.4. Polymer. The porous structure achieved with this technique is not as fully interconnected as in the case of phase separation. A porous corn starch and ethylene vinyl alcohol

DOI: 10.1021/acsbiomaterials.7b00615
ACS Biomater. Sci. Eng. XXXX, XXX, XXX−XXX

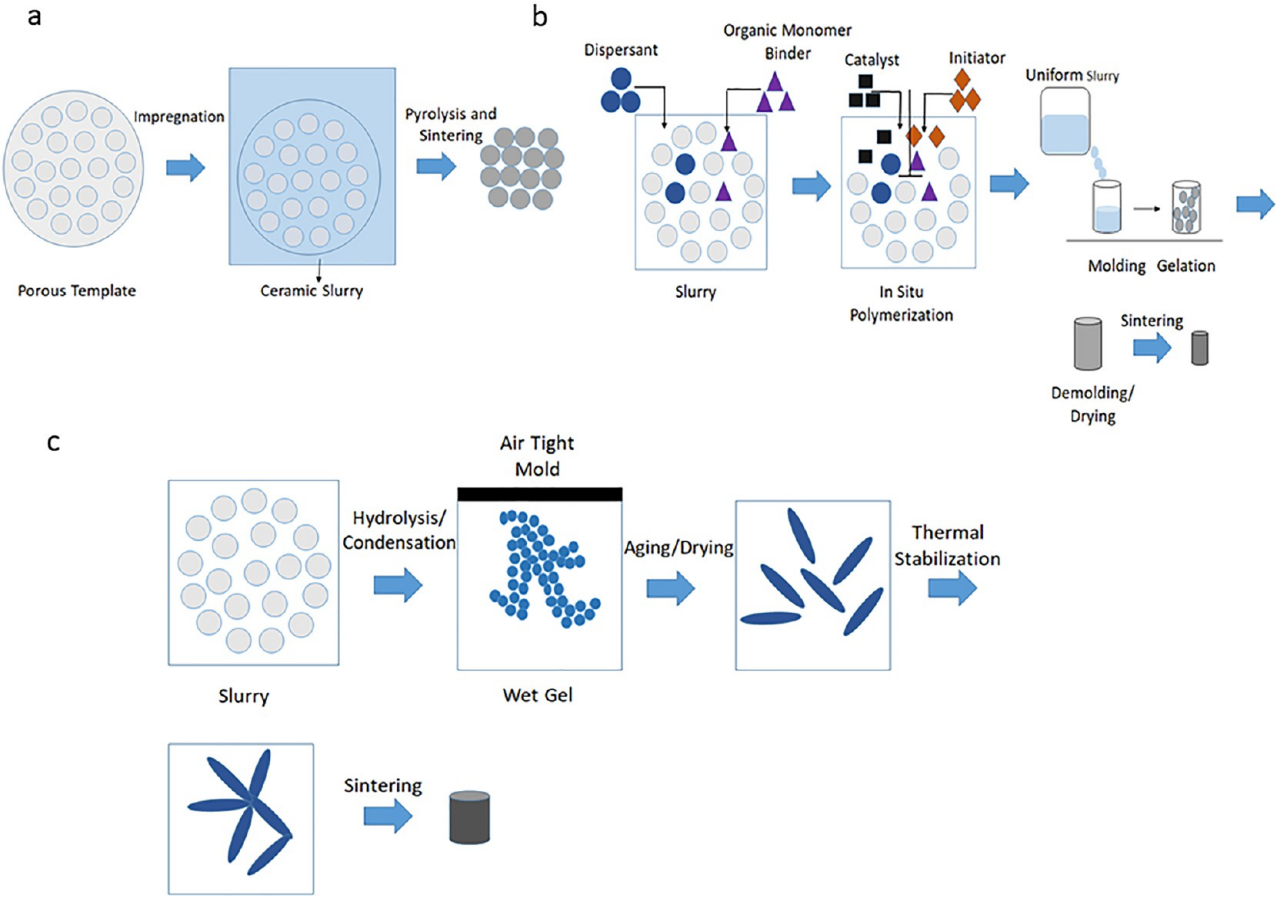

Figure 6. Random porosity generation by (a) polymeric sponge replication for metals and ceramics, (b) gel-casting for polymers, metals, and ceramics, and (c) sol–gel process for glasses and glass-ceramics.

scaffold was prepared using blowing agents based on carboxylic acids, which are made to react by heating, and followed by the release of CO_2 and water molecules.[99] In the physical blowing method, gas type, polymer composition, and molecular weight affect the resulting porosity. Amorphous PLGA with CO_2 acting as blowing agent can form a well-developed pore structure. This is a better strategy as opposed to crystalline PLGA due to increased gas dissolution in the amorphous polymer than its crystalline counterpart. Other gases like N_2 and He are also used to create porosity in PLGA. However, the pore structure is very fine.[100] A mixture of PLLA dissolved in an appropriate solvent containing dispersed ammonium bicarbonate salt particles was cast in a mold and subsequently immersed in a hot water solution.[101] As a result, ammonia and carbon dioxide were given off within the solidifying polymer matrix. The expansion of pores within the solidifying polymer created macropores with diameters ranging from 300 to 400 μm. A combined approach of salt leaching and gas foaming can further improve pore interconnectivity in polymeric foams.[101]

2.6. Porosity Using Polymeric Sponge Replication. This technique using a sacrificial polymeric foam is popular in producing macroporous ceramics and metals. One of the common sacrificial synthetic polymeric sponge template materials is polyurethane (PU). The polymeric template is soaked several times in a slurry of appropriate powders to impregnate the templates, and the leftover is drained and removed (squeezing the sponge to get rid of the excess slurry). The dried template is subsequently heat treated to decompose the organic sponges (pyrolysis). After the removal of the polymer template, the ceramic or metal structures are sintered at higher temperatures for the densification of strut walls (Figure 6a). Porosity content up to 90% can be obtained with open and interconnected cell sizes ranging from a few hundred micrometers to several millimeters.[24,87,102,103]

2.6.1. Metals. It is advantageous to start with a good dispersion and favorable rheological properties. A PU sponge is coated with a slurry consisting of TiH_2 powders, dispersant(s), and a binder. After the pyrolysis of sponges and conversion of TiH_2 to Ti metal, macroporous Ti scaffolds with dense struts are produced.[104] Compared to powder consolidation (e.g., dry pressing), slurry coating can create better packing uniformity in the green body, which leads to a better microstructural control during subsequent sintering.[105] Three-dimensionally (3D) interconnected porous TiNi scaffolds were also fabricated using this technique. The ultimate green scaffolds were heated at 400 °C for 2 h to burn out the polyurethane sponges and in high vacuum. The final pore content ranges from 65% to 72% and from 250 to 500 μm in size.[106]

2.6.2. Ceramic. The macroporous scaffolds have been prepared from HA with this technique. They showed a highly anisotropic pore structure with elongated pores parallel to the direction of the elongation of the polymeric sponge. Porous HA scaffolds with single and double coats showed porosity content of 82%, and 76%, respectively. The ranges of pore size were obtained parallel and normal to the direction of pore elongation roughly 700–950 μm and 750–1100 μm.[107]

2.7. Gel Casting. Gel casting is a near-net-shape method, which yields high homogeneity and strength of the green

DOI: 10.1021/acsbiomaterials.7b00615
ACS Biomater. Sci. Eng. XXXX, XXX, XXX–XXX

bodies.[108] As shown in Figure 6b, powders, organic monomers such as a mixture of methacrylamide and *N,N′*-methylenebis-(acrylamide), binders, dispersants, and solvents are mixed together to form a slurry. Next, a cross-linking reaction occurs when an initiator such as ammonium persulfate and catalyst such as *N,N,N′,N′*-tetramethylenediamine are added to cause an in situ polymerization of the green body. After solvent evaporation, the polymer (gel) acts to bind the powders and preserve the desired shape. The success of this technique depends on the production of well-dispersed and highly solid-loaded suspensions (up to 50 vol %).[108] The optimum concentration of the dispersant, the solid content, and times of mixing are important variables for the success of this technique.[108,109]

2.7.1. Bioglass. Gel-casting method combined with stereo-lithography was applied to fabricate of bioactive glass-ceramic (55-SiO_2; 41-CaO; 4-P_2O_5; mol %). A polymeric negative (replica of the desired structure) was obtained by stereo-lithography. The slurry was cast into the molds and then polymerized (gel-casting method). After sintering at 1300 °C, scaffolds with interconnected porosities, three-dimensional channels of 400−470 μm, and micropores of 1.4 μm were fabricated.[108] One strategy to improve mechanical properties can be sintering the foam at a relatively low temperature, taking advantage of viscous flow sintering with minimal crystallization. 45S5 Bioglass ($Na_2Ca_2Si_3O_9$) powder was added to PVA−water solution to prepare a bioglass slurry. A double coating of PU template was performed, dried, and then sintered using viscous flow sintering. The ultimate scaffold showed porosity of 90% and a cell diameter of 510−720 μm.[110] Gel casting can also be combined with foaming process. The mixture was vigorously agitated to produce foam with the help of the surfactant before polymerization step and introducing initiator. An open-porous structure of bioactive glass (49.46% SiO_2, 36.27% CaO, 6.6% Na_2O, 1.07% P_2O_5, and 6.6% K_2O, in mol %) could be fabricated with interconnected pores exceeding 100 μm in diameter while maintaining the amorphous structure of the glass. The porosity content of the final scaffold can be adjusted through glass powder composition and content, selection of the monomer, cross-linker, catalyst, initiator, dispersant, and surfactant. The size distribution of the glass powder particles appeared to be critical for sintering efficiency as also discussed previously.[111]

2.7.2. Ceramic. Gel-casting was also applied to porous or dense ceramic with or without the foaming step. Sepulveda et al. produced porous hydroxyapatite (HA) foams by introducing a foaming step into the original process prior to gelation.[91,92] The HA foam showed a better-interconnected pore structure as compared to those produced by the sacrificial space holder technique. The onset time of polymerization is a critical factor in the processing of ceramics. This factor is influenced by the number of variables such as the solid concentration, initial temperature, and pH. HA scaffolds were fabricated using this technique with 90% porosity and spherical interconnected pores with sizes ranging from 20 to 1000 μm.[91,92,112]

2.7.3. Metals. The gel-casting or gel-casting-foaming technique was adopted for metallic materials as well.[113] Ti−Mo and Ti−Nb alloys implants were fabricated with the gel-casting technique followed by sintering.[114] Initially, a premixed solution of the monomer and the cross-linkers was prepared by dissolving the polymers in deionized water at room temperature. Next, slurries were formed by adding elemental or prealloyed powders of Ti−Mo and Ti−Nb to the premixed solution. A suspending agent was used to obtain uniform slurry. The extents of solid loading, the monomer content, the ratio of monomer to the cross-linker affect the success of the process initially. The high temperature sintering conditions dictate the development of mechanical properties. By changing these variables, the volume of a polymeric network between the powder particles can be adjusted to vary the porosity content. The final scaffold showed total porosity content range between 39% and 50% and a pore size range of 5−120 μm. Furthermore, it was shown that the architecture of pores can be altered by changing the sintering conditions, leading to the formation of a three-dimensionally interconnected porosity.[114] As shown in Figure 5iii, with the increase of Mo content, the pore diameters and their connectivity increased for Ti−Mo alloys with the Mo content up to 17.5 wt %. A few closed-cell pore were located on the wall and edges of macropores can be seen. The pore diameter of Ti-7.5Mo, Ti-12.5Mo, and Ti 17.5Mo alloys were 98, 102 and 110 μm, respectively.

2.8. Other Fabrication Methods. *2.8.1. Bioglass. 2.8.1.1. Melt-Quenching Route.* This is a traditional method for bioglass fabrication. In this technique, oxides are melted together at high temperatures in the range of 1100−1300 °C in a platinum crucible and quenched in a graphite mold (to form rods or monoliths) or in water (to form glass-frits).[115,116] An important example is 45S5 bioglass. This technique can be adopted in combination with the other methods such as rapid prototyping and dip-coating processes to produce high porosity and interconnectivity. A melt-derived bioglass 45S5 can be crushed into fine powders for preparing the glass slurry. A commercially rapid-prototyped manufactured 3D graphite network can act as a template and uniformly dip coated with melt-derived glass slurry. A dip coated template can then be heat-treated at 900 or 1000 °C to remove the graphite template and sinter the glass−ceramic walls. The resultant scaffolds have high porosity content of 95%.[117]

2.8.1.2. Sol−Gel. This technique is a low-temperature one using organometallic reagents and simple to control. As shown in Figure 6c, the sol mixture composed of an organometallic alkoxide precursor, salt, and catalyst undergoes hydrolysis and condensation to form a gel. The condensation is catalyzed by adding an acidic compound upon completion of the hydrolysis stage. After the viscosity of the sol starts to rise, the sol is transferred to molds and sealed for aging. Aging takes place at specific temperatures for specific time periods. Subsequently, the gel is dried, and it gets thermally stabilized at temperatures typically varying in the range of 600−800 °C. Thermal stabilization allows for partial densification of the matrix.[115,118,119] 58S is an example of bioglass prepared by the sol−gel technique.[116] Sol−gel glass showed highly mesoporous structure compared to melt-derived bioglass and with a large content of nanoporosity in such products.[115] The glass composition, surfactant, and gelling agent concentration are the factors that affect the development of the pore network structure.[119,120] Polymerization-induced phase separation was adopted to fabricate porous ceramics with nano/macro-bimodal pore size distribution.[121,122] Generally in this approach, after mixing the appropriate constituting starting materials, polymer, or the gelation catalyst, the solution sits at a specific temperature in order to undergo the aging process and subsequent transition into thermodynamic phase separation. Finally, it gets thermally stabilized.[123] The SiO_2−CaO and SiO_2−CaO−P_2O_5 were also fabricated using polymerization-induced phase separation simultaneously with the sol−gel

DOI: 10.1021/acsbiomaterials.7b00615
ACS Biomater. Sci. Eng. XXXX, XXX, XXX−XXX

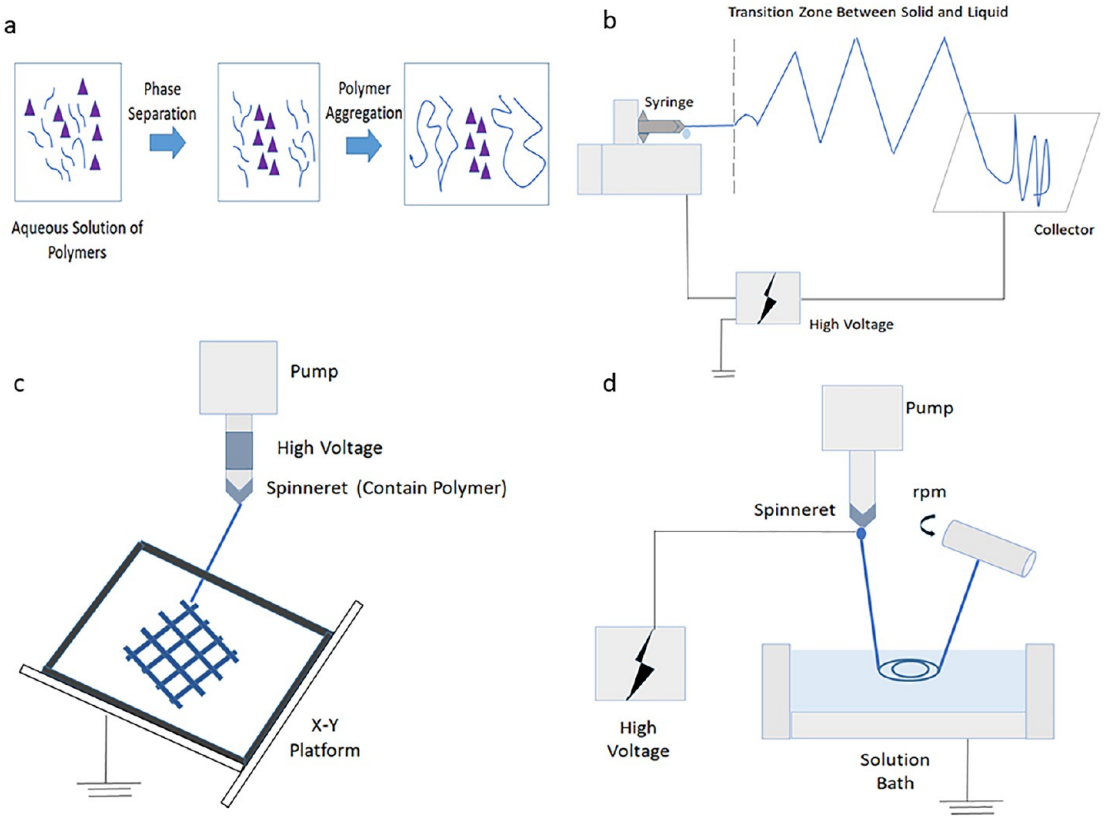

Figure 7. Random porosity generation by (a) Phase separation for polymers, (b) conventional electrospinning for polymers and polymer/ceramics, (c) melt electrospinning or direct writing for polymers, and (d) wet electrospinning.

transition when a water-soluble polymer such as (poly(ethylene oxide)) or a triblock copolymer (poly(ethylene oxide)−*block*−poly(propylene oxide)−*block*−poly(ethylene oxide)) was added to the sol−gel solution. The scaffold contained bimodal pore size distribution with interconnected macropores of 10−200 μm.[121]

2.8.2. Polymer. A number of techniques have been introduced to fabricate porous polymeric scaffolds, including phase separation process, fiber debonding, melt blending, and electrospinning, which are discussed as follows.

2.8.2.1. Phase Separation. The thermally induced phase separation processes involve liquid−liquid or solid−liquid separation that occurs in polymer/solvent mixture. This leads to the production of scaffolds with porosity content up to 97%. In this technique, thermal energy can be applied to separate the solution into a polymer-rich and a polymer-lean phase. This occurs by lowering the solution temperature below its solubility temperature or by adding a nonsolvent to the solution (Figure 7a). Scaffolds obtained with this technique are highly porous and can contain tubular pore morphology and extensive pore interconnectivity.[124,125] However, it is difficult to achieve a precise control of scaffold morphology. The pore morphology and porosity can be controlled by varying the polymer concentration in solution, the volume fraction of the secondary phase, quenching temperature, polymer and solvent nature, and incorporation of inorganic particles.[126,127] PLA was produced by using the thermally induced liquid−liquid phase separation and also solid−liquid phase separation. The addition of a nonsolvent (e.g., water) to polylactide−dioxane mixture can induce liquid−liquid phase separation of the polylactide solutions through the formation of cocontinuous phases. This produced isotropic foams with interconnected pores of 1−10 μm in diameter.[128] The solid−liquid separation of polylactide in pure dioxane produced highly anisotropic macroporosity.

2.8.2.2. Fiber Bonding (Unwoven Meshes). Fibers, if bonded together, can result in 3D structures with large surface areas and highly porous scaffolds. The fibers can be attached to each other via two different techniques. First, fibers (e.g., poly(glycolic acid), PGA) are immersed into a relevant solvent (e.g., PLA in chloroform). When the solvent evaporates, the network of PGA fibers is embedded in PLA. This fabrication technique yielded foamed-structures with porosities as high as 81% and pore diameters of up to 500 μm.[129] The second approach is bonding PGA fibers through atomization of PLA or PLGA to coat the fibers. PLA or PLGA is dissolved in chloroform and sprayed onto the PGA fibers. Pore sizes similar to those of the first approach can be attained.[130]

2.8.2.3. Melt Blending of Two Immiscible Polymers. Cocontinuous blends comprising PLA/PCL can be prepared by melt processing. By controlling the concentration and subsequent annealing step (above the melting temperature), it is possible to optimize the sizes of the cocontinuous phases. By subsequent extraction of the selective porogen phase like PCL, a fully interconnected porous PLA material with a void volume between 50% and 60% and pore size between 1.5 and 88 μm can be produced.[131] It is noted that pores in scaffolds prepared by polymer leaching are characterized by the interconnection of cylindrical pores. This is completely different than those scaffolds fabricated with the other techniques where the larger pores are generally interconnected through smaller openings.[65] This approach is able to produce controlled pore diameters with narrow pore size distribution and possessing substantial

DOI: 10.1021/acsbiomaterials.7b00615
ACS Biomater. Sci. Eng. XXXX, XXX, XXX−XXX

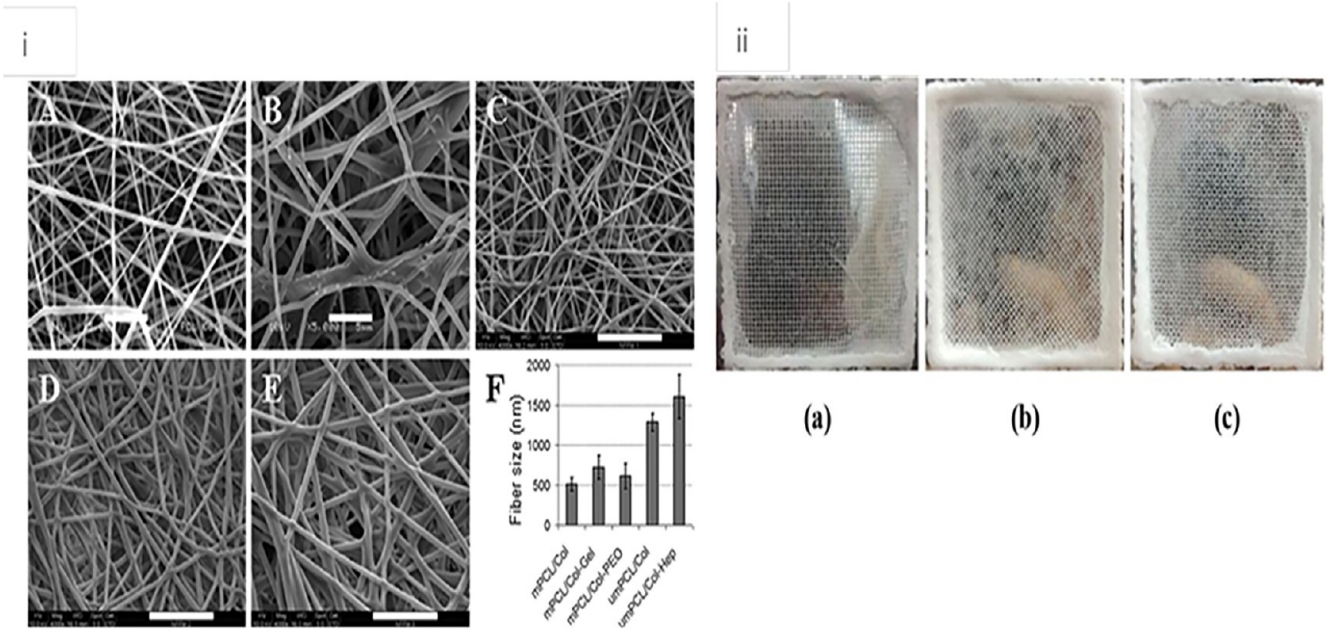

Figure 8. (i) Morphology of the electrospun fibrous meshes: (A) conventional electrospun mesh of PCL/Col showed fibers with diameters in the sub-micrometer range, (B, C) scaffolds based on PCl/Col cospun with PEO or gelatin. Coelectrospinning performed using the modified system yielded meshes with two different fiber groups noticeable by their difference in size (B, PCL/Col-PEO; C, PCL/Col-Gel). Using the modified electrospinning system with an increased PCL/Col solution concentration and selective leaching of a water-soluble fiber phase (poly(ethylene oxide) (PEO) or gelatin) resulted in fibers with micrometer-sized diameters. (D, E) Electrosprayed Heprasil in the structure of PCL/Col-Hep; image E could not be observed under SEM due to the dehydration process during specimen preparation. The resulting PCL/Col fiber diameters in all groups are shown graphically in part F. Scale bars are 5 μm in parts A and B and 20 μm in parts C–E.[155] Reproduced with permission from ref 155. Copyright 2008 American Chemical Society. (ii) Scaffold with nine layers fabricated via electrospinning-based rapid prototyping (a) 0°/90° pattern, (b) 45°/135° pattern, and (c) 45°-twist pattern.[156] Reproduced with permission from ref 156. Copyright 2015 Emerald Publishing Limited.

interconnectivity. Scaffolds with pore sizes from 1 μm to hundreds of micrometers can be fabricated by this technique,[132] which is shown in Figure 5iv. The increase in the annealing time leads to significantly increased phase and pore sizes over a wide range of scale.

2.8.2.4. Electrospinning. Electrospun scaffolds promote better cell/matrix interaction through the fabrication of macro- to nanoscaled fibers mimicking the size ranges of the extracellular matrices due to large surface to volume ratios. In this technique, a polymer solution is injected from an electrically conductive spinneret (needle) until it reaches a collector. A high voltage is applied from the tip of the spinneret to the collector, which is placed at a fixed position from the spinneret. When the electric potential applied to polymer solution overcomes the surface tension of formed droplet (Tylor cone), polymer jets eject from the needle and get collected onto the collector.[133] This result in an unwoven and randomly oriented fibrous polymer mesh with varying fiber diameter from 100 nm to a few micrometers based on particular polymer solution and electrospinning parameters (Figure 7b). The electrospinning process is inherently unable to control pore size and pore arrangement with regards to internal channels. However, the morphologies of electrospun scaffolds can be tailored through fabrication parameters. These parameters include concentrations of polymer solutions or voltage between nozzle and collector.[134,135] This technique is applicable to a variety of synthetic, natural polymer, biocomposite of polymer and CaP or MgP.[133,136] Synthetic polymers including polyesters such as PCL,[137] PLA,[138] PLGA, PGA,[139] poly(glycerol sebacate) (PGS),[140] PU[141] and functionalized polyolefins such as PVA,[142] poly(*N*-isopropylacrylamide) (PNIPAAM),[143] etc. Natural polymers and proteins include collagen,[141] gelatin,[141] silk,[144] fibrinogen,[145] elastin,[146] and polysaccharides like hyaluronic acid (HA),[144] chondroitin sulfate,[147] dextran,[148] alginate,[149] chitin,[142] chitosan[150] etc.

One problem associated with electrospinning is small pore sizes in scaffolds, which hinder cell infiltration in vitro and tissue in-growth into the scaffold in vivo. Two approaches can be employed to increase cell infiltration. In one such approach, cells are electrosprayed into a solution prior to fabrication or simultaneously adding cell during electrospinning. Another approach is increasing the pore size in final scaffold, which is discussed in the following.[136] Several postprocessing strategies can be applied to increase the pore size, including salt leaching,[151] cryogenic electrospinning,[152] ultrasound, sacrificial fibers,[135] or special collection techniques. Higher pore sizes can be produced by dissolving salt particles in the polymer solution during and leaching out postelectrospinning.[134] However, this technique affects the surface properties of the nanofibers and does not provide uniform morphology and stability.[134] Ultrasonication is applied to reduce packing density of fiber after electrospinning process that mechanically separates the fibers and increases the pore size.[153] Another strategy to increase the pore size is coelectrospinning of sacrificial fibers like PEO or gelatin with stable fibers. The removal of sacrificial fibers after electrospinning creates larger pores. In one study, the electrospun scaffolds comprised of PCL/collagen/HA, along with PEO sacrificial fibers. Use of PEO fibers increased mean pore size from almost 500 to 2000 μm, while enhancing infiltration of mesenchymal stem cells (MSCs).[135] By dissolving the sacrificial fibers, the continuous sections within the scaffold can be removed. The sudden removal of fibers can cause

DOI: 10.1021/acsbiomaterials.7b00615
ACS Biomater. Sci. Eng. XXXX, XXX, XXX–XXX

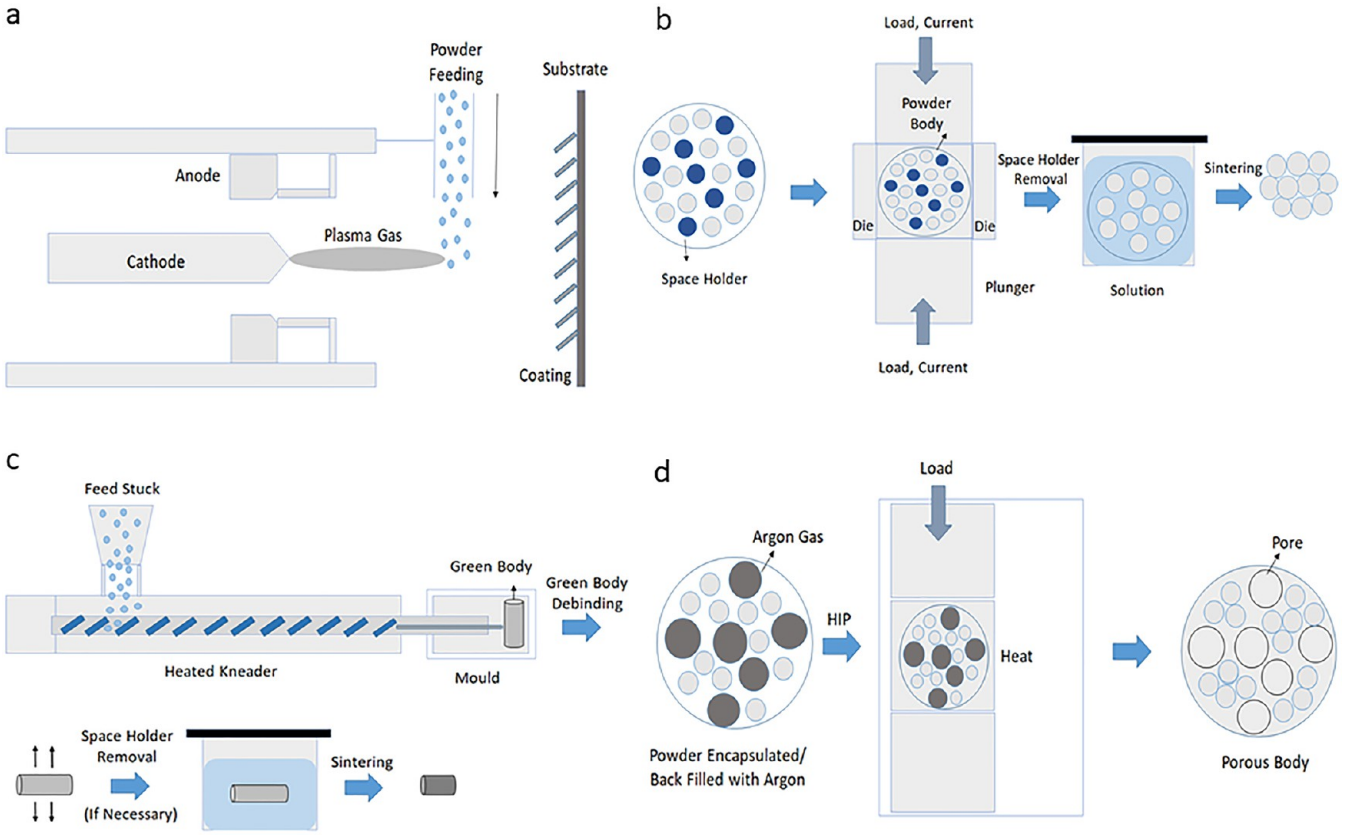

Figure 9. Random porosity generation by (a) plasma spraying of metals, (b) spark plasma sintering of metals, (c) metal injection molding, and (d) hot isostatic pressing of metals.

reorganization and contraction among fibers. This might block the newly created pores and collapse the mesh network of scaffolds.[154,155]

Electrospraying of hydrogels onto scaffolds during spinning is yet another strategy for increasing pore sizes. Fibrous PCL/collagen meshes with regions rich with the HA hydrogel were produced using this technique.[155] One of the problems associated with this technique is a nonuniform distribution of the hydrogel. Figure 8i indicates the difference in the morphology of scaffolds fabricated through conventional electrospinning, coelectrospinning with sacrificial fibers, and electrosprayed with hydrogel nanoparticles. Figures 8i-A–F show as-electrospun meshes and their respective average fiber dimensions, respectively. All fibers appeared to be uniform with minor variations in diameters. Co-electrospraying a drug, Heprasil, enlarged the fiber diameters slightly. The interfiber distances and pore sizes appeared visibly larger in Heprasil containing compositions.

An innovative technique to increase the pore size is to design special collectors.[134] In this technique, instead of the traditional flat-plate collector, a grounded spherical dish and an array of needle-like probes were used. This led to the three-dimensional cotton ball-like PCL scaffold with low-density nanofibers. This scaffold showed an open pore structure throughout, instead of superficial porous structures, which is the characteristic of a traditionally manufactured electrospun scaffold.

Electrospinning-based rapid prototyping (ESRP) technique was also developed for the fabrication of scaffolds to control deposition of fine fibers.[156] PLGA and β-TCP nanocomposites were fabricated with electrospinning-fused deposition modeling. Two different scaffolds with a simple design where microfilaments deposited at angles of 0° and 90° and complex design where microfilaments deposited at angles alternating between 0°, 90°, 45°, and −45° to produce specific pore architectures as shown in Figure 8ii.[156] In this RP process of fused deposition modeling, electrospinning is applied instead of extrusion to generate a continuous fiber from a liquid solution.

The two structures showed significantly different pore sizes and orientations. The results indicated that scaffolds with complex architecture appeared to degrade more slowly than those with simple architecture.[157] Electrospinning using molten nonconductive polymers instead of polymer solutions provided more control over the path and collection of fiber (e.g., pore morphology, size, shape, number, and porosity). This technique led to the fabrication of tubular scaffolds of PCL with 20 μm diameter by using a rotating collector on a translating stage. In this technique of melt electrospinning, especially in conjunction with direct writing process or programmable $x-y$ stage, matching of the translation speed of the collector to the speed of the melt electrospinning jet is the key experimental factor. This approach enables precise control of the location of fiber deposition, fiber diameter, and winding angle[158,159] (Figure 7c).

Dynamic liquid electrospinning technique is yet another technique designed to improve cell infiltration and vascularization. In this technique, electrospun nanofibers were deposited and twisted into yarns in a water vortex before collecting on a rotating mandrel. Preosteoblastic cells showed significantly higher proliferation rates in vitro than their traditional behavior on electrospun nanofiber scaffolds.[160] In wet electrospinning, the 3D scaffolds of PGA were fabricated by combining electrospinning and wet spinning systems. In the combined

DOI: 10.1021/acsbiomaterials.7b00615
ACS Biomater. Sci. Eng. XXXX, XXX, XXX−XXX

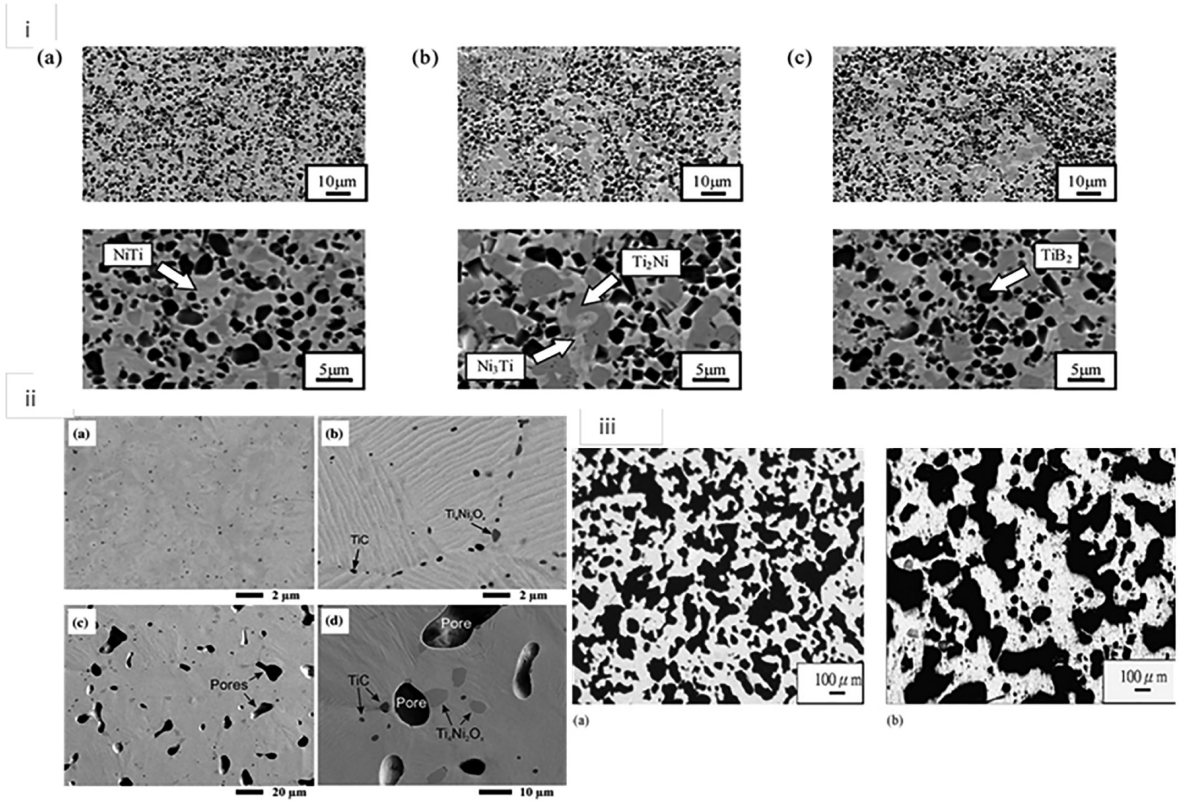

Figure 10. (i) NiTi alloy made by combustion synthesis with the help of ZrH_2 as foaming agent and TiB_2 as endothermic agent. (a) Ni powder classification = fine, and Ti powder denomination = fine; (b) Ni powder denomination = coarse, and Ti powder denomination = fine; (c) Ni powder denomination = fine, and Ti powder denomination = coarse.[171] Reproduced from ref 171, published by MDPI. (ii) NiTi parts made by metal injection molding: (a) powder particle, (b) distribution of secondary phases after HIP (1065 °C, 100 MPa, 3 h), (c) microstructure of NiTi sample made by MIM (1250 °C, 5 h, residual porosity 10%), and (d) detail of image c.[177] Reproduced with permission from ref 177. Copyright 2012 Springer. (iii) High porosity and large pore size shape memory alloys fabricated by using pore-forming agent (NH_4HCO_3) and capsule-free hot isostatic pressing. Optical micrographs of porous samples (a) without use of NH_4HCO_3 and (b) with 8.3% NH_4HCO_3.[183] Reproduced with permission from ref 183. Copyright 2007 Elsevier.

system, a spinning stainless bath filled with water and two different solvents was used as a grounded fiber collector[161] (Figure 7d). A low packing density of fibers can be achieved in this method in which the solvent was removed by freeze-drying. In another study, low density 3D scaffolds of poly(vinyl alcohol (PVA)−methacrylate) (PVA-MA) were spun into a bath of ethanol. Collecting fibers into liquid formed 3-D scaffolds without fiber compaction and fusion, which is a characteristic of solid form collection of fibers. However, the scaffolds manufactured did not have a defined overall morphology.[161,162]

In another combined rapid prototyping−electrospinning approach, (3D) scaffolds were fabricated by combining 3D fiber deposition and electrospinning. Rapid-prototyping of fibers provided an interconnected network of pores, while the randomly oriented fibers of electrospinning improved low cell seeding efficiency of rapid prototyping, leading to entrapping of more cells.[163]

Finally, needleless electrospinning has been invented to increase pore size compared to traditional needle electrospinning methods in which needles were used to eject polymer solution into the electrical field. In this technique, instead of generating a polymer jet from the needle, hundreds of jets of polymers formed from the surface of the polymer solution by means of rotating disks. At high rpm, the entire edge of the disk is covered with a thin layer of the PCL solution. When the PCL solution was charged with a high electrical voltage inside the solution vessel, numerous jets or filaments were generated from the edge of the disk, rotating at a high rpm. Fluffy three-dimensional nano- and macroporous PCL scaffolds were fabricated using disk-electrospinning with an average pore size of 26 μm, which is higher than that traditionally obtained with needle electrospinning.[164]

2.8.3. Metal. 2.8.3.1. Chemical Vapor Infiltration. Porous metallic foams comprised of approximately 99% tantalum and 1% vitreous carbon can be fabricated by this process. The product is processed via a chemical vapor infiltration (CVI) or deposition (CVD) where pure tantalum metal is precipitated into a reticulated vitreous carbon (RVC) skeleton. The synthesis begins by pyrolysis of a thermosetting polymer foam (e.g., PU) precursor to obtain a low-density vitreous carbon skeleton. This carbon skeleton has a repeating dodecahedral array of pores (about 700 μm) interconnected by smaller openings or portals (about 500 μm). Tantalum metal is subsequently deposited onto the carbon skeleton to create a porous metal construct. This material is comprised of 75−85% void space (pore volume) and is characterized by continuous interconnecting pores.[165,166]

2.8.3.2. Plasma Spraying. This technique can be used to create porous surface coatings on solid substrates and also fully porous structures where porous blocks can be cut from the sublayers using electric discharges.[167] An electric arc is generated between two water-cooled electrodes in a gun. The

DOI: 10.1021/acsbiomaterials.7b00615
ACS Biomater. Sci. Eng. XXXX, XXX, XXX−XXX

arc heats a gas to temperature as high as 36000 °F, partially ionizing it and forming a plasma jet. As shown in Figure 9a, the powder is injected into the plasma gas environment through a career gas. They are accelerated to a high speed, melted, and impacted onto the target substrates. Porous coatings with varying degrees of porosity and also graded porous coatings can be created on the substrate by adjusting the spraying parameters. The parameters include spraying distance between the substrate and nozzle, the flow rate of the transport gas, spraying power, and spraying pressure, as well as coating thickness (spraying time) in the case of fabrication of graded porous coatings.[168]

2.8.3.3. Combustion Synthesis. These reactions have the ability to generate high temperatures resulting in intermetallic compounds. Various processing parameters, including the particle size of reactant powder, the use of a binder, and the compaction pressure can affect the final microstructure and porosity. The process was used in fabricating porous NiTi alloy foams. The pore distribution was inhomogeneous and nonuniform but open and interconnected. Such foams have potential biomedical applications even though their shape memory behavior can be less than dense samples produced by conventional techniques.[169,170] Figure 10i shows that initial particle sizes of Ni and Ti affected the ignition temperature of the combustion reaction and the final microstructure of foams. By increasing the viscosity of the melt during the combustion foaming, the mechanical properties of NiTi foams can be controlled by reducing the rupture of cell walls and pore growth. Increasing the powder particle sizes of both Ni and Ti reduces the exothermicity of reactions, thus reducing the porosity content and their sizes. Nonspherical pores and large pore diameter can also be prevented by using diluents to control the exothermicity.[171]

2.8.3.4. Electrical Field Activated Sintering and Powder Metallurgy. This is an example of a rapid sintering process that can effectively consolidate metal powders within a short time. This technique avoids the main shortcoming of conventional powder sintering with a lengthy furnace cycle.[172] The technique is also known under different names, such as field assisted consolidation technique (FAST),[173] spark plasma sintering (SPS), plasma activated sintering (PAS), and electrical discharge compaction (EDC). Porous titanium implants were commercially manufactured with EDC.[174] The simultaneous application of electrical discharges along with pressure is the common theme in all of these methods. Products manufactured from Ti and Ti alloys are examples of successful applications of this technique. It has been argued that there is local generation of gas-plasma, which can melt local oxide surface films on the particles. This ensures good particle-to-particle bonding.[175] However, this hypothesis is not unequivocally proven. Several examples are discussed in the following.

2.8.3.4.1. SPS. This technique can be used to fabricate porous metal alloys, intermetallic materials and composites.[176] Porous Ti and Ti_5Mn alloy foams were prepared by the addition of both TiH_2 as a foaming agent and ammonium bicarbonate (NH_4HCO_3) as a space holder. The process is explained in Figure 9b.

2.8.3.4.2. EDC. This technique is capable of compaction as well as sintering of powders at the same time by discharging high voltage and high-density current in a short time less than 300 μs. The energy is instantaneously applied into the powders. The voltage and current values are simultaneously monitored. One issue associated with this technique is the formation of several comparatively large holes at the cross-section of central solids, which can affect the mechanical properties. Alternatively, multiple electrodischarging treatments in a low vacuum atmosphere resulted in graded porosities in Ti compacts. With more treatments, the density of initially formed compacts expanded outward, thus giving a gradient in pore content. In another variation, fully porous microstructures were produced with applications of electrical discharges to spherical Ti-powders.[174]

2.8.3.5. Metal Injection Molding (MIM). This technique can be applied to produce dense yet porous near-net-shape parts like NiTi or titanium alloys. As shown in Figure 9c, this process deals with the mixing of metal powder with or without a space holder (to act as the porogen) with one or more polymer binders in order to make the feedstock. This homogeneous mixture is then injected into a heated MIM tool to reach the mold. After cooling, the manufactured part in the mold, binder, and spacer are removed. Finally, sintering under vacuum is carried out to yield finished products.[177,178] Porous titanium was fabricated using NaCl as the space holder, followed by MIM. The results indicate that content of NaCl influences the porosity in titanium significantly, creating porosity in the range of 42−72% and pore sizes up to 300 μm.[179] Figure 10ii-a−d shows the evolution of pore morphology and size of oxygen-containing Ti_2Ni and TiC phases of starting powder after HIP (conducted at 1065 °C, 100 MPa, 3 h) and after MIM processing (sintering at 1250 °C, 5 h). With increasing sintering temperature, coarsening of both phases and increase in pore size took place, which is more noticeable in the case of oxygen-containing Ti_2Ni phase.

2.8.3.6. Hot Isostatic Pressing. Ti and Ti alloy powders, as well as TiNi, can be compacted with this technique. In conventional hot isostatic pressing (HIPing) powders are encapsulated in a can under a vacuum and compacted at high temperature with high gas pressure. This creates products with very little porosity. In comparison, a capsule-free HIP is useful for producing porous structures. In this technique, powders are cold pressed and then presintered at moderate temperatures. Afterward, the compacts are subjected to the HIP procedure. Porous manufactured parts using this technique showed nearly spherical pore shapes,[180] albeit with very low porosity content and small pore size. Combining with other methods such as using space holders plus gas expansion can create different porosities and pore morphologies and increased pore size.[181] HIP was applied to compress and trap Ar gas bubbles between metal (e.g., TiNi) powders. Sintering at reduced pressure leads to the expansion of trapped gas in the softened material at temperatures below melting. Subsequent sintering at a temperature above the melting temperature of NiTi resulted in Ar bubbles escaping to the top of the melt (Figure 9d). Using this technique, parts with different pore structures can be fabricated. In one variation, specimens with 50% porosity but with an average pore size of approximately 20 μm can be produced. Alternatively, specimens with 42% porosity and an average pore size of approximately 0.5 mm can be fabricated by slightly varying some of the HIP parameters.[182] The space holder technique in conjunction with HIPing can be also used to fabricate porous metal scaffolds, resulting in high porosity with large pore sizes. As an example, NiTi shape memory alloys were fabricated by using a pore-forming agent and capsule-free hot isostatic pressing process, which is shown in Figure 10iii. The porosity increased linearly with the addition of NH_4HCO_3 as a space holder and reached as high as nearly 50%. The

DOI: 10.1021/acsbiomaterials.7b00615
ACS Biomater. Sci. Eng. XXXX, XXX, XXX−XXX

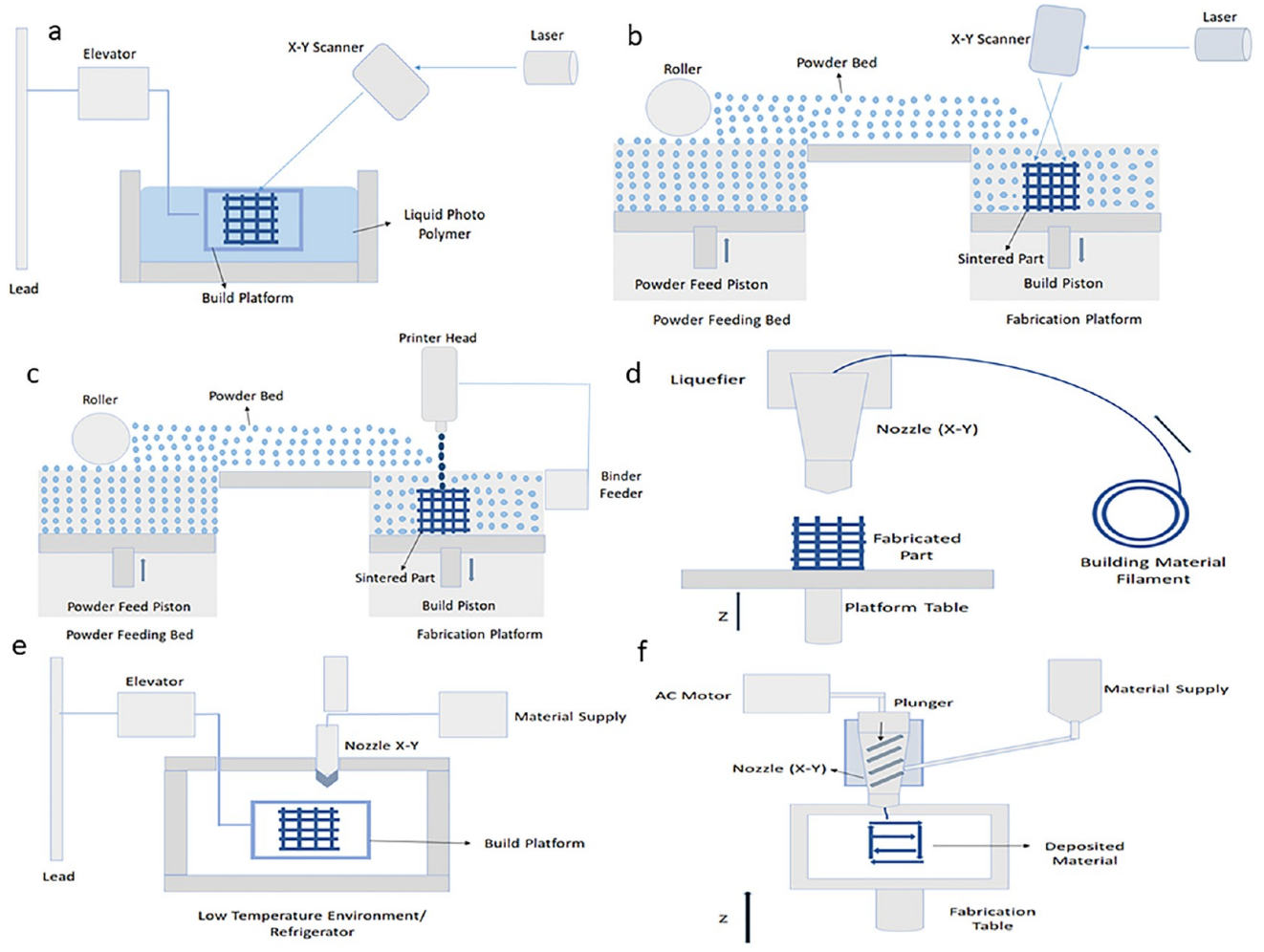

Figure 11. Generation of porosity by design using (a) stereolithography for polymers and polymer/ceramic slurries, (b) selective laser sintering for polymers, ceramics, metals, and composites, (c) 3-D printing for polymers, ceramics, metals, and polymer/ceramic, (d) fused deposition modeling for polymers, (e) low-temperature deposition modeling, and (f) bioextruder (single material deposition).

samples showed uniform pore distribution with most pores larger than 300 μm. Also, the pore shape is regular with less sharp angles and corners (Figure 10iii-b).[183−185]

2.8.3.7. Layer-by-Layer (LbL) Technique in Fabricating Orthopedic Biomaterial Scaffold: Layer-by-Layer Assembly. This technique involves layer-by-layer (LbL) deposition of metal nanoparticles (NPs) on polymeric surfaces, which may have potential applicability in biomaterials. In one study, LbL was successfully used to decorate electrospun nanofibers where Au NPs were incorporated in the pores and on the surface of polymeric hollow fiber membranes in order to modify the pores of hollow fibers without pore blockage. This strategy can enhance properties of as-fabricated scaffolds in terms of water permeability, contiguity, etc. The scaffolds showed maximum pore size of 0.5 μm. The incorporation of NPs occurs onto the fiber membranes via alternating adsorption of polyelectrolytes and negatively charged Au NPs. The stability of the deposited thin films is highly dependent on the solution pH and on the type of solubilized ions.[186−188]

2.9. Solid Free Form Fabrication (Porosity by Design). A large number of rapid prototyping (RP) or solid freeform fabrication techniques have been widely studied and used in fabricating porous structures. In RP, the digital representation of an object is mathematically sliced into a number of thin layers. Afterward, the layers are built and fused together to form 3D objects. These techniques are applicable in fabricating polymers, ceramic, and metals, both porous bioresorbable and nonresorbable. Examples of RP processes include stereolithography (STL), selective laser sintering (SLS), fused deposition modeling (FDM), and direct 3D printing. These techniques provide more control over fabricating of scaffolds with reproducible porosity and defined interconnectivity, geometry, orientation, and pore size due to selective spatial features of the scaffolds.[189,190] Hence, these processes are grouped together by their ability to create pores by design. FDM and SLS need thermoplastic polymers, STL requires the use of radical initiated polymerization, and 3DP includes the use of solvents and binders. Direct RP is usually associated with an anisotropic shrinkage during manufacturing. To address the limitations of direct RP, indirect Solid Freeform Fabrication (SFF)/RP has been developed for a variety of biomaterials, including ceramic slurries cast in STL fabricated molds. Designing of molds, casting methods, and mold removal techniques are the concerns of indirect RP. The main difference between direct RP and indirect RP is that in the former case, the scaffold is directly processed from a biomaterial, while in the latter; the scaffold is cast and processed in a RP mold.

DOI: 10.1021/acsbiomaterials.7b00615
ACS Biomater. Sci. Eng. XXXX, XXX, XXX−XXX

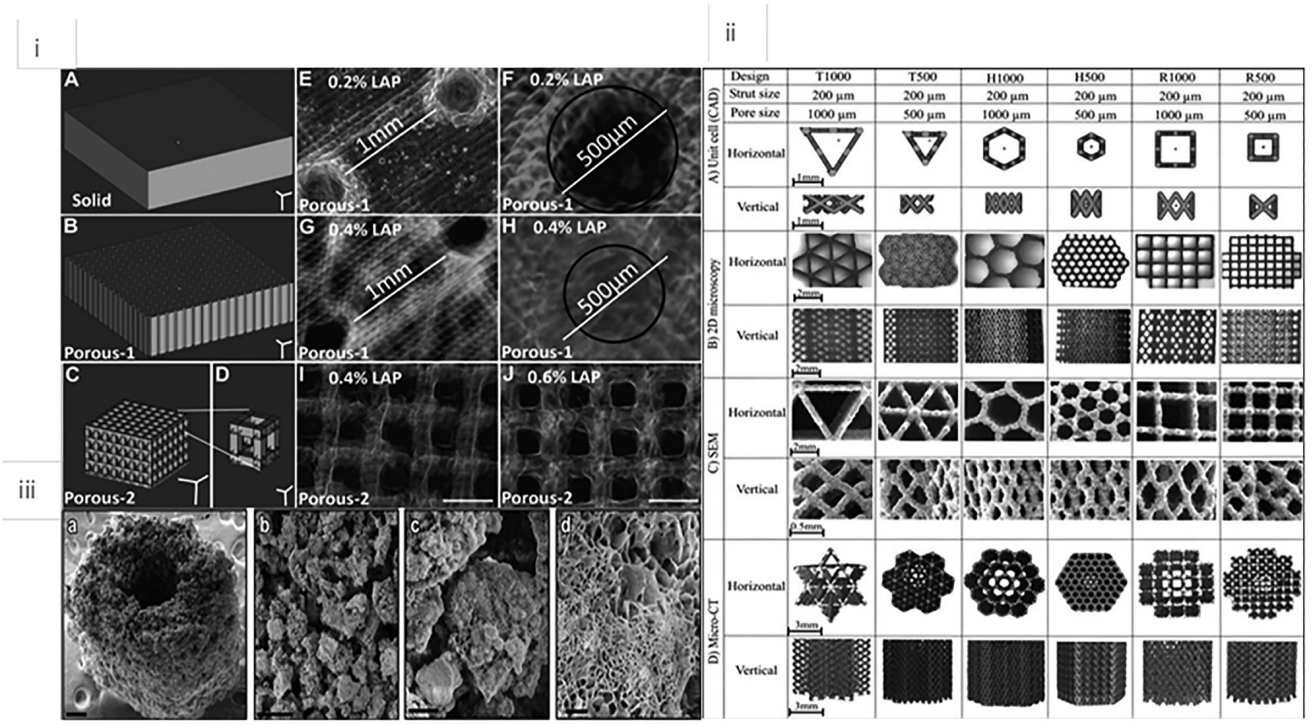

Figure 12. Evaluation of VL-PSL of cell laden scaffolds: (A–D) 3D models designed for (A) solid, (B) uniaxial (porous-1), and (C, D) biaxial (porous-2) porous structures. (E–H) The internal architectures of porous-1 PEG scaffolds produced with different initiator concentrations of LAP. The distance between 2 neighboring tubes was indicated by the white lines in parts E and G. Black circles in parts F and H indicate the approximate inner surface of the pores in porous-1 structures. The dimensions of the intended pore diameter of these structures were indicated by white lines, revealing the differences in fidelity of the photo-cross-linking using different LAP concentration. (I, J) The internal architectures of porous-2 PEG scaffold produced with different initiator concentrations. Bar in A, B = 2 mm. Bar in C = 1 mm. Bar in D = 200 μm. Bar in E, G = 1 mm. Bar in F, H, I and J = 500 μm.[192] Reproduced with permission from ref 192. Copyright 2013 Elsevier. (ii) Selective laser-melted Ti_6Al_4V bone scaffolds: (A) unit cells of the designed Ti_6Al_4V scaffolds, (B) optical light microscopy images of the as-produced Ti_6Al_4V scaffolds, (C) SEM images of the as-produced Ti_6Al_4V scaffolds, and (D) 3-D models from the micro-CT data sets of the as-produced Ti_6Al_4V scaffolds.[202] Reproduced with permission from ref 202. Copyright 2012 Elsevier. (iii) A 3D printed composite calcium phosphate and collagen murine femoral scaffold with microporosity and plate-like crystal: (a) murine-sized scaffold representing the geometry of the femoral middiaphysis. Scale bar is 250 μm. (b, c). The 3D printing process produces scaffolds with intrinsic microporosity, primarily in the range of 20–50 μm. Scale bars are 100 μm (b) and 10 μm (c). (d) Plate-like crystal growth occurs on the surface of unreacted calcium phosphate particles, which increases the specific surface area for protein or drug adsorption. Scale bar is 1 μm.[208] Reproduced with permission from ref 208. Copyright 2014 Elsevier.

2.9.1. Laser-Based Manufacturing. 2.9.1.1. Stereolithography (SLA). This is an important process among RP techniques, has been commercialized in 1988 (by 3D Systems Inc.), and is a laser-based system. In this technique, a UV laser scans over the top of a bath of a photopolymerizable liquid monomer. Laser initiates the photopolymerization process and controllably solidifies the resin. After formation of the first layer (2D layer) of the solid structure and adherence onto the support platform, the platform is moved away from the surface and liquid resin is recoated onto the built surface to solidify the second layer. As the depth of curing is slightly larger than the initial platform step, the 3D object is manufactured gradually through polymerization of the unreacted functional group by the forming of the second layer (Figure 11a). Once the formation of 3D structure is complete, the excess resin is drained. The finished model is further cured with UV to complete all the polymerization reactions and remove the surface irregularities. Polymers such as poly(ethylene glycol) (PEG) acrylate, PEG methacrylate, poly(vinyl alcohol) (PVA), and modified polysaccharides, such as hyaluronic acid and dextran methacrylate, polypropylene fumarate anhydride, and poly(ethylene oxide) (PEO) have been subjected to this technique. Multiple open channel geometries, including ellipses and rectangles, were developed to study the perfused culture of cells. Rectangular open channels with final dimensions of 350 μm by 850 μm were employed for subsequent studies that prolonged the maintenance of albumin production throughout the 7-day culture relative to 2D controls.[191]

A visible light-based projection stereolithography system (VL-PSL) has received attention due to a combination of high resolution, high fabrication speed, and possibility of culturing the live cells into the scaffold for organ printing. This method is based on projecting an entire image onto the surface of monomer solution to polymerize a whole layer. Poly(ethylene glycol) diacrylate (PEGDA) scaffolds were manufactured utilizing a visible light activated initiator and square shaped pore size of 300 μm × 300 μm that incorporated human adipose-derived stem cells as shown in Figure 12i.[192,193] To build a different architecture, it was important to determine the optimal concentration of the initiator (lithium phenyl-2,4,6-trimethylbenzoylphosphinate (LAP)). Various examples of successful attempts of architecture are shown in Figures 12i-A–D. The porous-1 design included pores formed by creating voids, 500 μm in diameter, through the *y*-axis (Figure 12i-B). The lattice-like porous-2 structure was designed using intersecting beams, 150 μm × 150 μm in height and width, spaced such that the resulting pore size was 300 μm × 300 μm (Figure 12i-C,D). Initially, a low concentration of 0.2% LAP

DOI: 10.1021/acsbiomaterials.7b00615
ACS Biomater. Sci. Eng. XXXX, XXX, XXX–XXX

was needed for the accurate 3D reproduction of the porous-1 design. As LAP concentration increased, the strut diameter decreased and distances between two struts increased (Figure 12i-E−H)). A concentration of 0.6% LAP was needed in precisely replicating the CAD design in porous-2 structure (Figure 12i-J). At 0.4% LAP, the individual layers were not strong enough to support stacking of the subsequent layers, resulting in an imperfect structure (Figure 12 i-I).[192]

The PCL scaffolds were manufactured via solvent-free stereolithography.[194] In solvent-free SL, photo-cross-linkable polymer was heated above the melting temperature to obtain an appropriate viscosity for use in the SL method, which prohibits the use of a solvent. As solvents were not used, material shrinkage does not occur for this technique after drying of the scaffolds. Therefore, the scaffolds accurately represent the exact structure modeled by computer-aided design for porosity, pore size, and interconnectivity. The scaffolds had porosity content of 70.5%, and the average pore size was 465 μm.

2.9.1.1.1. Ceramic. The SL technique has been adapted for the fabrication of three-dimensional (3D) ceramic by adding ceramic powders to photosensitive resins. This technique, called ceramic stereolithography (CSL), needs the preparation of photosensitive ceramic suspensions. The laser beam polymerizes ceramic slurries layer by layer. After building the green body, the binder is removed and then sintered. Osteochondral scaffolds, based on β-TCP and collagen, with 700−900 μm pore size, 200−500 μm interconnected pores size (fully interconnected), and 50−65% porosity were manufactured with CSL combined with gel casting.[195]

2.9.1.2. Selective Laser Sintering (SLS). In this technique, a computer-controlled CO_2 laser beam selectively scans over a bed of powder to sinter thin layers of powder material. Exposure to high temperatures fuses particles together to form 3D objects through melting or sintering. After finishing the first layer, a new powder layer is deposited by a roller, and the laser beam sinters the powder to form a new layer. This process continues until the building of the whole object is over.[196] At the end of the steps, the unbound powder is extracted from the product (Figure 11b). This technique does not require the binding of toxic components such as organic solvents, and it is applicable for polymer, ceramic, and multiphase metal materials.

2.9.1.2.1. Polymer. Both semicrystalline and amorphous thermoplastics have been subjected to SLS. Powders of the relevant polymers can be mixed homogeneously with NaCl powder as the porogen followed by sintering. A 3D interconnected flow-channel scaffold reached a high porosity content of 80% and pore sizes of 100−200 μm.[197] During sintering, the unwanted powders might bond to the pore channel interior surfaces, resulting in the actual total porosity of the scaffold being less than the nominally designed porosity. SLS processing parameters, including the laser power, the bed temperature, layer thickness, and hatch distance and the scan speed are the variables that affect the architecture of scaffolds. Biodegradable polymers such as PVA, PCL, PLLA, and PLGA and nonbiodegradable polymers PEEK, PE, and UHMWPE have been processed using the SLS method.

2.9.1.2.2. Ceramic/bioglass. SLS of ceramic materials can be performed either directly using powder or slurry or indirectly in which polymers can be used as binders with ceramic/bioglass powders. In the latter case, sacrificial molten polymers (lower melting point) are used to obtain a green part of ceramic (higher melting point). This actually is the binding mechanism to fuse layers in 3D structures.[198] Selective laser sintering (SLS) or selective laser melting was applied to produce bioglass scaffolds with five different pore geometries with 50% porosity, including gyroid, diamond, cubic, and spherical architectures, to study cell growth. The findings indicated that gyroid and diamond geometries provided sustained cell proliferation for 6 days of incubation compared to other scaffold architectures of cubic, spherical, and X geometries. SLS provides flexibility in the fabricating of complex pore geometries and lattice structures, as they do not require support structures during the part fabrication.[199]

2.9.1.2.3. Surface Selective Laser Sintering (SSLS). SSLS was also developed to manufacture the composite scaffolds of poly(lactic acid) (PLA) and TCP. In this technique, volume absorption of the CO_2 laser does not happen. Instead, the melting of particles occurs by laser radiation in the near IR range (λ= 0.97 μm) by a small number ($\leq$0.1 wt %) (up to 10 W) of carbon or gold nanoparticles uniformly distributed on the polymer surface. This technique prevents overheating of the polymer and the associated changes in the structures.[200] Cylindrical scaffolds with 3 D orthogonal periodic porous architectures were built from PCL using SSLS.[201] In HA−polyamide scaffold, it is reported that the average pore width, the proportion of pores of a suitable size, and open porosity are affected by the layer thickness of the powder bed. When the thickness of the powder layers is large, it can result in a lower extent of fusion between particles, lower densification, and higher open porosity.

2.9.1.2.4. Metals. Introduction of powerful, high-quality lasers has prompted their utilization in fabricating biometallic scaffolds through the selective laser melting (SLM) technique. Structures made of Ni−Ti shape memory alloys for spinal, orthopedic, and dental applications have been fabricated by SLM.[202] For example, as shown in Figure 12ii for Ti_6Al_4V scaffolds, the pore architecture in the horizontal plane could be precisely reproduced from respective CAD models. SEM images did not reveal any closed pores. In most situations, there were no significant differences between the designed and as-fabricated pore and strut sizes.

The final product reached approximately the same level of porosity of 77.5% compared to the porosity value of 76% using microcomputed tomography.[203] Ti_6Al_4V was fabricated via selective laser powder remelting/direct laser forming (DLF) with nominal average pore sizes of 500, 700, and 1000 μm. The particles stuck to surfaces were removed by sand blasting as a finishing step. In the SLM technique for metal powder processing, particles are partially melted and immediately sintered, leading to suboptimal bulk density. However, in DLF, metal particles are completely melted and fused in the focal area of the laser beam, which results in fabrication of parts with a wall density of almost 100% and improved mechanical properties. In DLF, the model of final 3D structure is split into layers with a defined thickness. This technique usually requires minimal surface finishing after manufacturing.[204]

2.9.1.3. Electron Beam Melting (EBM). This technology opened up a new fabrication possibility for the next generation of custom designed and fabricated implants made of metals. EBM has a greater energy density as compared to SLS/SLM. This reduces fabrication times and consequently reduces the manufacturing costs. The major difference between EBM and SLS is that the EBM process uses an electron beam to melt the powder, while SLS and SLM use a laser to melt the powder.

DOI: 10.1021/acsbiomaterials.7b00615
ACS Biomater. Sci. Eng. XXXX, XXX, XXX−XXX

The input of high energy can fully melt the metal powder particles, resulting in a dense wall with better control of the mechanical properties of the fabricated porous parts. This technique also eliminates expensive secondary processing, such as machining, forging, swaging, or forming. Melting the Ti_6Al_4V powder layer by layer by an electron beam and direct solidification of the melted powders creates porous Ti_6Al_4V parts with porosity ranging from 49.75% to 70.32% and pore sizes ranging from 765 to 1960 μm. Parts are fabricated in a vacuum chamber to eliminate impurities. Finally, blasting the porous structure with a high-pressure air stream containing silicon microbeads removes loosely stuck titanium powders.[205] An interesting variation can be to combine EBM with freeze casting. The electron beam melting can be used along with freeze casting technique for fabricating of composite scaffolds, such as the titanium scaffold manufactured via EBM. After manufacturing the porous Ti, a solution of chitosan/HA was cast onto the porous Ti scaffold and then lyophilized. The ultimate scaffold was highly porous with interconnected pore architecture.[206]

2.9.2. Printer Based Manufacturing. 2.9.2.1. 3D Printing. In this technique, an inkjet deposits a binder drop solution over a bed of powder. After the first layer is printed, a fresh bed of the powder layer is deposited and the printing cycle continues. The layers merge together when a fresh layer is printed onto the object until the whole model is created (Figure 11c). This technique has the limitation of removing the internal unbound powder, which affects the porosity content. Ceramics, polymers, and metals can be processed by inkjet 3DP. Biopolymers like starch, dextran, and gelatin are printed using distilled water as the binder. In ceramics, the binder can be water-soluble polymeric binder gluing the particles together and forming 3D objects via drying. During the process of 3D printing, the creation of random microporosity is also possible. The microporosities can be created from the space between the individual granules of powder. The particle size of powders affects the pore size distribution within the powder bed. The pore architecture can be varied via selective bonding of powders. Larger particles have lower surface per volume and are easier to spread. They result in larger pores during fabrication and create more homogeneous parts since the binders can penetrate better into the powder bed. On the other hand, smaller particle sizes are required to achieve finer details in microscale features.[207]

2.9.2.1.1. Ceramics. CaP−collagen scaffolds were manufactured via inkjet printing. CaP powder is bonded by an aqueous binder of phosphoric acid solutions in low-temperature 3D printing where collagen also is dissolved into the binder solution. The solution is delivered from the inkjets, and bonding occurs through a dissolution−precipitation reaction. In this scaffold, use of different average powder sizes of 30, 50, and 70 μm did not significantly affect porosity and pore size distributions, and the final 3D printed scaffold indicated pore sizes in the range of 20−50 μm. To create macropores of 0.5 mm, NaCl was used as the porogen[208] as shown in Figure 12iii-a−d. In another study, low-temperature direct 3D printing was also applied to produce self-setting cement implants of brushite and monetite as bone graft substitutes. Similar blocks with different channel geometry, consisting of either brushite or monetite with open pore channels (diameter of 1.3 mm, depth of 8 mm) and closed pores (diameter 1.3 mm, depth of 6 mm) were fabricated.[209] Parameters including powder characteristics (e.g., particle composition, size, and distribution), binder characteristics, and the process conditions (e.g., binder saturation, layer thickness and orientation, and location of the made-up parts) are controlling factors in this technique. For instance, the macropore interconnectivity, macropore dimension, and model accuracy for calcium phosphate scaffold decreased with the increase of binder saturation level.[210]

2.9.2.1.2. Metals. Titanium scaffolds with bimodal pore sizes and customized geometries are fabricated using suitable binder/powder/solvent systems. The parts can be subsequently sintered in a furnace to obtain enough strength. The surface and internal channels of the scaffolds were further coated by TiO_2 and HA. The total porosity was above 80%, 70% due to the pores created by design and 13−16% due to the pores produced by the process. The size of the pores was 23−25 μm and 1200−1400 μm for pores created by the process and pore created by design, respectively. After sintering, a linear shrinkage of 14−18% had occurred.[211]

2.9.2.1.3. Melt Infiltration after Creating Ordered Polymer Templates by 3D Printing. 3D printing was applied to fabricate a positive template of an acrylic polymer. The temporary polymeric template was infiltrated using a specially formulated sodium chloride (NaCl) slurry. Complete removal of the polymer by burning resulted in a negative NaCl template with the 1 mm × 1 mm square pore spacing. The negative template was used to infiltrate with liquid Mg in a furnace under a high purity protective gas atmosphere. Removal of the NaCl by solvent washing results in Mg porous scaffolds with ordered porosity, reproducing the macroscopic features of the CAD models.[212]

2.9.3. Nozzle-Based Manufacturing. The class of nozzle-based systems is available in a wide variety of configurations. Generally, fine nozzles can be used in complex designs, while larger nozzles are used for conventional sections.[213]

2.9.3.1. Fused Deposition Modeling (FDM). The fused deposition modeling (FDM) process was invented in 1990.[214] In this process, the candidate material in solid filament form is fed into a liquefier in order to create a semiliquid viscous melt. The melt or the softened material is extruded through a nozzle-head to deposit the melt material onto the building platform to form a layer. The liquefier can move in the horizontal *XY* plane generating heat and pump the filament through the nozzle onto the building platform. Once the top layer is completed, the stage moves down to deposit the next layer (Figure 11d). Biopolymers such as poly(ethylene glycol terephthalate)−poly(butylene terephthalate) (PEGT/PBT), PCL/CaP, poly-(glycolic acid) and poly(lactide-*co*-glycolide), hydroxyapatite, β-tricalcium phosphate, and biphasic calcium phosphates using a negative-mold RP technique are examples of materials manufactured using this technique. FDM process has many variations, such as precision extrusion deposition (PED), 3D fiber deposition, precise extrusion manufacturing (PEM), and multiphase jet solidification (MJS). All of them are based on gross material melting. Yet other AM modifications such as pressure-assisted microsyringe (PAM), low-temperature deposition manufacturing, 3D bioplotting, robocasting, direct-writing, and solvent-based extrusion-free forming are most commonly used without material melting.[207,215] Due to possible changes in properties of materials at high temperatures, researchers replaced the melting process with a dissolution process by adding a solvent.[216]

2.9.3.2. LDM. Low-temperature deposition manufacturing (LDM) is a type of melt−dissolution deposition that has the ability to fabricate scaffolds with heterogeneous materials and

DOI: 10.1021/acsbiomaterials.7b00615
ACS Biomater. Sci. Eng. XXXX, XXX, XXX−XXX

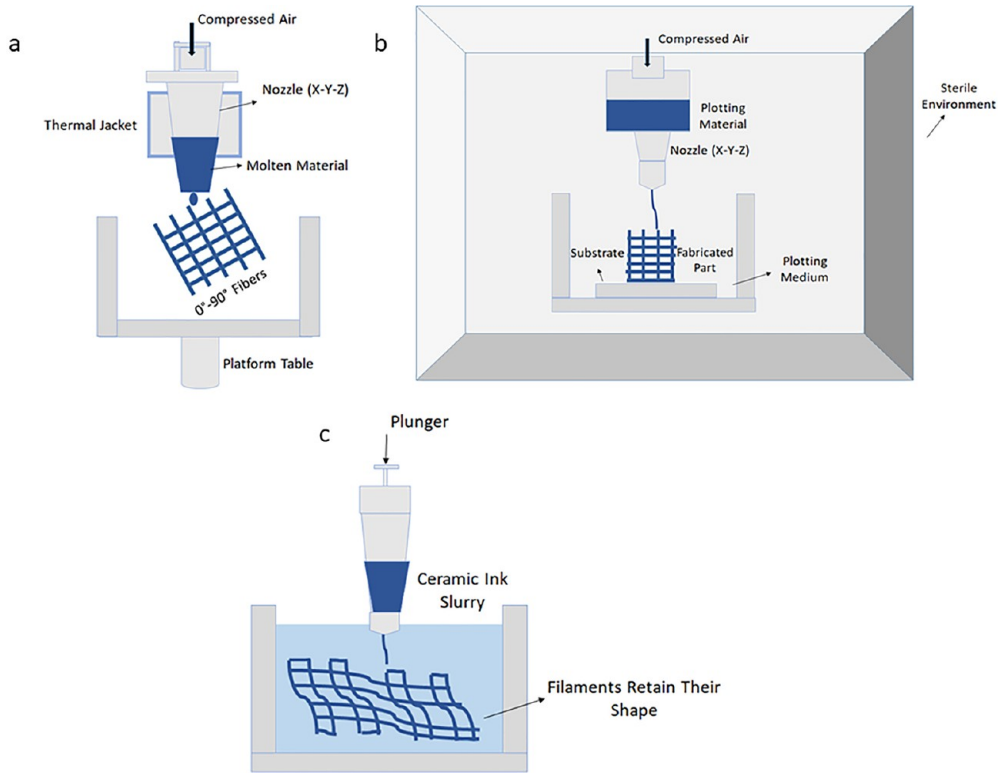

Figure 13. Generation of porosity by design using (a) 3-D fiber deposition, (b) bioplotter, or (c) robocasting.

gradient hierarchical porous structures (Figure 11e). Poly(L-lactic acid)/(tricalcium phosphate) composite scaffolds with porosity content up to 89.6% were fabricated using LDM. The LDM process has the capability to incorporate biomolecules and also preserve bioactivities of scaffold materials due to its nonheating liquefying materials.[217] Multinozzle low-temperature deposition manufacturing (M-LDM) is an improved version of LDM. This incorporates more jetting nozzles into the system. This technique resulted in functionally graded scaffolds with a range of materials and pore morphologies.[133]

2.9.3.3. Bioextruder. The main advantage of this technique is high reproducibility at a low cost. A large number of nozzle diameters ranging from 0.1 to 1 mm can be used.[218] Two different deposition mechanisms are possible in this technique: A rotational one for multimaterial deposition actuates by a pneumatic system. The second type of bioextruder is the single-material deposition, which is based on the extrusion process. Extrusion/deposition process of thin semimolten filaments is controlled by the liquefier temperature (LT), screw rotation velocity (SRV), deposition velocity (DV), and slice thickness (ST). These are important variables in this technique (Figure 11f). Among those parameters, DV and SRV have the highest influence on the porosity of structure for PCL scaffold made by layers of directionally aligned microfilaments.[207,214]

2.9.3.4. Three-Dimensional Fiber Deposition. Three-dimensional (3D) fiber deposition represents a modified 3D plotting.[190] Parameters such as the fiber diameter (depending on the nozzle diameter), the space between two continuous fibers within the same layer, and the thickness of each layer dictate the formation of the final 3D structure[219] (Figure 13a). Recently, hollow fibers were found to be useful in biomedical fields such as controlled tissue growth and drug delivery. 3D fiber deposition has the ability to fabricate hollow fibers with a tailored cavity spacing and wall thickness. This can be accomplished by extruding a molten blend of two or more miscible and immiscible polymers and by taking advantage of encapsulation of one by the other in the molten state. Parameters such as the relative contents of the constituents in the blend, the blend composition, and the extrusion nozzle diameter dictate the dimensions of the hollow cavity diameter and shell thickness. High strength cell-laden 3D structures with built-in microchannels were fabricated using hollow filaments based on calcium alginate. Controlling the cross-linking time can be used to fuse adjacent hollow filaments in layer-by-layer fabrication of the 3D structure. Curved, straight, stretched or fractured filaments can be formed by changing the filament extrusion speed or the platform movement speed.[220]

2.9.3.4.1. Metals. 3D porous Ti_6Al_4V scaffolds were directly fabricated by 3D fiber deposition (3DF). Scaffolds with different structures were fabricated by changing fiber spacing and fiber orientation (or deposition angle). 3DF is able to provide good control and reproducibility of the desired degree of porosity and the 3D structure.[221]

2.9.3.5. Bioplotter/Three-Dimensional Plotting. This technique was developed to produce scaffolds for soft tissue engineering and hydrogel purposes.[222] Computer-controlled deposition through a moving extruder head (*x*-*y*-*z* control) of material onto the stationary surface can create a layer-by-layer deposited object.[222] Continuous dispensing of microstrands or a discontinuous dispensing of microdots is possible via this technique.[223] Compressed air is applied to eject a liquid or paste in plotting liquid media. The strand thickness can be varied by altering material viscosity, deposition speed, tip diameter, and the applied pressure[215] (Figure 13b). Cell-laden gelatin−methacrylamide scaffolds were bioplotted with 100% interconnectivity. Increasing the gelatin concentration resulted in faster physical gelation and, therefore, more spherically deposited strands and pores. Additionally, precise temperature

DOI: 10.1021/acsbiomaterials.7b00615
ACS Biomater. Sci. Eng. XXXX, XXX, XXX−XXX

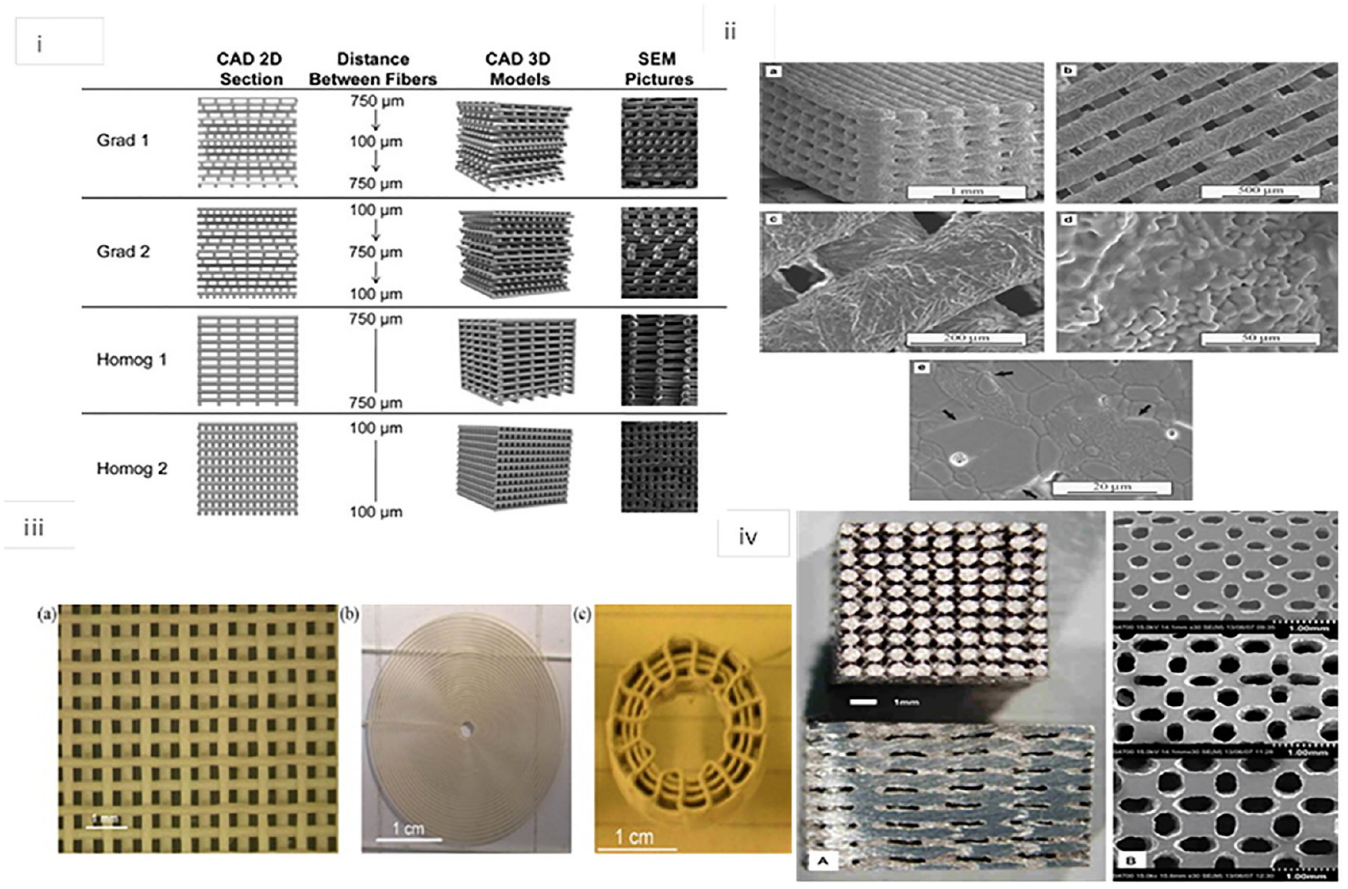

Figure 14. (i) Three-dimensional plotted scaffolds with controlled pore size gradients: CAD 2D sections, pore size along the scaffolds, 3D models, and SEM pictures for both homogeneous and pore size gradient PCL scaffolds designed and produced by 3D plotting technique.[244] Reproduced with permission from ref 244. Copyright 2011 Elsevier. (ii) The morphology of mesoscale porous β-tricalcium phosphate scaffolds fabricated via robocasting and then sintered at 1300 °C for 2 h: (a) general view, (b) *XY* plane view, (c) detail of the β-TCP rods, (d) detail of the rod surface, and (e) cross-section view showing the microstructure within the rods. Note in part e the presence of microcracks (marked by arrows) and the clearer secondary phase related to liquid present during sintering.[227] Reproduced with permission from ref 227. Copyright 2006 Elsevier. (iii) Structures fabricated by solvent-based extrusion free forming: (a) periodic woodpile structure (4 layers) fabricated with LMT ($La(Mg_{0.5},Ti_{0.5})O_3$) paste; (b) Circle ring structure (2 layers) fabricated with quartz paste; (c) cylindrical structure (8 layers) with alumina paste.[228] Reproduced with permission from ref 228. Copyright 2010 Elsevier. (iv) Porous titanium scaffolds fabricated via indirect RP: (A) Top and side profiles of a porous titanium scaffold with 59.1% porosity, (B) SEM of porous titanium scaffolds with pore sizes of 200, 300, and 400 μm. The scaffolds' porous characteristics were governed by a sacrificial wax template, fabricated using a commercial 3D-printer.[239] Reproduced with permission from ref 239. Copyright 2008 Elsevier.

control during the printing process creates the possibility to fabricate constructs with an interconnected pore network.[224] Examples of uniform and gradient pore-size containing scaffolds with different pores structures and sizes are shown in Figure 14i-a–d. Robocasting is also developed based on the bioplotter principle, which is discussed in the following.

2.9.3.6. Robocasting/Direct Writing Assembly. This is a robot-assisted deposition technique and uses filaments of materials. A computer controls the deposition of highly concentrated (typically 50–65 vol % ceramic powder) colloidal ceramic slurries.[207] In most cases, the robocasting setup has a stationary dispensing head, while the fabrication platform moves in the planar and vertical field.[215] This technique is different from FDM as it does not rely on solidification or drying to retain its shape after extrusion (Figure 13c).

The flocculated colloidal suspensions (or gels) are used as inks for robocasting of ceramics. Filament formation and initial shape retention are achieved by tailoring the ink viscosity, yield strength, and drying kinetics.[225] Robocasting in air enables ink deposition through nozzles with diameters exceeding 500 μm.[226] β-TCP scaffolds consisting of a 3-D network of β-TCP rods with an average diameter of ~200 μm and with tailored geometry and mesoscale porosity were fabricated with this technique, which is shown in Figure 14ii-a–e. For this study, concentrated β-TCP inks suitable for this fabrication route were optimized. Powder size and morphology was shown to play a major role in ink performance. Powders with reduced particle size and low specific surface area are more suitable for ink preparation.[227] This scaffold was printed at 10 mm/s speed through a tip of 250 μm diameter. An average linear shrinkage of around 20% was measured after sintering, and spacing between lines was around 75 μm. Typically, robocasting is a suitable technique for fabricating structures with characteristic feature sizes (i.e., line diameter and spacing) ranging from 100 μm to 1 mm.[220]

2.9.3.7. Solvent-Based Extrusion-Free Forming. This is a ceramic processing technique developed to produce bioceramic scaffolds. In this technique, a continuous flow of materials in the form of paste or particulate slurries is dispensed onto the surface with a three-axis table and extruder mounted on the *z*-

DOI: 10.1021/acsbiomaterials.7b00615
ACS Biomater. Sci. Eng. XXXX, XXX, XXX–XXX

axis. A 3D motion system is also incorporated with the nozzle. Solvent-based extrusion free forming is a relatively simple process in which phase change is based on solvent evaporation. Paste with high mechanical strength is also prepared by mixing appropriate polymers, ceramics, or metals and a solvent with specific ratios.[207] During extrusion, the material is in the liquid state so that extrusion pressure is low. After extrusion, the material changes rapidly into a solid state without sagging or other deformation defects. Control of colloidal forces is related to liquid-to-gel transition. To generate highly concentrated stable dispersions, the parameters of pH, ionic strength, or solvent quantity can be improved. Various suspensions for free forming, such as poly(vinyl pyrrolidone) (PVP) sol−gel ink and polyelectrolyte ink such as poly(ethylenimine) (PEI) have been processed.[213,228] Figure 14iii shows different examples of building a complex ceramic 3D structure with different shapes and porous characteristics via this technique.

2.9.3.8. Direct Writing/Direct Ink Writing. A wide range of inks can be patterned in both planar and 3D shapes where feature sizes are smaller than those achieved with 3D inkjet printing. In this technique, which is an extrusion-based system, compressed air is used to eject inks with controlled rheological properties through an individual nozzle. The dispensing process is controlled by motion control software, which provides accuracy and reproducibility of *XYZ* positioning of the dispensing nozzle. Printing speed and pressure, which depend on ink rheology and nozzle diameter, are the viable parameters. A wide range of inks including colloidal suspensions and gels, nanoparticle-filled inks, polymer melts, fugitive organic inks, hydrogels, sol−gel, and polyelectrolyte inks have been processed via direct-write assembly.[207,226] Chitosan scaffolds of diamond and orthogonal geometries led to the creation of different pore morphologies in scaffolds. The scaffold showed 76% and 79% porosity content, respectively, and pore size of 150 to 600 μm.[229] Poly(lactic acid) and a bioactive CaP-glass with two patterns of orthogonal and displaced double layer were fabricated in order to study pore size and pore distribution in the axial and transverse direction. The idea behind choosing different printing patterns was to decrease the pore size in the axial direction and increase that along the transverse one. Composite scaffolds showed lower porosity of 70%, whereas the polymer scaffolds (just PLA) with the same geometry showed 75% of porosity. This suggests that a lower content of polymer (the shrinkable phase during solvent evaporation) in the composite led to less shrinkage, smaller pore size, and lower porosity. Moreover, in both patterns, these scaffolds showed a combination of porosities from macroscale due to the initially designed pore size to the micro- and nanoscale due to the presence of glass particles and to the pores left by solvent evaporation.[230]

2.9.3.9. Bioprinting. Bioprinting is a versatile nozzle based RP technique that enables generation of 3D heterogeneous structures by precisely depositing polymers, biomolecules, and cells. The advantage here is its ability to construct heterogeneous tissues such as osteochondral tissues containing live cells and bone.[231] Using this method, (CAD/CAM)-based bioprinters can construct organs or tissues of viable cells and biomaterials within the exact space where they anatomically exist.[232] Composite mixtures of osteoblast-encapsulated collagen hydrogels and chondrocyte-encapsulated HA hydrogels were subjected to this process. The idea was to fabricate three-dimensional osteochondral constructs. The bioprinted collagen-hydrogel and HA hydrogels showed pore size diameters of 59.3 ± 33.7 μm, and 114.9 ± 95.3 μm, respectively. In vitro results indicated that viability and functions of each cell type were well maintained within the 3D structures for up to 14 days.[233] In another study, a cell-laden structure consisting of a PCL framework, chondrocytes, and osteoblasts was also produced with this technique. In the PCL scaffold, PCL line width was adjustable from 50 to 275 μm by changing the nozzle size, pressure, and feed rate resulting in pore sizes ranging from 50 to 600 μm. Interestingly, separately dispensed cells remained in position up to 7 days without significant fusion; however, conventional cell seeding methods are unable to achieve a separated cell arrangement. The flexibility of this technique leads to the generation of sophisticated designs and concurrently enables the direct recruitment of live cells.[234]

2.9.4. Indirect RP. Molds designed by a 3D CAD system with various pore patterns (round and square cross section, perpendicular and 60° orientation) can be manufactured via the 3D printer technique and subsequently impregnated with calcium phosphate slurries.[235] Wax inkjet printing allows for processing calcium phosphates into scaffolds with tailored architecture of pores and resulting-in mechanical properties. Molten wax is printed dropwise layer by layer on a building platform by a moving print head. After one layer is completed, the wax is built to a predefined slice thickness, the building platform is lowered, and the next layer is printed. Once the printing process is finished, the support wax and also residual wax are removed by a solvent. Then, the negative mold (printed wax mold) is used as the mold for casting a low viscosity ceramic slurry or cement paste. After drying the ceramic slurry, the wax, and the binder are removed by pyrolysis. Finally, the ceramic mold is sintered to yield final product.[235,236] This technique was also adopted for a composite of ceramic-polymer. The manufactured ceramic mold was used to prepare ceramic−polymer composites via casting of the polymer.[66,235,237,238] Indirect 3D printing of mold for a porous metallic scaffold was employed to produce 3D printed titanium scaffold. The porous architecture of scaffolds was controlled by a sacrificial wax template. By altering the wax design of templates, pore sizes ranging from 200 to 400 μm were produced as shown in Figure 14iv. The scaffold is a negative replica of the wax-template with interconnected networks of pores. The predominant factors governing the pore architecture in titanium scaffolds were the diameter of the struts in the sacrificial wax template unit-cell, as well as their height and the spacing. Both macro- and micropores existed in the as-fabricated scaffold. The powder metallurgical parameters were improved to generate fully interconnected pore networks with reproducible porosity and pore size of the titanium scaffolds. The controlling parameters include slurry concentration, compaction pressure, and sintering temperature.[239]

3. EFFECTS OF POROUS BONE SUBSTITUTION ON BIOLOGICAL RESPONSE

Macroporosities play major roles in responses in vitro with regard to cell penetration and in vivo with respect to tissue in-growth, vascularization, and osteointegration. If pores are too small, cell migration is limited, resulting in the formation of a cellular capsule around the edges of the scaffold and osteochondral ossification. If pores are too large, there is a decrease in specific surface area reducing the ligand density available for cells to bind. On the other hand, the pore sizes in the range of nano- and micrometers tend to modulate cell

DOI: 10.1021/acsbiomaterials.7b00615
ACS Biomater. Sci. Eng. XXXX, XXX, XXX−XXX

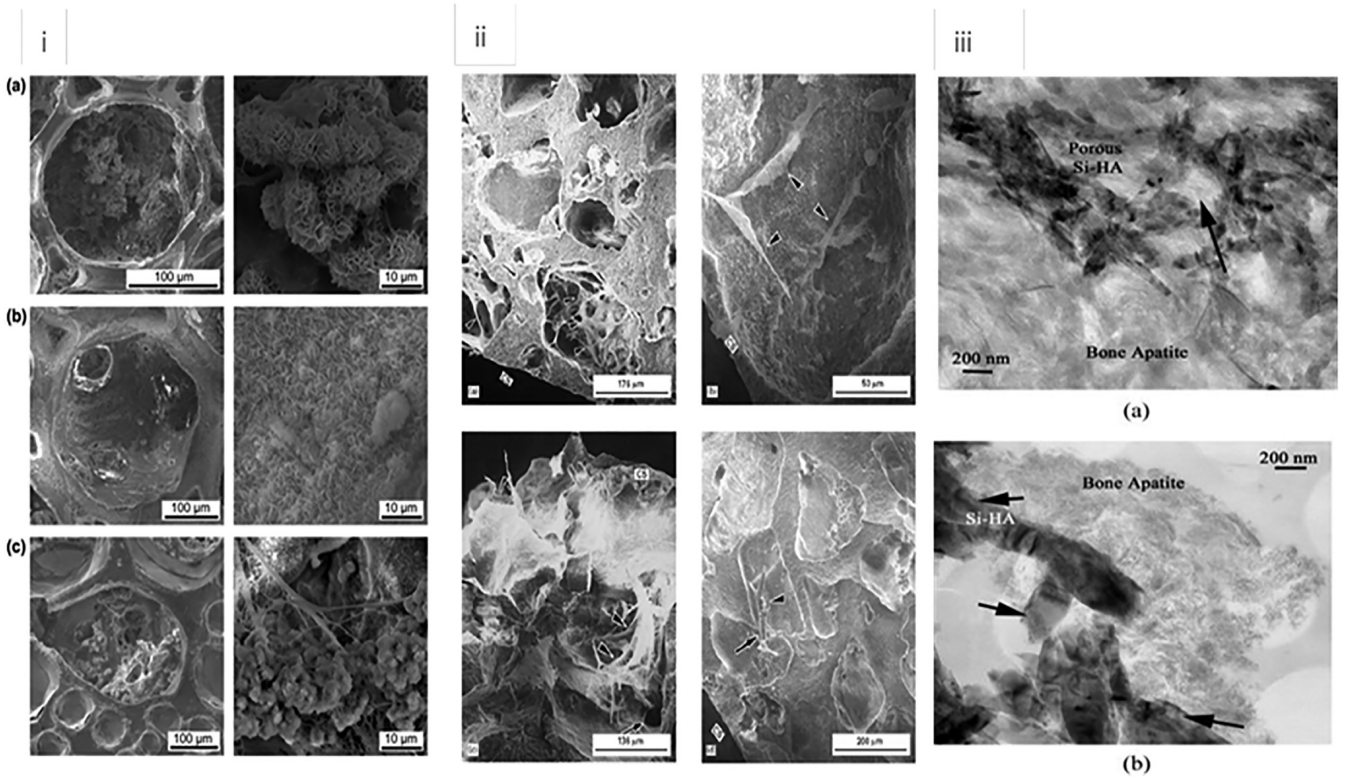

Figure 15. (i) Three-dimensional scaffolds cultured with preosteoblasts at 28 days for both uniform (inverse opal scaffolds) and nonuniform pore sizes and structures: inverse opal scaffolds with pore sizes of (a) 211 and (b) 313 μm, respectively, and (c) a nonuniform scaffold. Magnified views are shown in the right column.[246] Reproduced with permission from ref 246. Copyright 2010 American Chemical Society. (ii) Fracture surfaces of HA and β-TCP scaffolds with the same porosity of 50% and a mean pores size of 100−300 μm, and a mean interconnection size of 30−100 μm: (a, b) after 14 days of culture, and (c, d) after 28 days of culture. (a) β -TCP, showing numerous osteoblasts (short arrows) colonizing macropores near the contact surface (CS) between material and cells, (b) HA, showing a few osteoblasts (short arrows) located inside the pores near the CS, (c) β -TCP, showing osteoblasts (short arrows) going through the porous interconnection (long arrow), (d) HA, showing an osteoblast (short arrow) spreading across an interconnection (long arrow) and connecting two macropores.[253] Reproduced with permission from ref 253. Copyright 1999 Springer. (iii) The structure of the bond between bone and porous silicon-substituted HA shows organized crystallites of bone apatite after 6 weeks in vivo. (a) Apatite crystallites penetrated into the strut porosity (arrow), and also (b) apatite crystallites overlaid the Si-HA granules displaying darker contrast (arrows).[255] Reproduced with permission from ref 255. Copyright 2006 John Wiley and Sons.

differentiation and increase the protein adsorption. In view of these observations, a brief discussion on the correlations between pore sizes and the respective biological responses is provided in the following.

3.1. Macroporosity. *3.1.1. Pore Size and Porosity.* The effect of different porosities and pore sizes on the extent of osteogenesis in vitro and in vivo has been studied. In one study, the influence of the porosity (25%, 65%, and 75%) of β-tricalcium phosphate (TCP) ceramics on osteogenic differentiation of mesenchymal stem cells (MSC) was investigated both in vitro and in vivo. Alkaline phosphate (ALP) activity, a marker for osteogenic differentiation, was monitored in the aforementioned samples. Of the samples evaluated, the ALP expression was higher for the 65%, followed by 75% and 25% porosity containing samples. However, the specific ALP expression increased from day 1 to 21 and reached similar levels in all three specimens in vitro.[240] This suggests that higher porosity of scaffolds does not necessarily translate to a higher ALP activity. There are other important factors such as distribution of pores, size of the pores, and surface structure that would play an important role in osteogenic differentiation. There have been several studies focused on finding the optimum pore size. The minimum recommended pore size for bone substitute biomaterial is 100 μm.[241] Titanium plates with four different pore sizes of 50, 75, 100, and 125 μm were implanted in rabbit femoral defects under non-load-bearing conditions. The results indicated that bone in-growth was similar in all the pore sizes suggesting that 100 μm may not be the critical pore size for non-load-bearing conditions.[242] As opposed to that, there have been reports of the ability of the cells to proliferate and differentiate on porous Ti scaffolds with larger pore sizes between 313 and 390 μm. This resulted in enhanced ability to restore cancellous bone defects due to higher proliferation and bone in-growth compared to those with average pore sizes of 180 μm.

Nevertheless, porous titanium with an average pore size of 180 μm promoted more cell differentiation at the beginning.[243] Similarly, the effect of optimum pore size in scaffolds of collagen−glycosaminoglycan (CG) was investigated on osteoblast adhesion and early stage proliferation up to 7 days postseeding. These composite scaffolds with pore sizes ranging from 85 to 325 μm showed maximum cell numbers in scaffolds with the largest pore size of 325 μm. However, an early high cell number was also reported for the scaffolds with a mean pore size of 120 μm at time points up to 48 h postseeding.[80] This shows the importance of smaller pore size in the scaffold for initial attachment and bigger pore size for cell penetration and sustained cell proliferation. In view of these observations, gradient scaffolds were recently developed, which have shown higher cell seeding efficiency compared to monomodal

DOI: 10.1021/acsbiomaterials.7b00615
ACS Biomater. Sci. Eng. XXXX, XXX, XXX−XXX

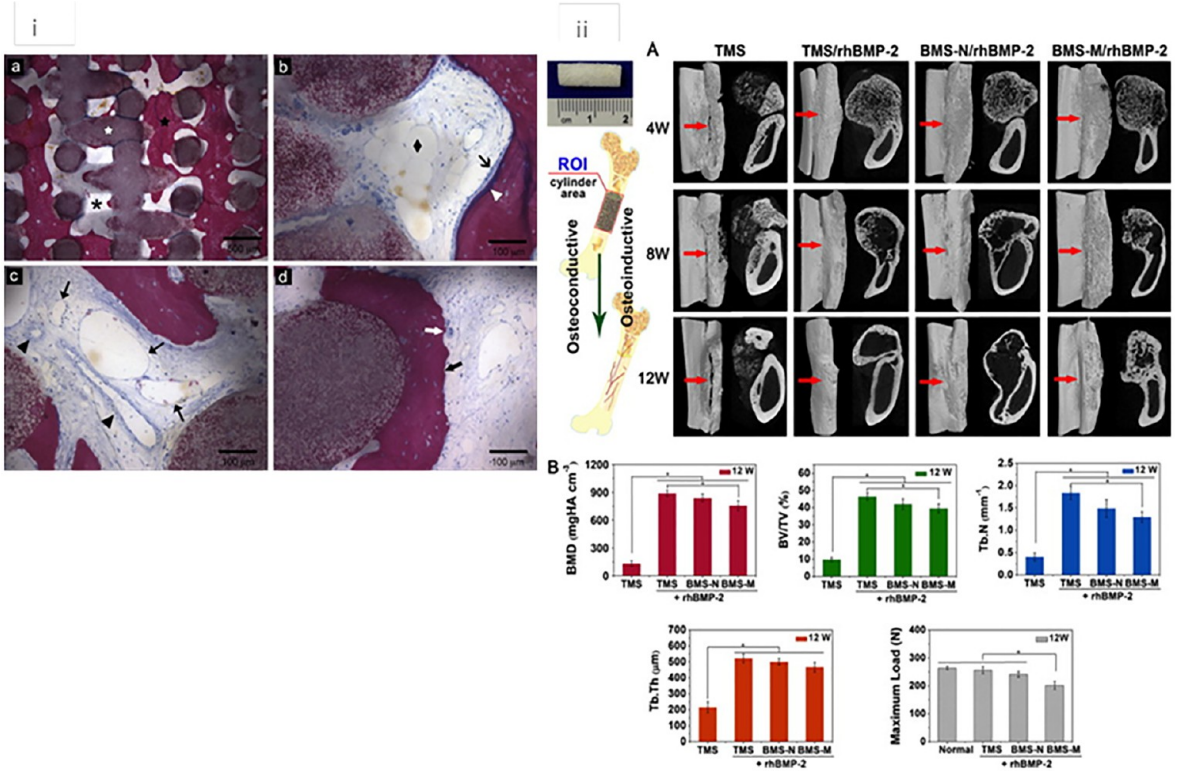

Figure 16. (i) Histological images show bone in the macropores. (a) Bone (∗) is present within scaffold macropores (★) and directly apposes scaffold rods (☆). (b) Aligned osteoblasts (→) deposit osteoid (▷) that subsequently undergoes mineralization and adipocytes constitute some of the loose connective tissue in the macropore space (⧫). (c) Blood vessels of varying sizes, including both veins (▶) and arteries (→), are present in macropores. (d) Osteoclasts (⇒) resorb bone, leaving scalloped edges (→). Mineralized bone, pink/red; osteoid, blue/purple; soft tissue, blue; cell nuclei, dark blue; cell cytoplasm, light blue. This shows the combined effect of BMP-2, a potent osteoinductive growth factor, and multiscale porosity BCP scaffolds, which implanted into porcine mandibular defects for 3, 6, 12, and 24 weeks.[257] Reproduced with permission from ref 257. Copyright 2010 Elsevier. (ii) Orthotopic bone formation in vivo on trimodal scaffolds (TMS) (size of segmental bone defect, 16 mm): (A) Micro-CT analyses at week 4, 8, and 12. (B) Quantitative histograms of bone formation at week 12. BMD, bone mineral density; BV/TV, bone volume/total volume; Tb Th, trabecular thickness; Tb N, trabecular number; Maximum load, the maximum bending load of the regenerated rabbit radius. TMS/rhBMP-2 showed a rapid bone bridging, basically recanalized medullary cavity, and completed reunion of the defects at week 4, 8, and 12, successively, while both the bimodal groups exhibited imperfect regeneration outcomes. Asterisks indicate significant differences, $p < 0.05$.[259] Reproduced with permission from ref 259. Copyright 2016 Elsevier.

scaffolds,[244] while higher proliferation and differentiation of MSCs at 14 days were observed on the monomodal PCL scaffolds.[245] This likely is due to more nutrition access for cell proliferation.[245] As opposed to those studies mentioned in the above, it is reported that the scaffolds with uniform (inverse opal scaffolds) size revealed a higher diffusion rate, a uniform distribution of cells, and a higher degree of differentiation of cells, as can be seen in Figure 15i. Such structures (pore size ∼211 μm) contained a large amount of inorganic and organic ECM. Very little fibrous organic ECM was deposited on the walls of pores of average size of 311 μm (Figure 15i-b). Also, most of the small pores were full of fibrous organic ECM (Figure 15i-c).[246]

Recently, there has been interest toward finding an optimum pore size in vivo, resulting in initial angiogenesis with subsequent to osteogenesis. The repair of bone defects depends on sufficient vascularization. Biphasic calcium phosphate particles with pore sizes in the ranges 40−70, 70−140, 140−210, and 210−280 μm were implanted in cranial defects, and angiogenesis and vascularization were monitored for 28 days. The results showed that the functional capillary density was significantly higher with ceramic particles with pore sizes between 210 and 280 μm than those with pore sizes less than 140 μm. Also, the newly formed bone deposited within the implants increased as the pore size increased.[247] Likewise, the results on porous β-TCP with different macropore size ranges of 300−400, 400−500, 500−600, and 600−700 μm and same interconnection size of 120 μm showed that the amount of fibrous tissue in-growth increases with the decrease of the pore size.[248] Thus, this study showed that the diameter of a pore smaller than 400 μm limits the growth of blood vessels and results in a smaller blood vessel diameter.[248]

3.1.2. Interconnectivity and Permeability. Interconnectivity is required for the transport of nutrients and waste for bone growth. Permeability is related to interconnectivity or accessible pore size to ensure ease of flow. From this perspective, the aforementioned terms interconnectivity and permeability are synonymous. Permeability depends on pore shape, orientation, and size.[249,250] For instance, the permeability of collagen−GAG scaffolds increased when the pore size increased.[251] Interconnectivity and permeability affect molecular transport, and non-interconnected pores lower the diffusion efficiency. An in vivo study on porous Ti scaffolds revealed that well-differentiated cells prefer pores with wider pore openings than those with narrow opening, which inhibit tissue differentiation in pores.[252] Two scaffolds of hydroxyapatite (HA) and β-tricalcium phosphate (β-TCP) with the same porosity content of about 50% and a mean pores size of 100−

DOI: 10.1021/acsbiomaterials.7b00615
ACS Biomater. Sci. Eng. XXXX, XXX, XXX−XXX

300 μm but different interconnection sizes of 30−100 μm were fabricated. The in vivo results revealed that the 20 μm interconnection size only allows cell penetration and chondroid tissue formation. However, the size of the interconnections must be over 50 μm to favor new bone in-growth inside the pores, as shown in Figure 15ii.[253] In Figure 15ii-a−d, the cellular morphology is similar for both biomaterials. A cellular layer spreads on the surfaces of the materials evenly covering the opened macropores. On the broken surface of discs, osteoblasts are observed to colonize the macropores. After 28 days of culture, their penetration is greater than that at 14 days (Figure 15ii-a,b). Some osteoblasts were observed in the interconnections (Figure 15ii-c,d).

3.2. Microporosity. Recently there have been interesting efforts toward the development of biomaterial with multiscale osteointegration ability.[53] This results in the fabrication of scaffold with multiscale porosity of macro- and micropore (<10 μm) size.[31,53] The combined macroporosity with microporosity interconnectivity translated into a scaffold with no "dead space", or discontinuities of bone. Multiscale osteointegration in the scaffolds with macroporosity increases bone-scaffold interface area by orders of magnitude compared to scaffolds without microporosity. There has been some evidence of bone growth into micropores at the periphery of scaffolds[254,255] and also deeper into struts.[53,256] TEM images of Figure 15iii-a,b show organized crystallites of bone apatite apposed to the mesoporous Si-HA implant and penetrating into the strut porosity after 6 weeks in vivo. Interestingly, in several regions, the apatite crystallites did not appear to directly abut against the implant surface, but instead they appeared to overlay the Si-HA [Figure 15ii-b]

The results from in vivo application of biphasic calcium phosphate scaffolds infused with bone morphogenetic protein-2 (BMP-2) showed that osteointegration into macropores improves when struts contain micropores (Figure 16i).[257] Figure 16ii-a−d shows histological images of biphasic calcium phosphate scaffolds implanted into porcine mandibular defects. Figure 16i-a shows that the mineralized bone located in macropores is directly integrated with calcium phosphate struts. Figure 16i-b depicts that osteoblasts align along an osteoid seam adjacent to the mineralized bone. The figure also shows the presence of adipocytes within macropores. Blood vessels, including arteries and veins of varying sizes, are visible within macropores (Figure 16i-c). Finally, Figure 16i-d presents clear proof that osteoclasts actively resorb mineralized bone, as evident by the presence of scalloped edges.

A study of porous HA scaffold with two different microporosities of 10% and 20% with total nominal porosity of 70% and 80% was performed. The results showed that within a short-term after implantation of the bone graft the scaffold with higher microporosity of 20% for both nominal porosities presented higher early bone integration and mineral apposition after 3 weeks. However, at 24 weeks a dominant factor in maintaining a high bone volume was total porosity or strut porosity. The 80% porous HA with 20% microporosity was able to maintain a high level of bone volume; while there was no significant difference between 10% and 20% microporosity for the 70% macroporous scaffolds. This suggested that higher microporosity of scaffolds can accelerate mineral apposition and osteointegration.[258] In a recent study, a trimodal macro-, micro-, and nanoporous bioglass scaffold (TMS) was loaded with BMP-2. A mesoporous structure with an average mesopore size of 7.5 nm was optimum for the entrapment of BMP-2 molecule to achieve sustained release and enhance bioactivity.[259] The results showed excellent cell attachment, in-growth, and osteogenesis in vitro.[259] Figure 16 ii-A reveals extensive bone formation throughout the entire defect site loaded with BMP-2, while absence of BMP-2 causes no satisfactory healing. Figure 16ii-B shows quantitative orthotopic bone formation at week 12. The importance of mesopores (and the sustained release of BMP-2) is clearly shown by the lowest quantity of regenerated bone in the bimodal scaffold BMS-M/rhBMP-2 group.

Habibovic et al.[209] studied porous HA and BCP and reported that there are synergic influences from microporosities. A higher microporosity was inherently linked with a higher specific surface area and hence could cause a major dissolution of ions. The higher ion dissolution can facilitate apatite formation in vivo, causing the coprecipitation of endogenous proteins such as BMPs. The osteoinductivity in macro- and microscaffolds was caused by the ability of scaffolds to entrap and adsorb certain types of serum proteins circulating around the biomaterial, which eventually controls cell fate.[260] Therefore, a combination of open macropores and interconnected micro- and nanopores within a scaffold seems to lead to a rough topography that encourages higher focal adhesion sites for cells to attach and interact with the scaffolds. This eventually can translate into cellular behavior such as adhesion, migration, proliferation, and differentiation, which results in osteoconductivity and osteoinductivity of scaffolds.[261,262]

3.3. Incorporation of Biomolecules for Drug Delivery. The porous structure inherently has the ability to incorporate different types of therapeutic agents and regulate the release profile. The pore size can be a controlling factor to customize the release rate and release fraction of the exogenous growth factors and other therapeutic agents. Scaffolds with different macroporosity sizes between 180 and 720 μm showed a faster release profile and higher release of BMP2 for 180 μm compared to scaffolds with bigger pore sizes of 720 μm. Releasing from porous material requires diffusion and transfer of therapeutic agents. Diffusion of drug molecules is the main mechanism of drug release. Larger pores in a scaffold means there is more space in which drug molecules can diffuse. More molecules must be released from the scaffold to fill these larger pore spaces to reach the same concentration level as the smaller pores. Thus, the average concentration of released growth factors within the bigger pores is lower than that within the smaller pores.

The therapeutic agents can be incorporated into ceramics and polymer scaffolds through RP techniques, adsorption into porous scaffolds using particles as carriers, and also self-setting ability in the cement.[263,264] Recently, the role of microporosity is also examined in drug release and proved to be quite effective in maintaining the sustained release profile of exogenic factors.[265] In one study, the role of nanopores in a mesoporous titania film in Mg adsorption and release was investigated.[266] Mesoporous films with average pore sizes of 2, 6 and 7 nm were fabricated and used as implant coatings in order to control the administration of magnesium to enhance initial osteoblast proliferation in vitro. Results showed a sustained release from all types of porous films. Higher magnesium adsorption was observed in 2 and 7 nm films, and the 7 nm film had the greatest effect on osteogenesis.[266]

3.3.1. Resorption of Bioceramics. The resorption behavior of a bone graft substitute is affected by both chemical composition and ultrastructure. Macropore size influenced the

DOI: 10.1021/acsbiomaterials.7b00615
ACS Biomater. Sci. Eng. XXXX, XXX, XXX−XXX

ceramic resorption and bone in-growth. β-TCP scaffolds with four different pore sizes of 150, 260, 510, and 1220 μm were fabricated. Resorption was significantly faster for a sample with 510 μm pores compared to the others, but it was also associated with less bone formation and more soft tissue.[267] High porosity was seen to facilitate the resorption process as the pores' external and internal surface areas are exposed to the medium. This increases Ca and P ion release into the intercellular medium for several micrometers beyond the graft.

Bohner and Baumgart[268] developed a theoretical model, which discussed the relationship between resorption and pore size. They determined that in resorbable bioceramics with a pore size range of 50−800 μm, it is the volume fraction of macroporosity, the size of the implant, and the size of the pore interconnections that are important, as opposed to the average pore size. However, in nonresorbable materials, the sizes of pores and their content are equally important.[267] Recently, the effect of different microporosity content (e.g., 10%, 25%) on in vivo resorption of β-TCP scaffolds was also investigated, and no significant differences were observed.[269]

4. MECHANICAL INTEGRITY OF POROUS SCAFFOLD

For proper implantation and tissue regeneration and implant success, there must be a balance between porosity requirements for transport of nutrients with resulting in-growth and mechanical properties during and after healing.[270] An important requirement of a synthetic bone graft substitute is that it should have a similar strength to that of the cortical or cancellous bone being replaced. Furthermore, the moduli of elasticity of the artificial substitute and the original bone should match. This prevents stress shielding as well as protects against fatigue fracture under cyclic loading.[271,272] Although the mechanical properties of scaffolds have been widely reported in the literature, most studied mechanical properties have focused on evaluating the strength and elastic modulus in compression of the as-fabricated scaffolds or scaffolds that were immersed in an aqueous phosphate solution such as a simulated body fluid.[273−275] Less attention has been paid to some load-bearing bones, such as long limb bones, that are subjected to multiple loading modes as well as cyclic loading.[273] In addition, data for the time-dependent mechanical response in vitro and in vivo[273] and strength reliability or the probability of failure especially for brittle materials under a given stress are other critically important factors for the design of scaffolds for load bearing applications.[270,275] The introduction of new and more sophisticated techniques for processing of scaffolds has allowed for the fabrication of tailored porous architectures with improved mechanical properties. In contrast, conventional methods generate random pores. However, by carefully monitoring the processing parameters, some kind of control over the porous architecture can be achieved. For example, in ceramic materials, this has been achieved by controlling the sintering temperature.[16]

The degradation rate of the scaffold plays an important role when comparing the properties of the degradable scaffold with the in-grown bone. For slowly (or non) degradable materials over the period of many weeks to years (e.g., HA), it is imperative that the strength and stiffness would increase with bone in-growth.[270]

Below are some examples in which the mechanical properties can be tuned to match the growth of bone tissue through an accurate design of porous characteristics.

Generally, it is demonstrated that pore size, fraction, distribution, interconnection, and architecture have an influence on the scaffolds' mechanical properties. An increase in the void volume content, macropore size, and interconnection in scaffolds with either designed pores or random pores results in a reduction in mechanical strength of the scaffolds.[276−278] For instance, studies on HA scaffolds showed that for a given pore fraction, smaller pore sizes yielded consistently higher compressive strengths.[279,280] Scaffolds based on blends of starch with poly(ε-caprolactone) were fabricated in homogeneous forms of 750 and 100 μm pore size and a gradient porous structure comprised of both 100 and 750 μm. The gradient macroporous scaffolds showed intermediate mechanical strength compared with those with homogeneous pore size distributions. Scaffolds with smaller homogeneous pore sizes presented the highest stress, and the scaffolds with larger homogeneous pore size showed the lowest values.[244] This suggests that gradient scaffolds have the ability to tailor mechanical properties of final scaffolds in a more complex way than homogeneous scaffolds, which may lead to a better compromise between enhanced mechanical properties and necessary pore size for biological response.

The effect of micropore size on mechanical properties was also investigated. HA scaffolds showed higher bending and compression strength in the presence of smaller micropores of an average size 5 μm compared to 16 μm.[270] This suggests that the composite scaffolds may yield tougher scaffolds through providing a mechanism to impede crack propagation.[28] In a study,[270] the mechanical behavior of porous HA and HA scaffolds with multiscale porosity was evaluated in order to investigate effects of average micropore size on strength and reliability. The results showed that HA scaffolds with multiscale porosity had strengths (8 MPa) closer to that of trabecular bone (1−7 MPa).[27,28] However, these values are much lower than the 140−200 MPa range reported for cortical bone. The microporous HA scaffold possessed better elastic properties than those of cortical or trabecular bone. For example, the elastic moduli of microporous HA scaffold from this study (28−30 GPa) was greater than the reported moduli for trabecular (11.4−18.1 GPa)[27,28] and cortical bone (15.8−25.9 GPa).[27,28] It is reported that in order to more closely match the modulus of cortical or trabecular bone, the microporosity content should be increased by decreasing the sintering temperature and time.[281,282] It is noted that the strength can also be modified by modifying the strut diameter and the spacing between the pores.

Pore morphology, orientation, such as aligned pores or stacking direction, hierarchy, and anisotropy have also been shown to significantly affect the mechanical properties. Scaffolds based on poly(L-lactic acid) (PLA) and ceramic fillers such as hydroxyapatite (HA) or β-tricalcium phosphate (β-TCP) were fabricated through foaming techniques. The structure showed anisotropy in morphology with pores oriented along the foaming direction. Compressive analysis demonstrated anisotropy in mechanical behavior, with an axial modulus up to 1.5 times greater than the transverse modulus.[283] In a recent study, the effects of pore morphology and pore shape anisotropy were studied on the fatigue resistance, failure reliability, flexural strength, and compressive strength in a highly porous three-dimensional glass−ceramic scaffold and compared to the strength of trabecular bone such as segmental bone defects (SBDs).[284] The scaffold was fabricated with direct ink writing with a variety of porosity

DOI: 10.1021/acsbiomaterials.7b00615
ACS Biomater. Sci. Eng. XXXX, XXX, XXX−XXX

contents (~50%, ~55%, ~60%, and ~70%; the diameter of the deposited struts at ~540 μm). The resultant scaffolds with anisotropic hexagonal design demonstrated a high fatigue resistance (1 000 000 cycles at 1−10 MPa compressive cyclic load), failure reliability, and flexural strength (30 MPa) compared to other conventional patterns (rectangular, curved, and zigzag).[284] Therefore, it appears that anisotropy in pore geometry is a useful strategy in tuning mechanical properties since bone can be considered as a hierarchically anisotropic composite material with a high compressive loading along the vertical direction. Thus, mimicking the architectural aspects of Haversian channels may enhance the mechanical properties. Other studies have shown that microporous (54−80 vol %) bioactive glass scaffolds with hierarchical porosity can support successful bone in-growth while maintaining adequate mechanical properties (12−20 MPa).[285,286]

Polycaprolactone and poly(lactic-*co*-glycolic acid) scaffolds with differently designed pore architectures (lattice, stagger, and triangle types) and stacking directions (horizontal and vertical directions) with identical porosity, line width, and pitch were fabricated using a multihead deposition system. The compressive strengths of the lattice-, stagger-, and triangle-type scaffolds were 6.05, 7.43, and 9.81 MPa, respectively. The compressive modulus of the triangle-type scaffold (178 MPa) was the highest among the three types of scaffolds as was the compressive strength. Also, the stacking direction affected the compressive strength of the scaffolds as well as pore shapes. The maximum compressive strength was achieved for the horizontally stacked scaffold (10.7 MPa), which was superior to vertically stacked scaffolds while being comparable to cortical bone.[274]

Similarly, HA/TCP scaffolds were fabricated using wax inkjet printing with different pore geometry of round and square cross sections and also with perpendicular and 60° inclined orientation. The scaffolds had average pore size of 300 μm and different porosity. The maximum strength (1.3−27.6 MPa) was observed for the scaffolds with the lowest amount of porosity and round pore morphology.[235] Additionally, they found that the compressive strength of the scaffolds was mainly influenced by the phase composition as well as the macroporosity content, although their influences exceeded that of pore geometry.[235]

While it is an accepted fact that porous biomaterials with tailored pore architecture can be fabricated using additive manufacturing techniques, it is unclear how mechanical properties, bone in-growth requirements, and manufacturing constraints affect the final characteristics. In an interesting study, tantalum scaffolds with tailored porosities were fabricated using selective laser melting to create two high-strength topologies, the tetrahedron and the octet truss.[287] Keeping the pore size constant, the structures were processed with four levels of pore content: 50%, 60%, 70%, and 75%. These values correspond to pore sizes used in canine models for bone in-growth study. The as-processed tetrahedron topology had an average porosity content of 55.51% and an average pore size of 438 μm. The manufactured octet truss had an average porosity content of 69.88% and an average pore size of 772 μm. The results showed that the maximum strength and stiffness ranged from 31 to 227 MPa and 1.23 to 4.5 GPa, respectively, for the two categories, and the maximum yield strength is almost 5 times more than that of tantalum foams. The results from this study showed that bone in-growth and manufacturing constraints can be easily integrated into architectural designs, which allow for a better understanding of the interplay between mechanical properties, bone in-growth, and manufacturing constraints, each affecting the properties of porous biomaterial for orthopedic applications.

5. SUMMARY AND FUTURE DIRECTION

During the past decade, remarkable research on different techniques has been devoted to producing porous biomaterial scaffolds. The efforts resulted in better control in porous structures and with improved properties. This paper reviewed different processing techniques, as well as biological correlation relationships with porous architectures of polymers, ceramics, metals, and glasses. The major conclusions of the present review are described in the following.

(1) Conventional techniques generate random pores. Combination of techniques can result in better interconnectivity. (2) Homogeneously porous ceramics with extremely narrow size distribution can be successfully fabricated by combining sintering with in situ chemical techniques. (3) Sol−gel foaming and gel casting foaming can be used to produce porous glass scaffolds with large channels and enough compressive strength comparable to those in porous bone. (4) In metal scaffolds, great progress has been made in the manufacturing of porous structures. However, achieving consistently homogeneous pore sizes, morphology distribution and wall thickness and low crack density is replete with issues. (5) Polymer scaffolds have also been extensively processed through various techniques including electrospinning. Despite recent advances in electrospinning methods, the low extent of cellular infiltration is still challenging. The more recent approach is to use a hybrid system of polymers to take advantage of individual components.

(6) Current methods based on rapid prototyping allow specific and precise control over porosity characteristics. Fabrication of graded and hierarchically porous scaffolds using SFF techniques has gained attention recently. (7) Polymers are the most studied and processed biomaterials using solid free form fabrication techniques. However, there is a lack of similarity in architecture between polymers or metals and natural bone. (8) The fabrication of scaffolds with graded pore-size distribution was mostly performed by solid free form fabrication technique. Combining electrospinning with SFF created the nanopores along with macropores, which seem to be useful. (9) It is also noted that porous scaffolds with a hierarchical porosity size distribution possessing macro-, meso-, micro-, and more recently nanopores (e.g., scaffolds for adsorption−delivery purpose, etc.) have attracted much attention in both academic and industrial fields. Tailoring the pore size distribution can create scaffolds that are able to act in a more complex way than homogeneous porous structures. This leads to improved mechanical properties and degradation kinetics, which are important issues in scaffolds with large pore sizes.

(10) From a biological response point of view, scaffolds with more uniform sized pores can provide higher colonization and better distribution of cells as long as their pores are large enough, such as >300 μm for bone in-growth and >400 μm for enough vascularization. In samples with heterogeneous pore size distribution, the cell penetration and colonization may be sufficient, but the porosity of smaller pore size should be carefully adjusted as it may impair the diffusion of nutrients. The interconnectivity and permeability, which are governed by macropore size and pore morphology, must also be controlled

DOI: 10.1021/acsbiomaterials.7b00615
ACS Biomater. Sci. Eng. XXXX, XXX, XXX−XXX

as they directly affect cellular infiltration. Inducing meso- and micropores within foam scaffolds is also proven to control cellular fate through the regulation of cellular protein adhesion.

Overall, the comparison of various methods and their physiochemical characteristics in the present review may be useful when choosing the right process for the right materials with specific functionality. However, further considerations should be taken into account such as mechanical properties, therapeutic agent loading, scalability, and the optimum properties of the microstructure.

AUTHOR INFORMATION

Corresponding Author

*E-mail: elham.babaie@rice.edu.

ORCID

Elham Babaie: 0000-0002-7173-9692

Notes

This paper is an updated version of part of the doctoral dissertation of E.B. at the University of Toledo.

The authors declare no competing financial interest.

ACKNOWLEDGMENTS

Partial support from the Third Frontier Program, Ohio, and NSF Grant 1706513 is gratefully acknowledged.

REFERENCES

(1) Gibson, L. J.; Ashby, M. F. *Cellular solids: structure and properties* new edition; Cambridge university press: 1999.

(2) Johnson, K. D.; Frierson, K. E.; Keller, T. S.; Cook, C.; Scheinberg, R.; Zerwekh, J.; Meyers, L.; Sciadini, M. F. Porous ceramics as bone graft substitutes in long bone defects: A biomechanical, histological, and radiographic analysis. *J. Orthop. Res.* **1996**, *14* (3), 351−369.

(3) Delécrin, J.; Takahashi, S.; Gouin, F.; Passuti, N. A synthetic porous ceramic as a bone graft substitute in the surgical management of scoliosis: a prospective, randomized study. *Spine* **2000**, *25* (5), 563−569.

(4) Kim, H.-W.; Knowles, J. C.; Kim, H.-E. Hydroxyapatite/poly (ε-caprolactone) composite coatings on hydroxyapatite porous bone scaffold for drug delivery. *Biomaterials* **2004**, *25* (7), 1279−1287.

(5) Rezwan, K.; Chen, Q.; Blaker, J.; Boccaccini, A. R. Biodegradable and bioactive porous polymer/inorganic composite scaffolds for bone tissue engineering. *Biomaterials* **2006**, *27* (18), 3413−3431.

(6) Korsmeyer, R. W.; Gurny, R.; Doelker, E.; Buri, P.; Peppas, N. A. Mechanisms of solute release from porous hydrophilic polymers. *Int. J. Pharm.* **1983**, *15* (1), 25−35.

(7) Kim, H.-W.; Lee, S.-Y.; Bae, C.-J.; Noh, Y.-J.; Kim, H.-E.; Kim, H.-M.; Ko, J. S. Porous ZrO2 bone scaffold coated with hydroxyapatite with fluorapatite intermediate layer. *Biomaterials* **2003**, *24* (19), 3277−3284.

(8) Ducheyne, P.; Van Raemdonck, W.; Heughebaert, J.; Heughebaert, M. Structural analysis of hydroxyapatite coatings on titanium. *Biomaterials* **1986**, *7* (2), 97−103.

(9) Langer, R. Biomaterials in drug delivery and tissue engineering: one laboratory's experience. *Acc. Chem. Res.* **2000**, *33* (2), 94−101.

(10) Entezari, A.; Roohani-Esfahani, S.-I.; Zhang, Z.; Zreiqat, H.; Dunstan, C. R.; Li, Q. *Sci. Rep.* **2016**, *6*, 28816.

(11) Campana, V.; Milano, G.; Pagano, E.; Barba, M.; Cicione, C.; Salonna, G.; Lattanzi, W.; Logroscino, G. Bone substitutes in orthopaedic surgery: from basic science to clinical practice. *J. Mater. Sci.: Mater. Med.* **2014**, *25* (10), 2445−2461.

(12) Ishizaki, K.; Komarneni, S.; Nanko, M. *Porous Materials: Process technology and applications*; Springer Science & Business Media: 2013; Vol. *4*.

(13) Davis, M. E. Ordered porous materials for emerging applications. *Nature* **2002**, *417* (6891), 813−821.

(14) Hollister, S. J. Porous scaffold design for tissue engineering. *Nat. Mater.* **2005**, *4* (7), 518−524.

(15) Ashby, M. The properties of foams and lattices. *Philos. Trans. R. Soc., A* **2006**, *364* (1838), 15−30.

(16) Perez, R. A.; Mestres, G. Role of pore size and morphology in musculo-skeletal tissue regeneration. *Mater. Sci. Eng., C* **2016**, *61*, 922−939.

(17) Salimon, A.; Brechet, Y.; Ashby, M.; Greer, A. Potential applications for steel and titanium metal foams. *J. Mater. Sci.* **2005**, *40* (22), 5793−5799.

(18) Albrektsson, T.; Johansson, C. Osteoinduction, osteoconduction and osseointegration. *Eur. Spine J.* **2001**, *10* (2), S96−S101.

(19) Miron, R. J.; Zhang, Y. F. Osteoinduction: A Review of Old Concepts with New Standards. *J. Dent. Res.* **2012**, *91* (8), 736−744.

(20) Hutmacher, D. W. Scaffolds in tissue engineering bone and cartilage. *Biomaterials* **2000**, *21* (24), 2529−2543.

(21) Hutmacher, D. W. Scaffold design and fabrication technologies for engineering tissues—state of the art and future perspectives. *J. Biomater. Sci., Polym. Ed.* **2001**, *12* (1), 107−124.

(22) Karageorgiou, V.; Kaplan, D. Porosity of 3D biomaterial scaffolds and osteogenesis. *Biomaterials* **2005**, *26* (27), 5474−5491.

(23) Chevalier, E.; Chulia, D.; Pouget, C.; Viana, M. Fabrication of porous substrates: a review of processes using pore forming agents in the biomaterial field. *J. Pharm. Sci.* **2008**, *97* (3), 1135−1154.

(24) Ohji, T.; Fukushima, M. Macro-porous ceramics: processing and properties. *Int. Mater. Rev.* **2012**, *57* (2), 115−131.

(25) *Quantitative Microscopy*. DeHoff, R. T., Rhines, F. N., Eds.; McGraw-Hill, 1968.

(26) *CRC Handbook of Chemistry and Physics*, 53rd ed.; Weast, R. C., Ed.; CRC Press, 1972.

(27) Rho, J.-Y.; Kuhn-Spearing, L.; Zioupos, P. Mechanical properties and the hierarchical structure of bone. *Medical Engineering & Physics* **1998**, *20* (2), 92−102.

(28) Wagoner Johnson, A. J.; Herschler, B. A. A review of the mechanical behavior of CaP and CaP/polymer composites for applications in bone replacement and repair. *Acta Biomater.* **2011**, *7* (1), 16−30.

(29) Veljović, D.; Jančić-Hajneman, R.; Balać, I.; Jokić, B.; Putić, S.; Petrović, R.; Janaćković, D. The effect of the shape and size of the pores on the mechanical properties of porous HAP-based bioceramics. *Ceram. Int.* **2011**, *37* (2), 471−479.

(30) Jones, A. C.; Arns, C. H.; Hutmacher, D. W.; Milthorpe, B. K.; Sheppard, A. P.; Knackstedt, M. A. The correlation of pore morphology, interconnectivity and physical properties of 3D ceramic scaffolds with bone ingrowth. *Biomaterials* **2009**, *30* (7), 1440−1451.

(31) Habibovic, P.; Yuan, H.; van der Valk, C. M.; Meijer, G.; van Blitterswijk, C. A.; de Groot, K. 3D microenvironment as essential element for osteoinduction by biomaterials. *Biomaterials* **2005**, *26* (17), 3565−3575.

(32) Babaie, E.; Ren, Y.; Bhaduri, S. B. Microwave sintering of fine grained MgP and Mg substitutes with amorphous tricalcium phosphate: Structural, and mechanical characterization. *J. Mater. Res.* **2016**, *31* (08), 995−1003.

(33) Ramesh, S.; Tan, C. Y.; Bhaduri, S. B.; Teng, W. D.; Sopyan, I. Densification behaviour of nanocrystalline hydroxyapatite bioceramics. *J. Mater. Process. Technol.* **2008**, *206* (1−3), 221−230.

(34) Borden, M.; Attawia, M.; Laurencin, C. T. The sintered microsphere matrix for bone tissue engineering: In vitro osteoconductivity studies. *J. Biomed. Mater. Res.* **2002**, *61* (3), 421−429.

(35) Borden, M.; El-Amin, S.; Attawia, M.; Laurencin, C. Structural and human cellular assessment of a novel microsphere-based tissue engineered scaffold for bone repair. *Biomaterials* **2003**, *24* (4), 597−609.

(36) Jiang, T.; Abdel-Fattah, W. I.; Laurencin, C. T. In vitro evaluation of chitosan/poly(lactic acid-glycolic acid) sintered microsphere scaffolds for bone tissue engineering. *Biomaterials* **2006**, *27* (28), 4894−4903.

(37) Bhamidipati, M.; Sridharan, B.; Scurto, A. M.; Detamore, M. S. Subcritical CO2 sintering of microspheres of different polymeric

DOI: 10.1021/acsbiomaterials.7b00615
ACS Biomater. Sci. Eng. XXXX, XXX, XXX−XXX

materials to fabricate scaffolds for tissue engineering. *Mater. Sci. Eng., C* **2013**, *33* (8), 4892−4899.
(38) Jeon, J. H.; Bhamidipati, M.; Sridharan, B.; Scurto, A. M.; Berkland, C. J.; Detamore, M. S. Tailoring of processing parameters for sintering microsphere-based scaffolds with dense-phase carbon dioxide. *J. Biomed. Mater. Res., Part B* **2013**, *101B* (2), 330−337.
(39) Vasconcellos, L. M. R. d.; Oliveira, M. V. d.; Graça, M. L. d. A.; Vasconcellos, L. G. O. d.; Carvalho, Y. R.; Cairo, C. A. A. Porous titanium scaffolds produced by powder metallurgy for biomedical applications. *Mater. Res.* **2008**, *11* (3), 275−280.
(40) Oh, I.-H.; Segawa, H.; Nomura, N.; Hanada, S. Microstructures and mechanical properties of porosity-graded pure titanium compacts. *Mater. Trans.* **2003**, *44* (4), 657−660.
(41) Murray, G.; Semple, J. Transfer of tensile loads from a prosthesis to bone using porous titanium. *J. Bone Jt. Surg., Br. Vol.* **1981**, *63-B* (1), 138−141.
(42) Spoerke, E. D.; Murray, N. G.; Li, H.; Brinson, L. C.; Dunand, D. C.; Stupp, S. I. A bioactive titanium foam scaffold for bone repair. *Acta Biomater.* **2005**, *1* (5), 523−533.
(43) Tang, C.; Wong, C.; Zhang, L.; Choy, M.; Chow, T.; Chan, K.; Yue, T.; Chen, Q. In situ formation of Ti alloy/TiC porous composites by rapid microwave sintering of Ti6Al4V/MWCNTs powder. *J. Alloys Compd.* **2013**, *557*, 67−72.
(44) Hong, T.; Guo, Z.; Yang, R. Fabrication of porous titanium scaffold materials by a fugitive filler method. *J. Mater. Sci.: Mater. Med.* **2008**, *19* (12), 3489−3495.
(45) Wen, C. E.; Mabuchi, M.; Yamada, Y.; Shimojima, K.; Chino, Y.; Asahina, T. Processing of biocompatible porous Ti and Mg. *Scr. Mater.* **2001**, *45* (10), 1147−1153.
(46) Wen, C.; Yamada, Y.; Shimojima, K.; Chino, Y.; Asahina, T.; Mabuchi, M. Processing and mechanical properties of autogenous titanium implant materials. *J. Mater. Sci.: Mater. Med.* **2002**, *13* (4), 397−401.
(47) Dabrowski, B.; Swieszkowski, W.; Godlinski, D.; Kurzydlowski, K. J. Highly porous titanium scaffolds for orthopaedic applications. *J. Biomed. Mater. Res., Part B* **2010**, *95* (1), 53−61.
(48) Kim, S. W.; Jung, H.-D.; Kang, M.-H.; Kim, H.-E.; Koh, Y.-H.; Estrin, Y. Fabrication of porous titanium scaffold with controlled porous structure and net-shape using magnesium as spacer. *Mater. Sci. Eng., C* **2013**, *33* (5), 2808−2815.
(49) Babaie, E.; Zhou, H.; Lin, B.; Bhaduri, S. B. Influence of ethanol content in the precipitation medium on the composition, structure and reactivity of magnesium−calcium phosphate. *Mater. Sci. Eng., C* **2015**, *53*, 204−211.
(50) Jones, A. C.; Arns, C. H.; Sheppard, A. P.; Hutmacher, D. W.; Milthorpe, B. K.; Knackstedt, M. A. Assessment of bone ingrowth into porous biomaterials using MICRO-CT. *Biomaterials* **2007**, *28* (15), 2491−2504.
(51) Babaie, E.; Lin, B.; Goel, V. K.; Bhaduri, S. B. Evaluation of amorphous magnesium phosphate (AMP) based non-exothermic orthopedic cements. *Biomed. Mater.* **2016**, *11* (5), 055010.
(52) Zhou, H.; Agarwal, A. K.; Goel, V. K.; Bhaduri, S. B. Microwave assisted preparation of magnesium phosphate cement (MPC) for orthopedic applications: a novel solution to the exothermicity problem. *Mater. Sci. Eng., C* **2013**, *33* (7), 4288−4294.
(53) Lan Levengood, S. K.; Polak, S. J.; Wheeler, M. B.; Maki, A. J.; Clark, S. G.; Jamison, R. D.; Wagoner Johnson, A. J. Multiscale osteointegration as a new paradigm for the design of calcium phosphate scaffolds for bone regeneration. *Biomaterials* **2010**, *31* (13), 3552−3563.
(54) Lopez-Heredia, M. A.; Sariibrahimoglu, K.; et al. Influence of the pore generator on the evolution of the mechanical properties and the porosity and interconnectivity of a calcium phosphate cement. *Acta Biomater.* **2012**, *8*, 404−414.
(55) Uchida, A.; Nade, S.; McCartney, E. R.; Ching, W. The use of ceramics for bone replacement. A comparative study of three different porous ceramics. *J. Bone Jt. Surg., Br. Vol.* **1984**, *66* (2), 269−275.
(56) Zhang, J.; Zhou, H.; Yang, K.; Yuan, Y.; Liu, C. RhBMP-2-loaded calcium silicate/calcium phosphate cement scaffold with hierarchically porous structure for enhanced bone tissue regeneration. *Biomaterials* **2013**, *34* (37), 9381−9392.
(57) Lickorish, D.; Guan, L.; Davies, J. A three-phase, fully resorbable, polyester/calcium phosphate scaffold for bone tissue engineering: evolution of scaffold design. *Biomaterials* **2007**, *28* (8), 1495−1502.
(58) Takagi, S.; Chow, L. Formation of macropores in calcium phosphate cement implants. *J. Mater. Sci.: Mater. Med.* **2001**, *12* (2), 135−139.
(59) Torres, Y.; Pavón, J. J.; Rodríguez, J. A. Processing and characterization of porous titanium for implants by using NaCl as space holder. *J. Mater. Process. Technol.* **2012**, *212* (5), 1061−1069.
(60) Thadavirul, N.; Pavasant, P.; Supaphol, P. Development of polycaprolactone porous scaffolds by combining solvent casting, particulate leaching, and polymer leaching techniques for bone tissue engineering. *J. Biomed. Mater. Res., Part A* **2014**, *102* (10), 3379−3392.
(61) Hou, Q.; Grijpma, D. W.; Feijen, J. Porous polymeric structures for tissue engineering prepared by a coagulation, compression moulding and salt leaching technique. *Biomaterials* **2003**, *24* (11), 1937−1947.
(62) Hou, Q.; Grijpma, D. W.; Feijen, J. Preparation of porous poly(ε-caprolactone) structures. *Macromol. Rapid Commun.* **2002**, *23* (4), 247−252.
(63) Mano, J. F.; Hungerford, G.; Ribelles, J. L. G. Bioactive poly (L-lactic acid)-chitosan hybrid scaffolds. *Mater. Sci. Eng., C* **2008**, *28* (8), 1356−1365.
(64) Oh, S. H.; Kang, S. G.; Kim, E. S.; Cho, S. H.; Lee, J. H. Fabrication and characterization of hydrophilic poly (lactic-co-glycolic acid)/poly (vinyl alcohol) blend cell scaffolds by melt-molding particulate-leaching method. *Biomaterials* **2003**, *24* (22), 4011−4021.
(65) Reignier, J.; Huneault, M. A. Preparation of interconnected poly (ε-caprolactone) porous scaffolds by a combination of polymer and salt particulate leaching. *Polymer* **2006**, *47* (13), 4703−4717.
(66) Taboas, J.; Maddox, R.; Krebsbach, P.; Hollister, S. Indirect solid free form fabrication of local and global porous, biomimetic and composite 3D polymer-ceramic scaffolds. *Biomaterials* **2003**, *24* (1), 181−194.
(67) Van Tienen, T. G.; Heijkants, R. G.; Buma, P.; de Groot, J. H.; Pennings, A. J.; Veth, R. P. Tissue ingrowth and degradation of two biodegradable porous polymers with different porosities and pore sizes. *Biomaterials* **2002**, *23* (8), 1731−1738.
(68) Stähli, C.; Bohner, M.; Bashoor-Zadeh, M.; Doebelin, N.; Baroud, G. Aqueous impregnation of porous b-tricalcium phosphate scaffolds. *Acta Biomater.* **2010**, *6*, 2760−2772.
(69) Bohner, M.; van Lenthe, G. H.; Grünenfelder, S.; Hirsiger, W.; Evison, R.; Müller, R. Synthesis and characterization of porous -tricalcium phosphate blocks. *Biomaterials* **2005**, *26* (31), 6099−6105.
(70) Barralet, J. E.; Grover, L.; Gaunt, T.; Wright, A. J.; Gibson, I. R. Preparation of macroporous calcium phosphate cement tissue engineering scaffold. *Biomaterials* **2002**, *23* (15), 3063−3072.
(71) Wu, C.; Zhang, Y.; Zhou, Y.; Fan, W.; Xiao, Y. A comparative study of mesoporous glass/silk and non-mesoporous glass/silk scaffolds: Physiochemistry and in vivo osteogenesis. *Acta Biomater.* **2011**, *7* (5), 2229−2236.
(72) Wegst, U. G. K.; Schecter, M.; Donius, A. E.; Hunger, P. M. Biomaterials by freeze casting. *Philos. Trans. R. Soc., A* **2010**, *368*, 2099.
(73) Deville, S. Freeze-casting of porous biomaterials: structure, properties and opportunities. *Materials* **2010**, *3* (3), 1913−1927.
(74) Li, J. C.; Dunand, D. C. Mechanical properties of directionally freeze-cast titanium foams. *Acta Mater.* **2011**, *59* (1), 146−158.
(75) Li, W.; Lu, K.; Walz, J. Freeze casting of porous materials: review of critical factors in microstructure evolution. *Int. Mater. Rev.* **2012**, *57* (1), 37−60.
(76) Yook, S.-W.; Kim, H.-E.; Koh, Y.-H. Fabrication of porous titanium scaffolds with high compressive strength using camphene-based freeze casting. *Mater. Lett.* **2009**, *63* (17), 1502−1504.
(77) Yook, S.-W.; Yoon, B.-H.; Kim, H.-E.; Koh, Y.-H.; Kim, Y.-S. Porous titanium (Ti) scaffolds by freezing TiH2/camphene slurries. *Mater. Lett.* **2008**, *62* (30), 4506−4508.

DOI: 10.1021/acsbiomaterials.7b00615
ACS Biomater. Sci. Eng. XXXX, XXX, XXX−XXX

(78) Chino, Y.; Dunand, D. C. Directionally freeze-cast titanium foam with aligned, elongated pores. *Acta Mater.* **2008**, *56* (1), 105−113.
(79) Florczyk, S. J.; Wang, K.; Jana, S.; Wood, D. L.; Sytsma, S. K.; Sham, J. G.; Kievit, F. M.; Zhang, M. Porous chitosan-hyaluronic acid scaffolds as a mimic of glioblastoma microenvironment ECM. *Biomaterials* **2013**, *34* (38), 10143−10150.
(80) Murphy, C. M.; Haugh, M. G.; O'Brien, F. J. The effect of mean pore size on cell attachment, proliferation and migration in collagen−glycosaminoglycan scaffolds for bone tissue engineering. *Biomaterials* **2010**, *31* (3), 461−466.
(81) Whang, K.; Thomas, C. H.; Healy, K. E.; Nuber, G. A novel method to fabricate bioabsorbable scaffolds. *Polymer* **1995**, *36* (4), 837−842.
(82) Deville, S.; Saiz, E.; Tomsia, A. P. Freeze casting of hydroxyapatite scaffolds for bone tissue engineering. *Biomaterials* **2006**, *27* (32), 5480−5489.
(83) Fu, Q.; Rahaman, M. N.; Dogan, F.; Bal, B. S. Freeze casting of porous hydroxyapatite scaffolds. I. Processing and general microstructure. *J. Biomed. Mater. Res., Part B* **2008**, *86B* (1), 125−135.
(84) Landi, E.; Valentini, F.; Tampieri, A. Porous hydroxyapatite/gelatine scaffolds with ice-designed channel-like porosity for biomedical applications. *Acta Biomater.* **2008**, *4* (6), 1620−1626.
(85) Yook, S.-W.; Jung, H.-D.; Park, C.-H.; Shin, K.-H.; Koh, Y.-H.; Estrin, Y.; Kim, H.-E. Reverse freeze casting: A new method for fabricating highly porous titanium scaffolds with aligned large pores. *Acta Biomater.* **2012**, *8* (6), 2401−2410.
(86) Mooney, D. J.; Baldwin, D. F.; Suh, N. P.; Vacanti, J. P.; Langer, R. Novel approach to fabricate porous sponges of poly (D, L-lactic-co-glycolic acid) without the use of organic solvents. *Biomaterials* **1996**, *17* (14), 1417−1422.
(87) Li, Z.; Chen, X.; Zhao, N.; Dong, H.; Li, Y.; Lin, C. Stiff macroporous bioactive glass−ceramic scaffold: Fabrication by rapid prototyping template, characterization and in vitro bioactivity. *Mater. Chem. Phys.* **2013**, *141* (1), 76−80.
(88) Almirall, A.; Larrecq, G.; Delgado, J. A.; Martínez, S.; Planell, J. A.; Ginebra, M. P. Fabrication of low temperature macroporous hydroxyapatite scaffolds by foaming and hydrolysis of an α-TCP paste. *Biomaterials* **2004**, *25* (17), 3671−3680.
(89) Binner, J.; Reichert, J. Processing of hydroxyapatite ceramic foams. *J. Mater. Sci.* **1996**, *31* (21), 5717−5723.
(90) Song, H. Y.; Islam, S.; Lee, B. T. A novel method to fabricate unidirectional porous hydroxyapatite body using ethanol bubbles in a viscous slurry. *J. Am. Ceram. Soc.* **2008**, *91* (9), 3125−3127.
(91) Sepulveda, P.; Binner, J. G. P. Processing of cellular ceramics by foaming and in situ polymerisation of organic monomers. *J. Eur. Ceram. Soc.* **1999**, *19* (12), 2059−2066.
(92) Sepulveda, P.; Binner, J.; Rogero, S.; Higa, O.; Bressiani, J. Production of porous hydroxyapatite by the gel-casting of foams and cytotoxic evaluation. *J. Biomed. Mater. Res.* **2000**, *50* (1), 27−34.
(93) Li, X.; van Blitterswijk, C. A.; Feng, Q.; Cui, F.; Watari, F. The effect of calcium phosphate microstructure on bone-related cells in vitro. *Biomaterials* **2008**, *29* (23), 3306−3316.
(94) Del Real, R.; Wolke, J.; Vallet-Regı, M.; Jansen, J. A new method to produce macropores in calcium phosphate cements. *Biomaterials* **2002**, *23* (17), 3673−3680.
(95) Babaie, E.; Lin, B.; Bhaduri, S. B. A new method to produce macroporous Mg-phosphate bone growth substitutes. *Mater. Sci. Eng., C* **2017**, *75* (1), 602−609.
(96) Chen, Y.; Feng, B.; Zhu, Y.; Weng, J.; Wang, J.; Lu, X. Preparation and characterization of a novel porous titanium scaffold with 3D hierarchical porous structures. *J. Mater. Sci.: Mater. Med.* **2011**, *22* (4), 839−844.
(97) Lefebvre, L.-P.; Thomas, Y.; Gauthier, M. Method of making open cell material. US Patents, US6660224B2, 2003.
(98) St-Pierre, J.-P.; Gauthier, M.; Lefebvre, L.-P.; Tabrizian, M. Three-dimensional growth of differentiating MC3T3-E1 pre-osteoblasts on porous titanium scaffolds. *Biomaterials* **2005**, *26* (35), 7319−7328.
(99) Gomes, M. E.; Ribeiro, A.; Malafaya, P.; Reis, R.; Cunha, A. A new approach based on injection moulding to produce biodegradable starch-based polymeric scaffolds: morphology, mechanical and degradation behaviour. *Biomaterials* **2001**, *22* (9), 883−889.
(100) Sheridan, M.; Shea, L.; Peters, M.; Mooney, D. Bioabsorbable polymer scaffolds for tissue engineering capable of sustained growth factor delivery. *J. Controlled Release* **2000**, *64* (1), 91−102.
(101) Nam, Y. S.; Yoon, J. J.; Park, T. G. A novel fabrication method of macroporous biodegradable polymer scaffolds using gas foaming salt as a porogen additive. *J. Biomed. Mater. Res.* **2000**, *53* (1), 1−7.
(102) Brown, D. D.; Green, D. J. Investigation of strut crack formation in open cell alumina ceramics. *J. Am. Ceram. Soc.* **1994**, *77* (6), 1467−1472.
(103) Mallick, K. K.; Winnett, J.; van Grunsven, W.; Lapworth, J.; Reilly, G. C. Three-dimensional porous bioscaffolds for bone tissue regeneration: Fabrication via adaptive foam reticulation and freeze casting techniques, characterization, and cell study. *J. Biomed. Mater. Res., Part A* **2012**, *100* (11), 2948−2959.
(104) Lee, J.-H.; Kim, H.-E.; Koh, Y.-H. Highly porous titanium (Ti) scaffolds with bioactive microporous hydroxyapatite/TiO 2 hybrid coating layer. *Mater. Lett.* **2009**, *63* (23), 1995−1998.
(105) Cachinho, S. C.; Correia, R. N. Titanium porous scaffolds from precursor powders: rheological optimization of TiH 2 slurries. *Powder Technol.* **2007**, *178* (2), 109−113.
(106) Li, J.; Yang, H.; Wang, H.; Ruan, J. Low elastic modulus titanium−nickel scaffolds for bone implants. *Mater. Sci. Eng., C* **2014**, *34* (0), 110−114.
(107) Jo, I.-H.; Shin, K.-H.; Soon, Y.-M.; Koh, Y.-H.; Lee, J.-H.; Kim, H.-E. Highly porous hydroxyapatite scaffolds with elongated pores using stretched polymeric sponges as novel template. *Mater. Lett.* **2009**, *63* (20), 1702−1704.
(108) Padilla, S.; Sánchez-Salcedo, S.; Vallet-Regí, M. Bioactive glass as precursor of designed-architecture scaffolds for tissue engineering. *J. Biomed. Mater. Res., Part A* **2007**, *81A* (1), 224−232.
(109) Li, Y.; Yang, C.; Zhao, H.; Qu, S.; Li, X.; Li, Y. New developments of Ti-based alloys for biomedical applications. *Materials* **2014**, *7* (3), 1709−1800.
(110) Chen, Q. Z.; Thompson, I. D.; Boccaccini, A. R. 45S5 Bioglass®-derived glass−ceramic scaffolds for bone tissue engineering. *Biomaterials* **2006**, *27* (11), 2414−2425.
(111) Wu, Z. Y.; Hill, R. G.; Yue, S.; Nightingale, D.; Lee, P. D.; Jones, J. R. Melt-derived bioactive glass scaffolds produced by a gel-cast foaming technique. *Acta Biomater.* **2011**, *7* (4), 1807−1816.
(112) Sepulveda, P.; Binner, J. Evaluation of the in situ polymerization kinetics for the gelcasting of ceramic foams. *Chem. Mater.* **2001**, *13* (11), 3882−3887.
(113) Singh, R.; Lee, P. D.; Jones, J. R.; Poologasundarampillai, G.; Post, T.; Lindley, T. C.; Dashwood, R. J. Hierarchically structured titanium foams for tissue scaffold applications. *Acta Biomater.* **2010**, *6* (12), 4596−4604.
(114) Yang, D.; Guo, Z.; Shao, H.; Liu, X.; Ji, Y. Mechanical properties of porous Ti-Mo and Ti-Nb alloys for biomedical application by gelcasting. *Procedia Eng.* **2012**, *36*, 160−167.
(115) Sepulveda, P.; Jones, J. R.; Hench, L. L. Characterization of melt-derived 45S5 and sol-gel−derived 58S bioactive glasses. *J. Biomed. Mater. Res.* **2001**, *58* (6), 734−740.
(116) Jones, J. R. Review of bioactive glass: From Hench to hybrids. *Acta Biomater.* **2013**, *9* (1), 4457−4486.
(117) Jun, I.-K.; Koh, Y.-H.; Kim, H.-E. Fabrication of a highly porous bioactive glass−ceramic scaffold with a high surface area and strength. *J. Am. Ceram. Soc.* **2006**, *89* (1), 391−394.
(118) Hench, L. L.; West, J. K. The sol-gel process. *Chem. Rev.* **1990**, *90* (1), 33−72.
(119) Sepulveda, P.; Jones, J. R.; Hench, L. L. Bioactive sol-gel foams for tissue repair. *J. Biomed. Mater. Res.* **2002**, *59* (2), 340−348.
(120) Jones, J. R.; Ehrenfried, L. M.; Hench, L. L. Optimising bioactive glass scaffolds for bone tissue engineering. *Biomaterials* **2006**, *27* (7), 964−973.

DOI: 10.1021/acsbiomaterials.7b00615
ACS Biomater. Sci. Eng. XXXX, XXX, XXX−XXX

(121) Marques, A. C.; Jain, H.; Almeida, R. M. Sol-gel derived nano/macroporous scaffolds. *Phys. Chem. Glasses: Eur. J. Glass Sci. Technol. B* **2007**, *48* (2), 65−68.
(122) Marques, A. C.; Almeida, R. M.; Thiema, A.; Wang, S.; Falk, M.; Jain, H. Sol-gel-derived glass scaffold with high pore interconnectivity and enhanced bioactivity. *J. Mater. Res.* **2009**, *24* (12), 3495−3502.
(123) Wang, S.; Falk, M.; Rashad, A.; Saad, M.; Marques, A.; Almeida, R.; Marei, M.; Jain, H. Evaluation of 3D nano−macro porous bioactive glass scaffold for hard tissue engineering. *J. Mater. Sci.: Mater. Med.* **2011**, *22* (5), 1195−1203.
(124) Yang, F.; Qu, X.; Cui, W.; Bei, J.; Yu, F.; Lu, S.; Wang, S. Manufacturing and morphology structure of polylactide-type microtubules orientation-structured scaffolds. *Biomaterials* **2006**, *27* (28), 4923−4933.
(125) Hu, X.; Shen, H.; Yang, F.; Bei, J.; Wang, S. Preparation and cell affinity of microtubular orientation-structured PLGA(70/30) blood vessel scaffold. *Biomaterials* **2008**, *29* (21), 3128−3136.
(126) Boccaccini, A. R.; Maquet, V. Bioresorbable and bioactive polymer/Bioglass® composites with tailored pore structure for tissue engineering applications. *Compos. Sci. Technol.* **2003**, *63* (16), 2417−2429.
(127) Yang, F.; Murugan, R.; Ramakrishna, S.; Wang, X.; Ma, Y.-X.; Wang, S. Fabrication of nano-structured porous PLLA scaffold intended for nerve tissue engineering. *Biomaterials* **2004**, *25* (10), 1891−1900.
(128) Schugens, C.; Maquet, V.; Grandfils, C.; Jerome, R.; Teyssie, P. Polylactide macroporous biodegradable implants for cell transplantation. II. Preparation of polylactide foams by liquid-liquid phase separation. *J. Biomed. Mater. Res.* **1996**, *30* (4), 449−461.
(129) Mikos, A. G.; Bao, Y.; Cima, L. G.; Ingber, D. E.; Vacanti, J. P.; Langer, R. Preparation of poly(glycolic acid) bonded fiber structures for cell attachment and transplantation. *J. Biomed. Mater. Res.* **1993**, *27* (2), 183−189.
(130) Mooney, D. J.; Mazzoni, C. L.; Breuer, C.; McNamara, K.; Hern, D.; Vacanti, J. P.; Langer, R. Stabilized polyglycolic acid fibre-based tubes for tissue engineering. *Biomaterials* **1996**, *17* (2), 115−124.
(131) Sarazin, P.; Roy, X.; Favis, B. D. Controlled preparation and properties of porous poly (L-lactide) obtained from a co-continuous blend of two biodegradable polymers. *Biomaterials* **2004**, *25* (28), 5965−5978.
(132) Ghavidel Mehr, N.; Li, X.; Ariganello, M.; Hoemann, C.; Favis, B. Poly(ε-caprolactone) scaffolds of highly controlled porosity and interconnectivity derived from co-continuous polymer blends: model bead and cell infiltration behavior. *J. Mater. Sci.: Mater. Med.* **2014**, *25* (9), 2083−2093.
(133) Zhou, H.; Lawrence, J. G.; Bhaduri, S. B. Fabrication aspects of PLA-CaP/PLGA-CaP composites for orthopedic applications: a review. *Acta Biomater.* **2012**, *8* (6), 1999−2016.
(134) Blakeney, B. A.; Tambralli, A.; Anderson, J. M.; Andukuri, A.; Lim, D.-J.; Dean, D. R.; Jun, H.-W. Cell infiltration and growth in a low density, uncompressed three-dimensional electrospun nanofibrous scaffold. *Biomaterials* **2011**, *32* (6), 1583−1590.
(135) Phipps, M. C.; Clem, W. C.; Grunda, J. M.; Clines, G. A.; Bellis, S. L. Increasing the pore sizes of bone-mimetic electrospun scaffolds comprised of polycaprolactone, collagen I and hydroxyapatite to enhance cell infiltration. *Biomaterials* **2012**, *33* (2), 524−534.
(136) Wade, R. J.; Burdick, J. A. Advances in nanofibrous scaffolds for biomedical applications: From electrospinning to self-assembly. *Nano Today* **2014**, *9* (6), 722−742.
(137) Duling, R. R.; Dupaix, R. B.; Katsube, N.; Lannutti, J. Mechanical characterization of electrospun polycaprolactone (PCL): a potential scaffold for tissue engineering. *J. Biomech. Eng.* **2008**, *130* (1), 011006.
(138) Yang, F.; Murugan, R.; Wang, S.; Ramakrishna, S. Electrospinning of nano/micro scale poly(l-lactic acid) aligned fibers and their potential in neural tissue engineering. *Biomaterials* **2005**, *26* (15), 2603−2610.
(139) Bashur, C. A.; Dahlgren, L. A.; Goldstein, A. S. Effect of fiber diameter and orientation on fibroblast morphology and proliferation on electrospun poly(d,l-lactic-co-glycolic acid) meshes. *Biomaterials* **2006**, *27* (33), 5681−5688.
(140) Yi, F.; LaVan, D. A. Poly (glycerol sebacate) nanofiber scaffolds by core/shell electrospinning. *Macromol. Biosci.* **2008**, *8* (9), 803−806.
(141) Kidoaki, S.; Kwon, I. K.; Matsuda, T. Mesoscopic spatial designs of nano- and microfiber meshes for tissue-engineering matrix and scaffold based on newly devised multilayering and mixing electrospinning techniques. *Biomaterials* **2005**, *26* (1), 37−46.
(142) Shalumon, K. T.; Binulal, N. S.; Selvamurugan, N.; Nair, S. V.; Menon, D.; Furuike, T.; Tamura, H.; Jayakumar, R. Electrospinning of carboxymethyl chitin/poly(vinyl alcohol) nanofibrous scaffolds for tissue engineering applications. *Carbohydr. Polym.* **2009**, *77* (4), 863−869.
(143) Chen, M.; Dong, M.; Havelund, R.; Regina, V. R.; Meyer, R. L.; Besenbacher, F.; Kingshott, P. Thermo-responsive core− sheath electrospun nanofibers from poly (N-isopropylacrylamide)/polycaprolactone blends. *Chem. Mater.* **2010**, *22* (14), 4214−4221.
(144) Kim, T. G.; Chung, H. J.; Park, T. G. Macroporous and nanofibrous hyaluronic acid/collagen hybrid scaffold fabricated by concurrent electrospinning and deposition/leaching of salt particles. *Acta Biomater.* **2008**, *4* (6), 1611−1619.
(145) Fang, Z.; Fu, W.; Dong, Z.; Zhang, X.; Gao, B.; Guo, D.; He, H.; Wang, Y. Preparation and biocompatibility of electrospun poly(l-lactide-co-ε-caprolactone)/fibrinogen blended nanofibrous scaffolds. *Appl. Surf. Sci.* **2011**, *257* (9), 4133−4138.
(146) Rnjak-Kovacina, J.; Wise, S. G.; Li, Z.; Maitz, P. K.; Young, C. J.; Wang, Y.; Weiss, A. S. Tailoring the porosity and pore size of electrospun synthetic human elastin scaffolds for dermal tissue engineering. *Biomaterials* **2011**, *32* (28), 6729−6736.
(147) Yan, S.; Zhang, Q.; Wang, J.; Liu, Y.; Lu, S.; Li, M.; Kaplan, D. L. Silk fibroin/chondroitin sulfate/hyaluronic acid ternary scaffolds for dermal tissue reconstruction. *Acta Biomater.* **2013**, *9* (6), 6771−6782.
(148) Pan, H.; Jiang, H.; Chen, W. Interaction of dermal fibroblasts with electrospun composite polymer scaffolds prepared from dextran and poly lactide-co-glycolide. *Biomaterials* **2006**, *27* (17), 3209−3220.
(149) Ma, G.; Fang, D.; Liu, Y.; Zhu, X.; Nie, J. Electrospun sodium alginate/poly (ethylene oxide) core−shell nanofibers scaffolds potential for tissue engineering applications. *Carbohydr. Polym.* **2012**, *87* (1), 737−743.
(150) Du, F.; Wang, H.; Zhao, W.; Li, D.; Kong, D.; Yang, J.; Zhang, Y. Gradient nanofibrous chitosan/poly ε-caprolactone scaffolds as extracellular microenvironments for vascular tissue engineering. *Biomaterials* **2012**, *33* (3), 762−770.
(151) Wright, L. D.; Andric, T.; Freeman, J. W. Utilizing NaCl to increase the porosity of electrospun materials. *Mater. Sci. Eng., C* **2011**, *31* (1), 30−36.
(152) Leong, M. F.; Rasheed, M. Z.; Lim, T. C.; Chian, K. S. In vitro cell infiltration and in vivo cell infiltration and vascularization in a fibrous, highly porous poly(D,L-lactide) scaffold fabricated by cryogenic electrospinning technique. *J. Biomed. Mater. Res., Part A* **2009**, *91A* (1), 231−240.
(153) Lee, J. B.; Jeong, S. I.; Bae, M. S.; Yang, D. H.; Heo, D. N.; Kim, C. H.; Alsberg, E.; Kwon, I. K. Highly porous electrospun nanofibers enhanced by ultrasonication for improved cellular infiltration. *Tissue Eng., Part A* **2011**, *17* (21−22), 2695−2702.
(154) Lowery, J. L.; Datta, N.; Rutledge, G. C. Effect of fiber diameter, pore size and seeding method on growth of human dermal fibroblasts in electrospun poly(ε-caprolactone) fibrous mats. *Biomaterials* **2010**, *31* (3), 491−504.
(155) Ekaputra, A. K.; Prestwich, G. D.; Cool, S. M.; Hutmacher, D. W. Combining electrospun scaffolds with electrosprayed hydrogels leads to three-dimensional cellularization of hybrid constructs. *Biomacromolecules* **2008**, *9* (8), 2097−2103.
(156) Chanthakulchan, A.; Koomsap, P.; Auyson, K.; Supaphol, P. Development of an electrospinning-based rapid prototyping for scaffold fabrication. *Rapid Prototyp J.* **2015**, *21* (3), 329−339.

DOI: 10.1021/acsbiomaterials.7b00615
ACS Biomater. Sci. Eng. XXXX, XXX, XXX−XXX

(157) Kim, J.; McBride, S.; Tellis, B.; Alvarez-Urena, P.; Song, Y.-H.; Dean, D. D.; Sylvia, V. L.; Elgendy, H.; Ong, J.; Hollinger, J. O. Rapid-prototyped PLGA/β-TCP/hydroxyapatite nanocomposite scaffolds in a rabbit femoral defect model. *Biofabrication* **2012**, *4* (2), 025003.
(158) Brown, T. D.; Slotosch, A.; Thibaudeau, L.; Taubenberger, A.; Loessner, D.; Vaquette, C.; Dalton, P. D.; Hutmacher, D. W. Design and fabrication of tubular scaffolds via direct writing in a melt electrospinning mode. *Biointerphases* **2012**, *7* (1), 13.
(159) Farrugia, B. L.; et al. Dermal fibroblast infiltration of poly(ε-caprolactone) scaffolds fabricated by melt electrospinning in a direct writing mode. *Biofabrication* **2013**, *5* (2), 025001.
(160) Wu, J.; Huang, C.; Liu, W.; Yin, A.; Chen, W.; He, C.; Wang, H.; Liu, S.; Fan, C.; Bowlin, G. L.; Mo, X. Cell infiltration and vascularization in porous nanoyarn scaffolds prepared by dynamic liquid electrospinning. *J. Biomed. Nanotechnol.* **2014**, *10* (4), 603−614.
(161) Yokoyama, Y.; Hattori, S.; Yoshikawa, C.; Yasuda, Y.; Koyama, H.; Takato, T.; Kobayashi, H. Novel wet electrospinning system for fabrication of spongiform nanofiber 3-dimensional fabric. *Mater. Lett.* **2009**, *63* (9−10), 754−756.
(162) Kim, M. S.; Son, J.; Lee, H.; Hwang, H.; Choi, C. H.; Kim, G. Highly porous 3D nanofibrous scaffolds processed with an electrospinning/laser process. *Curr. Appl. Phys.* **2014**, *14* (1), 1−7.
(163) Moroni, L.; Schotel, R.; Hamann, D.; de Wijn, J. R.; van Blitterswijk, C. A. 3D Fiber-deposited electrospun integrated scaffolds enhance cartilage tissue formation. *Adv. Funct. Mater.* **2008**, *18* (1), 53−60.
(164) Li, D.; Wu, T.; He, N.; Wang, J.; Chen, W.; He, L.; Huang, C.; Ei-Hamshary, H. A.; Al-Deyab, S. S.; Ke, Q.; Mo, X. Three-dimensional polycaprolactone scaffold via needleless electrospinning promotes cell proliferation and infiltration. *Colloids Surf., B* **2014**, *121* (0), 432−443.
(165) Bobyn, J.; Stackpool, G.; Hacking, S.; Tanzer, M.; Krygier, J. Characteristics of bone ingrowth and interface mechanics of a new porous tantalum biomaterial. *J. Bone Jt. Surg., Br. Vol.* **1999**, *81* (5), 907−914.
(166) Zardiackas, L. D.; Parsell, D. E.; Dillon, L. D.; Mitchell, D. W.; Nunnery, L. A.; Poggie, R. Structure, metallurgy, and mechanical properties of a porous tantalum foam. *J. Biomed. Mater. Res.* **2001**, *58* (2), 180−187.
(167) Fujibayashi, S.; Neo, M.; Kim, H.-M.; Kokubo, T.; Nakamura, T. Osteoinduction of porous bioactive titanium metal. *Biomaterials* **2004**, *25* (3), 443−450.
(168) Yang, Y.; Tian, J.; Tian, J.; Chen, Z.; Deng, X.; Zhang, D. Preparation of graded porous titanium coatings on titanium implant materials by plasma spraying. *J. Biomed. Mater. Res.* **2000**, *52* (2), 333−337.
(169) Zhang, X.; Ayers, R.; Thorne, K.; Moore, J.; Schowengerdt, F. Combustion synthesis of porous materials for bone replacement. *Biomed. Sci. Instrum.* **2000**, *37*, 463−468.
(170) Li, B.-Y.; Rong, L.-J.; Li, Y.-Y.; Gjunter, V. A recent development in producing porous Ni−Ti shape memory alloys. *Intermetallics* **2000**, *8* (8), 881−884.
(171) Arakawa, Y.; Kobashi, M.; Kanetake, N. Effect of elemental powder size on foaming behavior of NiTi alloy made by combustion synthesis. *Materials* **2012**, *5* (7), 1267.
(172) Lee, J. H.; Park, H. J.; Hong, S. H.; Kim, J. T.; Lee, W. H.; Park, J. M.; Kim, K. B. Characterization and deformation behavior of Ti hybrid compacts with solid-to-porous gradient structure. *Mater. Eng.* **2014**, *60* (0), 66−71.
(173) Zou, X.; Li, H.; Bünger, M.; Egund, N.; Lind, M.; Bünger, C. Bone ingrowth characteristics of porous tantalum and carbon fiber interbody devices: an experimental study in pigs. *Spine J.* **2004**, *4* (1), 99−105.
(174) Lifland, M.; Okazaki, K. Properties of titanium dental implants produced by electro-discharge compaction. *Clin. Mater.* **1994**, *17* (4), 203−209.
(175) Ibrahim, A.; Zhang, F.; Otterstein, E.; Burkel, E. Processing of porous Ti and Ti5Mn foams by spark plasma sintering. *Mater. Eng.* **2011**, *32* (1), 146−153.
(176) Wen, M.; Wen, C.; Hodgson, P.; Li, Y. Fabrication of Ti−Nb−Ag alloy via powder metallurgy for biomedical applications. *Mater. Eng.* **2014**, *56* (0), 629−634.
(177) Bram, M.; Bitzer, M.; Buchkremer, H.; Stöver, D. Reproducibility study of NiTi parts made by metal injection molding. *J. Mater. Eng. Perform.* **2012**, *21* (12), 2701−2712.
(178) Köhl, M.; Habijan, T.; Bram, M.; Buchkremer, H. P.; Stöver, D.; Köller, M. Powder metallurgical near-net-shape fabrication of porous NiTi shape memory alloys for use as long-term implants by the combination of the metal injection molding process with the space-holder technique. *Adv. Eng. Mater.* **2009**, *11* (12), 959−968.
(179) Chen, L.-j.; Li, T.; Li, Y.-m.; He, H.; Hu, Y.-h. Porous titanium implants fabricated by metal injection molding. *Trans. Nonferrous Met. Soc. China* **2009**, *19* (5), 1174−1179.
(180) Yuan, B.; Zhang, X. P.; Chung, C. Y.; Zhu, M. The effect of porosity on phase transformation behavior of porous Ti-Ni shape memory alloys prepared by capsule-free hot isostatic pressing. *Mater. Sci. Eng., A* **2006**, *438−440* (0), 585−588.
(181) Bansiddhi, A.; Sargeant, T. D.; Stupp, S. I.; Dunand, D. C. Porous NiTi for bone implants: A review. *Acta Biomater.* **2008**, *4* (4), 773−782.
(182) Lagoudas, D. C.; Vandygriff, E. L. Processing and characterization of NiTi porous SMA by elevated pressure sintering. *J. Intell. Mater. Syst. Struct.* **2002**, *13* (12), 837−850.
(183) Zhang, Y. P.; Yuan, B.; Zeng, M. Q.; Chung, C. Y.; Zhang, X. P. High porosity and large pore size shape memory alloys fabricated by using pore-forming agent (NH4HCO3) and capsule-free hot isostatic pressing. *J. Mater. Process. Technol.* **2007**, *192−193* (0), 439−442.
(184) Elahinia, M. H.; Hashemi, M.; Tabesh, M.; Bhaduri, S. B. Manufacturing and processing of NiTi implants: a review. *Prog. Mater. Sci.* **2012**, *57* (5), 911−946.
(185) Andani, M. T.; Shayesteh Moghaddam, N.; Haberland, C.; Dean, D.; Miller, M. J.; Elahinia, M. Metals for bone implants. Part 1. Powder metallurgy and implant rendering. *Acta Biomater.* **2014**, *10* (10), 4058−4070.
(186) Dotzauer, D. M.; Dai, J.; Sun, L.; Bruening, M. L. Catalytic Membranes Prepared Using Layer-by-Layer Adsorption of Polyelectrolyte/Metal Nanoparticle Films in Porous Supports. *Nano Lett.* **2006**, *6* (10), 2268−2272.
(187) Ouyang, L.; Dotzauer, D. M.; Hogg, S. R.; Macanás, J.; Lahitte, J.-F.; Bruening, M. L. Catalytic hollow fiber membranes prepared using layer-by-layer adsorption of polyelectrolytes and metal nanoparticles. *Catal. Today* **2010**, *156* (3), 100−106.
(188) Dumee, L. F.; He, L.; Lin, B.; Ailloux, F.-M.; Lemoine, J.-B.; Velleman, L.; She, F.; Duke, M. C.; Orbell, J. D.; Erskine, G.; Hodgson, P. D.; Gray, S.; Kong, L. The fabrication and surface functionalization of porous metal frameworks - a review. *J. Mater. Chem. A* **2013**, *1* (48), 15185−15206.
(189) Park, S. A.; Lee, S. H.; Kim, W. D. Fabrication of porous polycaprolactone/hydroxyapatite (PCL/HA) blend scaffolds using a 3D plotting system for bone tissue engineering. *Bioprocess Biosyst. Eng.* **2011**, *34* (4), 505−513.
(190) Gloria, A.; Causa, F.; Russo, T.; Battista, E.; Della Moglie, R.; Zeppetelli, S.; De Santis, R.; Netti, P.; Ambrosio, L. Three-dimensional poly (ε-caprolactone) bioactive scaffolds with controlled structural and surface properties. *Biomacromolecules* **2012**, *13* (11), 3510−3521.
(191) Neiman, J. A. S.; Raman, R.; Chan, V.; Rhoads, M. G.; Raredon, M. S. B.; Velazquez, J. J.; Dyer, R. L.; Bashir, R.; Hammond, P. T.; Griffith, L. G. Photopatterning of hydrogel scaffolds coupled to filter materials using stereolithography for perfused 3D culture of hepatocytes. *Biotechnol. Bioeng.* **2015**, *112* (4), 777−787.
(192) Lin, H.; Zhang, D.; Alexander, P. G.; Yang, G.; Tan, J.; Cheng, A. W.-M.; Tuan, R. S. Application of visible light-based projection stereolithography for live cell-scaffold fabrication with designed architecture. *Biomaterials* **2013**, *34* (2), 331−339.
(193) Gauvin, R.; Chen, Y.-C.; Lee, J. W.; Soman, P.; Zorlutuna, P.; Nichol, J. W.; Bae, H.; Chen, S.; Khademhosseini, A. Microfabrication of complex porous tissue engineering scaffolds using 3D projection stereolithography. *Biomaterials* **2012**, *33* (15), 3824−3834.

DOI: 10.1021/acsbiomaterials.7b00615
ACS Biomater. Sci. Eng. XXXX, XXX, XXX−XXX

(194) Elomaa, L.; Teixeira, S.; Hakala, R.; Korhonen, H.; Grijpma, D. W.; Seppälä, J. V. Preparation of poly (ε-caprolactone)-based tissue engineering scaffolds by stereolithography. *Acta Biomater.* **2011**, *7* (11), 3850−3856.
(195) Bian, W.; Li, D.; Lian, Q.; Li, X.; Zhang, W.; Wang, K.; Jin, Z. Fabrication of a bio-inspired beta-Tricalcium phosphate/collagen scaffold based on ceramic stereolithography and gel casting for osteochondral tissue engineering. *Rapid Prototyp J.* **2012**, *18* (1), 68−80.
(196) Eshraghi, S.; Das, S. Mechanical and microstructural properties of polycaprolactone scaffolds with one-dimensional, two-dimensional, and three-dimensional orthogonally oriented porous architectures produced by selective laser sintering. *Acta Biomater.* **2010**, *6* (7), 2467−2476.
(197) Huang, H.; Oizumi, S.; Kojima, N.; Niino, T.; Sakai, Y. Avidin−biotin binding-based cell seeding and perfusion culture of liver-derived cells in a porous scaffold with a three-dimensional interconnected flow-channel network. *Biomaterials* **2007**, *28* (26), 3815−3823.
(198) Amorim, F. L.; Lohrengel, A.; Neubert, V.; Higa, C. F.; Czelusniak, T. Selective laser sintering of Mo-CuNi composite to be used as EDM electrode. *Rapid Prototyp J.* **2014**, *20* (1), 59−68.
(199) Kolan, K. C.; Thomas, A.; Leu, M. C.; Hilmas, G. In vitro assessment of laser sintered bioactive glass scaffolds with different pore geometries. *Rapid Prototyp J.* **2015**, *21* (2), 152−158.
(200) Antonov, E.; Barinov, S.; Vakhrushev, I.; Komlev, V.; Popov, V.; Fedotov, A. Y.; Yarygin, K. Selective laser sintering of bioactive composite matrices for bone tissue engineering. *Inorganic Materials: Applied Research* **2015**, *6* (2), 171−178.
(201) Chen, C.-H.; Shyu, V. B.-H.; Chen, J.-P.; Lee, M.-Y. Selective laser sintered poly-ε-caprolactone scaffold hybridized with collagen hydrogel for cartilage tissue engineering. *Biofabrication* **2014**, *6* (1), 015004.
(202) Van Bael, S.; Chai, Y. C.; Truscello, S.; Moesen, M.; Kerckhofs, G.; Van Oosterwyck, H.; Kruth, J.-P.; Schrooten, J. The effect of pore geometry on the in vitro biological behavior of human periosteum-derived cells seeded on selective laser-melted Ti6Al4V bone scaffolds. *Acta Biomater.* **2012**, *8* (7), 2824−2834.
(203) Hoffmann, W.; Bormann, T.; Rossi, A.; Müller, B.; Schumacher, R.; Martin, I.; de Wild, M.; Wendt, D. Rapid prototyped porous nickel−titanium scaffolds as bone substitutes. *J. Tissue Eng.* **2014**, *5*, 2041731414540674.
(204) Hollander, D. A.; Von Walter, M.; Wirtz, T.; Sellei, R.; Schmidt-Rohlfing, B.; Paar, O.; Erli, H.-J. Structural, mechanical and in vitro characterization of individually structured Ti−6Al−4V produced by direct laser forming. *Biomaterials* **2006**, *27* (7), 955−963.
(205) Parthasarathy, J.; Starly, B.; Raman, S.; Christensen, A. Mechanical evaluation of porous titanium (Ti6Al4V) structures with electron beam melting (EBM). *J. Mech. Behav. Biomed. Mater.* **2010**, *3* (3), 249−259.
(206) Li, X.; Ma, X.-Y.; Feng, Y.-F.; Wang, L.; Wang, C. A novel composite scaffold consisted of porous titanium and chitosan sponge for load-bearing applications: Fabrication, characterization and cellular activity. *Compos. Sci. Technol.* **2015**, *117* (0), 78−84.
(207) Vaezi, M.; Seitz, H.; Yang, S. A review on 3D micro-additive manufacturing technologies. *Int. J. Adv. Manuf. Technol.* **2013**, *67* (5−8), 1721−1754.
(208) Inzana, J. A.; Olvera, D.; Fuller, S. M.; Kelly, J. P.; Graeve, O. A.; Schwarz, E. M.; Kates, S. L.; Awad, H. A. 3D printing of composite calcium phosphate and collagen scaffolds for bone regeneration. *Biomaterials* **2014**, *35* (13), 4026−4034.
(209) Habibovic, P.; Gbureck, U.; Doillon, C. J.; Bassett, D. C.; van Blitterswijk, C. A.; Barralet, J. E. Osteoconduction and osteoinduction of low-temperature 3D printed bioceramic implants. *Biomaterials* **2008**, *29* (7), 944−953.
(210) Castilho, M.; Gouveia, B.; Pires, I.; Rodrigues, J.; Pereira, M. The role of shell/core saturation level on the accuracy and mechanical characteristics of porous calcium phosphate models produced by 3Dprinting. *Rapid Prototyp J.* **2015**, *21* (1), 43−55.
(211) Maleksaeedi, S.; Wang, J. K.; El-Hajje, A.; Harb, L.; Guneta, V.; He, Z.; Wiria, F. E.; Choong, C.; Ruys, A. J. Toward 3D printed bioactive titanium scaffolds with bimodal pore size distribution for bone ingrowth. *Procedia CIRP* **2013**, *5* (0), 158−163.
(212) Kirkland, N. T.; Kolbeinsson, I.; Woodfield, T.; Dias, G. J.; Staiger, M. P. Synthesis and properties of topologically ordered porous magnesium. *Mater. Sci. Eng., B* **2011**, *176* (20), 1666−1672.
(213) Grida, I.; Evans, J. R. G. Extrusion freeforming of ceramics through fine nozzles. *J. Eur. Ceram. Soc.* **2003**, *23* (5), 629−635.
(214) Domingos, M.; Chiellini, F.; Gloria, A.; Ambrosio, L.; Bartolo, P.; Chiellini, E. Effect of process parameters on the morphological and mechanical properties of 3D Bioextruded poly(ε-caprolactone) scaffolds. *Rapid Prototyp J.* **2012**, *18* (1), 56−67.
(215) Billiet, T.; Vandenhaute, M.; Schelfhout, J.; Van Vlierberghe, S.; Dubruel, P. A review of trends and limitations in hydrogel-rapid prototyping for tissue engineering. *Biomaterials* **2012**, *33* (26), 6020−6041.
(216) Yeong, W.-Y.; Chua, C.-K.; Leong, K.-F.; Chandrasekaran, M. Rapid prototyping in tissue engineering: challenges and potential. *Trends Biotechnol.* **2004**, *22* (12), 643−652.
(217) Xiong, Z.; Yan, Y.; Wang, S.; Zhang, R.; Zhang, C. Fabrication of porous scaffolds for bone tissue engineering via low-temperature deposition. *Scr. Mater.* **2002**, *46* (11), 771−776.
(218) Domingos, M.; Dinucci, D.; Cometa, S.; Alderighi, M.; Bártolo, P. J.; Chiellini, F. Polycaprolactone scaffolds fabricated via bioextrusion for tissue engineering applications. *Int. J. Biomater.* **2009**, *2009*, 239643.
(219) Moroni, L.; Schotel, R.; Sohier, J.; de Wijn, J. R.; van Blitterswijk, C. A. Polymer hollow fiber three-dimensional matrices with controllable cavity and shell thickness. *Biomaterials* **2006**, *27* (35), 5918−5926.
(220) Gao, Q.; He, Y.; Fu, J.-z.; Liu, A.; Ma, L. Coaxial nozzle-assisted 3D bioprinting with built-in microchannels for nutrients delivery. *Biomaterials* **2015**, *61*, 203−215.
(221) Li, J.; De Wijn, J.; Van Blitterswijk, C.; De Groot, K. The effect of scaffold architecture on properties of direct 3D fiber deposition of porous Ti6Al4V for orthopedic implants. *J. Biomed. Mater. Res., Part A* **2010**, *92* (1), 33−42.
(222) Hoque, M. E.; Chuan, Y. L.; Pashby, I. Extrusion based rapid prototyping technique: an advanced platform for tissue engineering scaffold fabrication. *Biopolymers* **2012**, *97* (2), 83−93.
(223) Landers, R.; Mülhaupt, R. Desktop manufacturing of complex objects, prototypes and biomedical scaffolds by means of computer-assisted design combined with computer-guided 3D plotting of polymers and reactive oligomers. *Macromol. Mater. Eng.* **2000**, *282* (1), 17−21.
(224) Billiet, T.; Gevaert, E.; De Schryver, T.; Cornelissen, M.; Dubruel, P. The 3D printing of gelatin methacrylamide cell-laden tissue-engineered constructs with high cell viability. *Biomaterials* **2014**, *35* (1), 49−62.
(225) Cesarano, J.; Segalman, R.; Calvert, P. Robocasting provides moldless fabrication from slurry deposition. *Ceram. Ind.* **1998**, *148* (4), 94.
(226) Lewis, J. A.; Smay, J. E.; Stuecker, J.; Cesarano, J. Direct ink writing of three-dimensional ceramic structures. *J. Am. Ceram. Soc.* **2006**, *89* (12), 3599−3609.
(227) Miranda, P.; Saiz, E.; Gryn, K.; Tomsia, A. P. Sintering and robocasting of β-tricalcium phosphate scaffolds for orthopaedic applications. *Acta Biomater.* **2006**, *2* (4), 457−466.
(228) Lu, X.; Lee, Y.; Yang, S.; Hao, Y.; Evans, J. R. G.; Parini, C. G. Solvent-based paste extrusion solid freeforming. *J. Eur. Ceram. Soc.* **2010**, *30* (1), 1−10.
(229) Almeida, C. R.; Serra, T.; Oliveira, M. I.; Planell, J. A.; Barbosa, M. A.; Navarro, M. Impact of 3-D printed PLA-and chitosan-based scaffolds on human monocyte/macrophage responses: unraveling the effect of 3-D structures on inflammation. *Acta Biomater.* **2014**, *10* (2), 613−622.

DOI: 10.1021/acsbiomaterials.7b00615
ACS Biomater. Sci. Eng. XXXX, XXX, XXX−XXX

(230) Serra, T.; Planell, J. A.; Navarro, M. High-resolution PLA-based composite scaffolds via 3-D printing technology. *Acta Biomater.* **2013**, *9* (3), 5521−5530.
(231) Fedorovich, N. E.; Schuurman, W.; Wijnberg, H. M.; Prins, H.-J.; van Weeren, P. R.; Malda, J.; Alblas, J.; Dhert, W. J. A. Biofabrication of Osteochondral Tissue Equivalents by Printing Topologically Defined, Cell-Laden Hydrogel Scaffolds. *Tissue Eng., Part C* **2012**, *18* (1), 33−44.
(232) Mironov, V.; Kasyanov, V.; Markwald, R. R. Organ printing: from bioprinter to organ biofabrication line. *Curr. Opin. Biotechnol.* **2011**, *22* (5), 667−673.
(233) Park, J. Y.; et al. A comparative study on collagen type I and hyaluronic acid dependent cell behavior for osteochondral tissue bioprinting. *Biofabrication* **2014**, *6* (3), 035004.
(234) Shim, J.-H.; et al. Bioprinting of a mechanically enhanced three-dimensional dual cell-laden construct for osteochondral tissue engineering using a multi-head tissue/organ building system. *J. Micromech. Microeng.* **2012**, *22* (8), 085014.
(235) Schumacher, M.; Deisinger, U.; Detsch, R.; Ziegler, G. Indirect rapid prototyping of biphasic calcium phosphate scaffolds as bone substitutes: influence of phase composition, macroporosity and pore geometry on mechanical properties. *J. Mater. Sci.: Mater. Med.* **2010**, *21* (12), 3119−3127.
(236) Schumacher, M.; Uhl, F.; Detsch, R.; Deisinger, U.; Ziegler, G. Static and dynamic cultivation of bone marrow stromal cells on biphasic calcium phosphate scaffolds derived from an indirect rapid prototyping technique. *J. Mater. Sci.: Mater. Med.* **2010**, *21* (11), 3039−3048.
(237) Yeong, W.-Y.; Chua, C.-K.; Leong, K.-F.; Chandrasekaran, M.; Lee, M.-W. Comparison of drying methods in the fabrication of collagen scaffold via indirect rapid prototyping. *J. Biomed. Mater. Res., Part B* **2007**, *82B* (1), 260−266.
(238) Deisinger, U.; Hamisch, S.; Schumacher, M.; Uhl, F.; Detsch, R.; Ziegler, G. In Fabrication of tailored hydroxyapatite scaffolds: comparison between a direct and an indirect rapid prototyping technique, Key Eng. *Key Eng. Mater.* **2008**, *361-363*, 915−918.
(239) Ryan, G. E.; Pandit, A. S.; Apatsidis, D. P. Porous titanium scaffolds fabricated using a rapid prototyping and powder metallurgy technique. *Biomaterials* **2008**, *29* (27), 3625−3635.
(240) Kasten, P.; Beyen, I.; Niemeyer, P.; Luginbuhl, R.; Bohner, M.; Richter, W. Porosity and pore size ofb-tricalcium phosphate scaffold can influence protein production and osteogenic differentiation of human mesenchymal stem cells: An in vitro and in vivo study. *Acta Biomater.* **2008**, *4*, 1904−1915.
(241) Hulbert, S. F.; Young, F. A.; Mathews, R. S.; Klawitter, J. J.; Talbert, C. D.; Stelling, F. H. Potential of ceramic materials as permanently implantable skeletal prostheses. *J. Biomed. Mater. Res.* **1970**, *4* (3), 433−456.
(242) Itala, A. I.; Ylanen, H. O.; Ekholm, C.; Karlsson, K. H.; Aro, H. T. Pore diameter of more than 100 microm is not requisite for bone ingrowth in rabbits. *J. Biomed. Mater. Res.* **2001**, *58* (6), 679−83.
(243) Chang, B.; Song, W.; Han, T.; Yan, J.; Li, F.; Zhao, L.; Kou, H.; Zhang, Y. Influence of pore size of porous titanium fabricated by vacuum diffusion bonding of titanium meshes on cell penetration and bone ingrowth. *Acta Biomater.* **2016**, *33*, 311−321.
(244) Sobral, J. M.; Caridade, S. G.; Sousa, R. A.; Mano, J. F.; Reis, R. L. Three-dimensional plotted scaffolds with controlled pore size gradients: Effect of scaffold geometry on mechanical performance and cell seeding efficiency. *Acta Biomater.* **2011**, *7* (3), 1009−1018.
(245) Salerno, A.; Guarnieri, D.; Iannone, M.; Zeppetelli, S.; Netti, P. A. Effect of micro- and macroporosity of bone tissue three-dimensional-poly(ε-caprolactone) scaffold on human mesenchymal stem cells invasion, proliferation, and differentiation in vitro. *Tissue Eng., Part A* **2010**, *16* (8), 2661−2673.
(246) Choi, S.-W.; Zhang, Y.; Xia, Y. Three-dimensional scaffolds for tissue engineering: the importance of uniformity in pore size and structure. *Langmuir* **2010**, *26* (24), 19001−19006.
(247) Klenke, F. M.; Liu, Y.; Yuan, H.; Hunziker, E. B.; Siebenrock, K. A.; Hofstetter, W. Impact of pore size on the vascularization and osseointegration of ceramic bone substitutes in vivo. *J. Biomed. Mater. Res., Part A* **2008**, *85* (3), 777−786.
(248) Feng, B.; Jinkang, Z.; Zhen, W.; Jianxi, L.; Jiang, C.; Jian, L.; Guolin, M.; Xin, D. The effect of pore size on tissue ingrowth and neovascularization in porous bioceramics of controlled architecture in vivo. *Biomed. Mater.* **2011**, *6* (1), 015007.
(249) Bohner, M.; Loosli, Y.; Baroud, G.; Lacroix, D. Commentary: Deciphering the link between architecture and biological response of a bone graft substitute. *Acta Biomater.* **2011**, *7* (2), 478−484.
(250) Ho, S. T.; Hutmacher, D. W. A comparison of micro CT with other techniques used in the characterization of scaffolds. *Biomaterials* **2006**, *27* (8), 1362−1376.
(251) O'Brien, F. J.; Harley, B. A.; Waller, M. A.; Yannas, I. V.; Gibson, L. J.; Prendergast, P. J. The effect of pore size on permeability and cell attachment in collagen scaffolds for tissue engineering. *Technol. Health Care* **2007**, *15* (1), 3−17.
(252) Otsuki, B.; Takemoto, M.; Fujibayashi, S.; Neo, M.; Kokubo, T.; Nakamura, T. Pore throat size and connectivity determine bone and tissue ingrowth into porous implants: Three-dimensional micro-CT based structural analyses of porous bioactive titanium implants. *Biomaterials* **2006**, *27* (35), 5892−5900.
(253) Lu, J.; Flautre, B.; Anselme, K.; Hardouin, P.; Gallur, A.; Descamps, M.; Thierry, B. Role of interconnections in porous bioceramics on bone recolonization in vitro and in vivo. *J. Mater. Sci.: Mater. Med.* **1999**, *10* (2), 111−120.
(254) Grandfield, K.; Palmquist, A.; Ericson, F.; Malmstrom, J.; Emanuelsson, L.; Slotte, C.; Adolfsson, E.; Botton, G. A.; Thomsen, P.; Engqvist, H. Bone response to free-form fabricated hydroxyapatite and zirconia scaffolds: a transmission electron microscopy study in the human maxilla. *Clin. Implant. Dent. Relat. Res.* **2012**, *14* (3), 461−9.
(255) Porter, A. E.; Buckland, T.; Hing, K.; Best, S. M.; Bonfield, W. The structure of the bond between bone and porous silicon-substituted hydroxyapatite bioceramic implants. *J. Biomed. Mater. Res., Part A* **2006**, *78* (1), 25−33.
(256) Simon, J. L.; Michna, S.; Lewis, J. A.; Rekow, E. D.; Thompson, V. P.; Smay, J. E.; Yampolsky, A.; Parsons, J. R.; Ricci, J. L. In vivo bone response to 3D periodic hydroxyapatite scaffolds assembled by direct ink writing. *J. Biomed. Mater. Res., Part A* **2007**, *83* (3), 747−58.
(257) Lan Levengood, S. K.; Polak, S. J.; Poellmann, M. J.; Hoelzle, D. J.; Maki, A. J.; Clark, S. G.; Wheeler, M. B.; Wagoner Johnson, A. J. The effect of BMP-2 on micro- and macroscale osteointegration of biphasic calcium phosphate scaffolds with multiscale porosity. *Acta Biomater.* **2010**, *6* (8), 3283−3291.
(258) Hing, K.; Annaz, B.; Saeed, S.; Revell, P.; Buckland, T. Microporosity enhances bioactivity of synthetic bone graft substitutes. *J. Mater. Sci.: Mater. Med.* **2005**, *16* (5), 467−475.
(259) Tang, W.; Lin, D.; Yu, Y.; Niu, H.; Guo, H.; Yuan, Y.; Liu, C. Bioinspired trimodal macro/micro/nano-porous scaffolds loading rhBMP-2 for complete regeneration of critical size bone defect. *Acta Biomater.* **2016**, *32*, 309−323.
(260) Lutolf, M.; Hubbell, J. Synthetic biomaterials as instructive extracellular microenvironments for morphogenesis in tissue engineering. *Nat. Biotechnol.* **2005**, *23* (1), 47−55.
(261) Lord, M. S.; Foss, M.; Besenbacher, F. Influence of nanoscale surface topography on protein adsorption and cellular response. *Nano Today* **2010**, *5* (1), 66−78.
(262) Cox, S. C.; Thornby, J. A.; Gibbons, G. J.; Williams, M. A.; Mallick, K. K. 3D printing of porous hydroxyapatite scaffolds intended for use in bone tissue engineering applications. *Mater. Sci. Eng., C* **2015**, *47*, 237−247.
(263) Perez, R. A.; Kim, T. H.; Kim, M.; Jang, J. H.; Ginebra, M. P.; Kim, H. W. Calcium phosphate cements loaded with basic fibroblast growth factor: Delivery and in vitro cell response. *J. Biomed. Mater. Res., Part A* **2013**, *101* (4), 923−931.
(264) Dorj, B.; Won, J.-E.; Purevdorj, O.; Patel, K. D.; Kim, J.-H.; Lee, E.-J.; Kim, H.-W. A novel therapeutic design of microporous-structured biopolymer scaffolds for drug loading and delivery. *Acta Biomater.* **2014**, *10* (3), 1238−1250.

DOI: 10.1021/acsbiomaterials.7b00615
ACS Biomater. Sci. Eng. XXXX, XXX, XXX−XXX

(265) Polak, S. J.; Levengood, S. K. L.; Wheeler, M. B.; Maki, A. J.; Clark, S. G.; Johnson, A. J. W. Analysis of the roles of microporosity and BMP-2 on multiple measures of bone regeneration and healing in calcium phosphate scaffolds. *Acta Biomater.* **2011**, *7* (4), 1760−1771.
(266) Cecchinato, F.; Atefyekta, S.; Wennerberg, A.; Andersson, M.; Jimbo, R.; Davies, J. R. Modulation of the nanometer pore size improves magnesium adsorption into mesoporous titania coatings and promotes bone morphogenic protein 4 expression in adhering osteoblasts. *Dent. Mater.* **2016**, *32*, e148.
(267) Von Doernberg, M. C.; Von Rechenberg, B.; et al. In vivo behavior of calcium phosphate scaffolds with four different pore sizes. *Biomaterials* **2006**, *27*, 5186−5198.
(268) Bohner, M.; Baumgart, F. Theoretical model to determine the effects of geometrical factors on the resorption of calcium phosphate bone substitutes. *Biomaterials* **2004**, *25*, 3569−3582.
(269) Lapczyna, H.; Galea, L.; Wüst, S.; Bohner, M.; Jerban, S.; Sweedy, A.; Doebelin, N.; Van Garderen, N.; Hofmann, S.; Baroud, G.; Müller, R.; von Rechenberg, B. Effect of grain size and microporosity on the in vivo behaviour of β-tricalcium phosphate scaffolds. *Eur. Cells Mater.* **2014**, *28*, 299−319.
(270) Cordell, J. M.; Vogl, M. L.; Johnson, A. J. W. The influence of micropore size on the mechanical properties of bulk hydroxyapatite and hydroxyapatite scaffolds. *J. Mech. Behav. Biomed. Mater.* **2009**, *2* (5), 560−570.
(271) Moore, W. R.; Graves, S. E.; Bain, G. I. Synthetic bone graft substitutes. *Aust. N. Z. J. Surg.* **2001**, *71* (6), 354−361.
(272) Sabree, I.; Gough, J. E.; Derby, B. Mechanical properties of porous ceramic scaffolds: Influence of internal dimensions. *Ceram. Int.* **2015**, *41* (7), 8425−8432.
(273) Liu, X.; Rahaman, M. N.; Hilmas, G. E.; Bal, B. S. Mechanical properties of bioactive glass (13−93) scaffolds fabricated by robotic deposition for structural bone repair. *Acta Biomater.* **2013**, *9* (6), 7025−7034.
(274) Lee, J. S.; Cha, H. D.; Shim, J. H.; Jung, J. W.; Kim, J. Y.; Cho, D. W. Effect of pore architecture and stacking direction on mechanical properties of solid freeform fabrication-based scaffold for bone tissue engineering. *J. Biomed. Mater. Res., Part A* **2012**, *100* (7), 1846−53.
(275) Baino, F.; Vitale-Brovarone, C. Mechanical properties and reliability of glass−ceramic foam scaffolds for bone repair. *Mater. Lett.* **2014**, *118*, 27−30.
(276) Chin Ang, K.; Fai Leong, K.; Kai Chua, C.; Chandrasekaran, M. Investigation of the mechanical properties and porosity relationships in fused deposition modelling-fabricated porous structures. *Rapid Prototyp J.* **2006**, *12* (2), 100−105.
(277) Sudarmadji, N.; Tan, J.; Leong, K.; Chua, C.; Loh, Y. Investigation of the mechanical properties and porosity relationships in selective laser-sintered polyhedral for functionally graded scaffolds. *Acta Biomater.* **2011**, *7* (2), 530−537.
(278) Wu, C.; Ramaswamy, Y.; Zreiqat, H. Porous diopside (CaMgSi2O6) scaffold: a promising bioactive material for bone tissue engineering. *Acta Biomater.* **2010**, *6* (6), 2237−2245.
(279) Le Huec, J. C.; Schaeverbeke, T.; Clement, D.; Faber, J.; Le Rebeller, A. Influence of porosity on the mechanical resistance of hydroxyapatite ceramics under compressive stress. *Biomaterials* **1995**, *16* (2), 113−118.
(280) Liu, D.-M. Influence of porosity and pore size on the compressive strength of porous hydroxyapatite ceramic. *Ceram. Int.* **1997**, *23* (2), 135−139.
(281) Prokopiev, O.; Sevostianov, I. Dependence of the mechanical properties of sintered hydroxyapatite on the sintering temperature. *Mater. Sci. Eng., A* **2006**, *431* (1), 218−227.
(282) Prokopiev, O.; Sevostianov, I. On the Possibility of Approximation of Irregular Porous Microstructure by Isolated Spheroidal Pores. *Int. J. Fract.* **2006**, *139* (1), 129−136.
(283) Mathieu, L. M.; Mueller, T. L.; Bourban, P.-E.; Pioletti, D. P.; Müller, R.; Månson, J.-A. E. Architecture and properties of anisotropic polymer composite scaffolds for bone tissue engineering. *Biomaterials* **2006**, *27* (6), 905−916.
(284) Roohani-Esfahani, S.-I.; Newman, P.; Zreiqat, H. Design and Fabrication of 3D printed Scaffolds with a mechanical strength comparable to cortical bone to repair large bone defects. *Sci. Rep.* **2016**, *6*, 19468.
(285) Wu, C.; Luo, Y.; Cuniberti, G.; Xiao, Y.; Gelinsky, M. Three-dimensional printing of hierarchical and tough mesoporous bioactive glass scaffolds with a controllable pore architecture, excellent mechanical strength and mineralization ability. *Acta Biomater.* **2011**, *7* (6), 2644−2650.
(286) Vitale-Brovarone, C.; Baino, F.; Miola, M.; Mortera, R.; Onida, B.; Verné, E. Glass−ceramic scaffolds containing silica mesophases for bone grafting and drug delivery. *J. Mater. Sci.: Mater. Med.* **2009**, *20* (3), 809.
(287) Arabnejad, S.; Burnett Johnston, R.; Pura, J. A.; Singh, B.; Tanzer, M.; Pasini, D. High-strength porous biomaterials for bone replacement: A strategy to assess the interplay between cell morphology, mechanical properties, bone ingrowth and manufacturing constraints. *Acta Biomater.* **2016**, *30*, 345−356.
(288) Bashoor-Zadeh, M.; Baroud, G.; Bohner, M. Geometric analysis of porous bone substitutes using micro-computed tomography and fuzzy distance transform. *Acta Biomater.* **2010**, *6* (3), 864−875.
(289) Del Valle, S.; Miño, N.; Muñoz, F.; González, A.; Planell, J. A.; Ginebra, M.-P. In vivo evaluation of an injectable macroporous calcium phosphate cement. *J. Mater. Sci.: Mater. Med.* **2007**, *18* (2), 353−361.
(290) Potoczek, M.; Zima, A.; Paszkiewicz, Z.; Ślósarczyk, A. Manufacturing of highly porous calcium phosphate bioceramics via gel-casting using agarose. *Ceram. Int.* **2009**, *35* (6), 2249−2254.
(291) Ramay, H. R.; Zhang, M. Preparation of porous hydroxyapatite scaffolds by combination of the gel-casting and polymer sponge methods. *Biomaterials* **2003**, *24* (19), 3293−3302.
(292) Zhou, J.; Gao, C.; Feng, P.; Xiao, T.; Shuai, C.; Peng, S. Calcium sulfate bone scaffolds with controllable porous structure by selective laser sintering. *J. Porous Mater.* **2015**, *22*, 1171.
(293) Zhang, Y.; Fan, W.; Ma, Z.; Wu, C.; Fang, W.; Liu, G.; Xiao, Y. The effects of pore architecture in silk fibroin scaffolds on the growth and differentiation of mesenchymal stem cells expressing BMP7. *Acta Biomater.* **2010**, *6* (8), 3021−3028.
(294) Lam, C. X. F.; Mo, X.; Teoh, S.-H.; Hutmacher, D. Scaffold development using 3D printing with a starch-based polymer. *Mater. Sci. Eng., C* **2002**, *20* (1), 49−56.
(295) Shuai, C.; Mao, Z.; Lu, H.; Nie, Y.; Hu, H.; Peng, S. Fabrication of porous polyvinyl alcohol scaffold for bone tissue engineering via selective laser sintering. *Biofabrication* **2013**, *5* (1), 015014.
(296) Wieding, J.; Lindner, T.; Bergschmidt, P.; Bader, R. Biomechanical stability of novel mechanically adapted open-porous titanium scaffolds in metatarsal bone defects of sheep. *Biomaterials* **2015**, *46* (0), 35−47.
(297) Chen, Y.; Feng, B.; Zhu, Y.; Weng, J.; Wang, J.; Lu, X. Fabrication of porous titanium implants with biomechanical compatibility. *Mater. Lett.* **2009**, *63* (30), 2659−2661.
(298) Hong, T. F.; Guo, Z. X.; Yang, R. Fabrication of porous titanium scaffold materials by a fugitive filler method. *J. Mater. Sci.: Mater. Med.* **2008**, *19* (12), 3489−3495.
(299) Kutty, M. G.; De, A.; Bhaduri, S. B.; Yaghoubi, A. Microwave-assisted fabrication of titanium implants with controlled surface topography for rapid bone healing. *ACS Appl. Mater. Interfaces* **2014**, *6* (16), 13587−13593.
(300) Li, J. P.; de Wijn, J. R.; Van Blitterswijk, C. A.; de Groot, K. Porous Ti 6 Al 4 V scaffold directly fabricating by rapid prototyping: preparation and in vitro experiment. *Biomaterials* **2006**, *27* (8), 1223−1235.

DOI: 10.1021/acsbiomaterials.7b00615
ACS Biomater. Sci. Eng. XXXX, XXX, XXX−XXX